Development and Modeling of Conducting Polymer Actuators and the Fabrication of a Conducting Polymer Based Feedback Loop

by

Peter Geoffrey Alexander Madden

B.Apsc., University of British Columbia (1993)
M.Eng. McGill University (1996)

Submitted to the Department of Mechanical Engineering
in Partial Fulfillment of the Requirements for the Degree of

Doctor of Philosophy in Mechanical Engineering

at the

MASSACHUSETTS INSTITUTE OF TECHNOLOGY

AUGUST 2003

Signature of Author .....
Department of Mechanical Engineering
August 1, 2003

Certified by .....
Ian W. Hunter
Hatsopoulos Professor of Mechanical Engineering
Thesis Supervisor

Accepted by .....
Ain A. Sonin
Professor of Mechanical Engineering
Chairman, Department Committee on Graduate Students

Development and Modeling of Conducting Polymer Actuators and the Fabrication of a Conducting Polymer Based Feedback Loop

by

Peter Geoffrey Alexander Madden

Submitted to the Department of Mechanical Engineering
on August 1, 2003 in Partial Fulfillment of the
Requirements for the Degree of Doctor of Philosophy in
Mechanical Engineering

ABSTRACT

Conducting polymers as a class of materials can be used to build a diverse range of devices. Conducting polymer based actuators (muscles), transistors (neurons), strain gages (muscle spindles), force sensors (Golgi tendon organs), light emitting diodes, photodetectors (eyes), batteries and supercapacitors (energy storage), and chemical sensors (noses) can all be manufactured. The range of behaviors makes conducting polymers the only class of materials that might be able to mimic the full range of functions needed to build a truly lifelike artificial system. In this thesis, a conducting polymer actuator and conducting polymer strain gage are used for the first time to build a reflex or position feedback loop that rejects position disturbances. The successful operation of the conducting polymer based reflex loop is an important step towards building an all polymer reflex loop that is directly integrated into a bulk material. Such a reflex loop could be used to control position, to control force or to dynamically change the material stiffness and viscosity. In the course of the project, an improved understanding of conducting polymer actuators has led to mathematical descriptions of the charging and discharging of long linear actuators and to equations describing the deflection and force of three layer bending beam actuators. These equations can be used as design tools to build actuators that satisfy given performance requirements. Finally, the performance of the actuators has been related to specific material properties to help direct research into new conducting polymeric materials.

Thesis Supervisor: Ian W. Hunter
Title: Professor of Mechanical Engineering

Acknowledgements

It is not often enough that we pause to think of and to thank those who have helped us through the events of our lives. A thesis involves far more than just the experiments and the written document. There are moments of joy as there are times of discouragement. There are moments of understanding sometimes interspersed between months of frustration. And through it all, there are those who encourage, those who discuss, and those who support.

I owe a special thanks to all the people who first welcomed me into the lab at McGill University. Ian Hunter has shaped the way I think about research and illustrates every day that learning is a lifelong process. Many thanks to Lynette Jones and to Serge Lafontaine, who have always been tremendously hospitable and helpful in the lab and out.

I also owe a tremendous amount to my committee members Professor Seth Lloyd, Professor Donald Sadoway, and Professor Timothy Swager. Each of them has helped direct the research and encouraged me as I have matured along the route to finishing this thesis.

I enjoyed working with the conducting polymer group at MIT tremendously. Patrick, Nate, Rachel, and Nicola have all helped me innumerable times.

Many friends inside the lab and out have taught me and changed me more during my Ph.D. than they would ever suspect and perhaps without even knowing. Many thanks to James, who proves you can have both carefully considerate maturity and side-splitting immaturity; thanks to Dom for teaching me to live both in the lab and in the mountains; and thanks to Aimee for showing me that life should be balanced and that everyone is human.

My mother and father have always been more than supportive, and I should say, more than patient, during my Ph.D. While gently encouraging me to finish and yet understanding that I wasn't finished, they have provided sound advice and support.

A very special thanks goes to my brother John who spent many years in the lab as well. John was subject to more of the vagaries of my mood than anyone and yet was ever tolerant and always helpful. John also taught me a tremendous amount about conducting polymers and his thesis is the foundation upon which my work strives to build. And finally, a special thanks to my nephew Alex and sister in law Ann for telling me (without words) what life is about.

Table of Contents

Abstract 3
Acknowledgements 5

1. Introduction 9
2. Understanding of the diffusive elastic model 23
3. Finite Conductivity Effects in Long Actuators 41
4. Derivation of the Trilayer Force and Displacement Equations 63
5. Trimorphs in Liquid Electrolyte 69
6. Analysis of Trimorph Deflection in Air 81
7. Position Feedback Loop Using a Conducting Polymer Actuator and Strain Gage 91
8. Conclusions 121

Appendices

A. Measurement of Gel Electrolyte Properties 127
B. Matlab Code for Frame Analysis of Trilayer Actuator Motion 129
C. Experiments on Coated Lycra Strain Gages 135

1. Introduction

Mechanical properties of materials are often thought of as being fixed once the material has been manufactured. Yet in nature, the stiffness and viscosity of muscle can be changed dramatically via neural control, sometimes on millisecond time scales. Natural muscle incorporates the elements of a feedback loop to control not only position and force but also stiffness and viscosity. All the components of the feedback loop are built using high molecular weight materials: the actin-myosin filaments generate force and displacement; muscle spindle fibers measure displacement and velocity; Golgi tendon organs measure the muscle force; neurons perform computation and control the muscle.

Conducting polymers comprise the only class of artificial high molecular weight materials from which all of the same feedback loop components can be manufactured. Conducting polymer actuators, strain gages, and transistors have all been built (Madden, Madden, and Hunter, 2001; Mazzoldi, Della Santa, and De Rossi, 1999; De Rossi, Della Santa and Mazzoldi, 1999; Okuzaki, Ishihara and Ashizawa, 2003). In fact, conducting polymers can perform many other functions that nature has evolved over billions of years. Conducting polymer batteries can store energy, conducting polymer light sensors can act as eyes, or conducting polymer chemical sensors can be artificial noses, to list just a few.

This thesis describes the construction of a feedback loop that uses a conducting polymer actuator and a conducting polymer strain gage. The demonstration of a conducting polymer actuator and strain gage feedback loop is a big step towards an ongoing goal of building a feedback loop entirely out of conducting polymers. Like integrated circuits where transistors, resistors and capacitors are fabricated together out of silicon, the aim is to integrate an actuator, a strain gage, and transistors into a bulk material made from conducting polymers. The new material would implement a feedback loop to dynamically alter the stiffness, viscosity, or other properties of the material or to control position or force. In the work described in this thesis, the transistors used for control are external in a computer.

An all conducting polymer feedback loop could eventually be used as a self-contained system to both actuate and control motion. The system could be used as the actuator and control in robotics, a dynamically adjustable shock absorber via changes in stiffness and viscosity, or eventually as part of a conducting polymer lifelike system with a brain (transistors), ears (vibrations sensors), eyes (photosensors), energy storage (batteries and supercapacitors), and movement control (muscles, position sensors, and force sensors).

Conducting polymer actuators are relatively new materials, having first been described in 1991 (Baughman, Shacklette, and Elsenbaumer, 1991). For this thesis, many of the experiments on the route to building a feedback loop were done to elucidate the behavior of the actuators and to transition the materials from a laboratory phenomenon to a practical engineering tool with behavior that can be predicted, whose limitations are understood, and which can be designed into systems based on performance requirements.

The work described herein uses the conducting polymer polypyrrole (Figure 1.1). However, newer materials are being designed to make stronger faster materials (Madden,

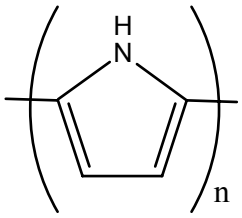

Figure 1.1: Chemical structure of polypyrrole. The chemical formula of the monomer is C_4NH_5

Yu, Anquetil, Swager and Hunter, 2000; Marsella and Reid, 1999). Until now, the search for new materials has focused very much on improving strain to charge ratio. In his Ph.D. thesis, J. Madden developed a model to describe the electrical impedance of a conducting polymer in an electrolyte (Madden, 2000). The model forms the foundation that is used in this thesis to relate specific material properties of the polymer to specific actuator performance metrics (Chapter 2). The relevance of electrolyte properties is discussed as they too affect the actuator function. With a better conception of the effect of other properties (such as the conductivity, the rate of diffusion, and the voltage at which materials degrade), the selection of research directions for material improvement can be refined and the benefits and tradeoffs that result from enhancement of one material property can be grasped from a more comprehensive viewpoint.

Understanding the impact of material properties is very important but there is also a need to model and predict the behavior of actuators. A practical engineering issue that has plagued development of linear polymer muscles is a reduction in strain with longer polymer devices (Della Santa, De Rossi and Mazzoldi, 1997). The reduction in strain is related to ohmic voltage drops along the length of the polymer as it charges. In Chapter 3 of this thesis, the voltage profile along a conducting polymer strip as it is being charged is measured for the first time. A model is developed to show how the local strain varies along polymer strip as a function of geometry and material properties. The model can be used to choose actuator geometries based on required strain and strain rate at specific frequencies.

Many research groups have used bimorphs or trimorphs to get large motion from the few percent strains that are typical of conducting polymers. A model for the displacement of bimorphs (Pei and Inganas, 1992) can be used to predict the displacement as a function of charge. No models have been presented in the literature to predict the displacement of trimorphs or the force from bimorph or trimorph actuators. Such a model is presented here and has been used to guide the fabrication of >100 mN trimorph actuators (which we believe to be the record force for conducting polymer bimorphs or trimorphs). These actuators are already being used in preliminary tests to adjust camber in propeller blades (Madden, J. D., Schmid, B., Lafontaine, S. R., Madden, P. G., Hover, F. S., McLetchi, K. and Hunter, I. W., in press). Chapters 4 through 6 describe the model and the trimorph experiments.

With a better understanding of polymer actuators, they can be incorporated into engineering systems. In mammalian movement, a fundamental system of motion is the reflex loop. Muscle spindles within the muscle signal the length of the muscle and, in the spinal cord, neurons signal back to the muscle to maintain position. In Chapter 7 of this thesis, a feedback loop is constructed which uses conducting polymer strain gages and a conducting polymer actuator to successfully reject position disturbances. Construction of

a feedback loop is a big step towards all polymer flexible robotics that can mimic or improve upon nature's capabilities.

In the rest of this introduction, short overviews are given of conducting polymer materials (Section 1.1) and of other muscle like actuators (Section 1.2) and Section 1.3 gives short descriptions of the contents of each chapter.

1.1. Conducting Polymer Materials

Conducting organic materials offer an incredible range of diversity in function and properties. Like silicon, conducting polymers are semiconductors with a bandgap that can be changed by adjusting the doping level. Unlike silicon, the doping level can be changed quite easily and reversibly by introduction of ions into the material. Here is a partial list of devices that can be fabricated using conducting polymers:

- actuators (Baughman and others, 1991; Mazzoldi and others, 1999; Otero and Sansinena, 1998; Hutchison, Lewis, Moulton, Spinks and Wallace, 2000),
- transistors (Epstein, Hsu, Chiou and Prigodin, 2002),
- strain gages (De Rossi, Della Santa, and Mazzoldi, 1999; Spinks, Wallace, Liu and Zhou, 2003),
- chemical sensors (Swager, 2002; Swager and Wosnick, 2002; Shepherd, Barisci, Collier, Hart, Partridge and Wallace, 2002; Guadarrama, Fernandez, Inguez, Souto and De Saja, 2001),
- batteries and supercapacitors (Levi, Gofer and Aurbach, 2002; Talbi, Just and Dao, 2003),
- and photodiodes (Luzzati, Panigoni and Catellani, 2001; Miquelino, Depaoli and Genies, 1994).

Good overviews of conducting polymer synthesis and properties can be found in any of several handbooks that have been published (for example (Skotheim, Terje A., Elsenbaumer, Ronald L., and Reynolds, John R., 98) or (Osada, Y. and De Rossi, D. E., 2000)).

The wide range of electrical and optical properties of organic materials is coupled with mechanical properties that are very different from traditional metal and semiconducting materials. Polymeric and oligomeric organic materials are typically much more flexible than semiconductor crystals or metal, opening up a range of new applications such a flexible integrated circuits and displays.

While discrete devices made from polymer and oligomeric materials do not generally perform as well as their inorganic counterparts, the strength of organic materials is in their range of properties, the compatibility of manufacturing methods needed to achieve those properties, and, particularly for polymers and oligomers, the ease of processability of the materials. These strengths have made it possible to create integrated systems such as mechanically flexible organic transistor driven organic LEDs (Sirringhaus, Kawase, Friend, Shimoda, Inbasekaran, Wu and Woo, 2000).

Such integrated circuits offer tremendous advantages for ease of manufacturing and therefore cost per unit. When silicon integrated circuits were first introduced in the late 1950s[1], the individual transistors, resistors, and capacitors on the integrated circuits did not perform as well as discrete devices and many engineers thought that they would

[1] The integrated circuit was invented by Jack Kilby at Texas Instruments in September, 1958.

not be successful. The key advantage of these circuits has proven to be the complexity of the circuitry that can be manufactured at very low unit cost.

Little attention has been paid so far to opportunities available for integration of organic actuators with other devices. One integrated electro-mechanical application has been to use polypyrrole actuators as variable thickness interference devices to control reflection from a gold surface (Smela, 1999). Small scale manipulators have also been built by combining silicon lithography techniques with conducting polymer actuators (Smela, Kallenbach and Holdenried, 1999). The polypyrrole actuators were grown electrochemically in place onto gold electrode patterns formed on a silicon wafer.

The work described in this thesis is the first report of research whose goal is to create an all polymer feedback system that integrates an actuator, a strain gage, and transistors.

Actuators

Conducting polymer actuators have demonstrated high stresses (up to tens of MPa) and reasonable strains (typically 1 to 2% and as much as 15 to 20%) (Madden and others, 2001; Spinks, Wallace, Liu, and Zhou, 2003; Anquetil, Patrick A., Yu, Hsiao-hua, Madden, John D., Madden, Peter G., Swager, T. M. and Hunter, Ian W., 2002). In the past, limited strain rates as low as 0.03%/s have prevented the development of conducting polymers as effective actuators. However, using thin actuators and high activation potentials, J. Madden et al. observed strain rates above 3%/s (Madden, Cush, Kanigan and Hunter, 2000). At the higher strain rates, a peak power to mass ratio of 150 W/kg was observed, matching the power to mass ratio of mammalian muscle (Hunter, I. W. and Lafontaine, S., 92).

Polymer actuators offer unique possibilities for the design of systems. The relatively high stress, strain, and mechanical flexibility give them a combination of properties lacking in traditional actuators (e.g. electromagnetic, piezo-electric).

Expansion or contraction is the result of an ion movement into and out of the polymer. The actuators are immersed in an electrochemical solution, gel, or solid electrolyte. As the polymer potential is changed, ions enter or leave and the volume of the polymer changes. The change in volume is generally found to be linearly proportional to the injected charge density:

$$\varepsilon = \alpha \frac{Q}{V},$$

where ε is the strain, Q is the injected charge, α is the strain to charge density ratio, and V is the polymer volume (Mazzoldi and others, 1999; Madden and others, 2001; Madden, 2000). Typical values of α for polypyrrole are on the order of 10^{-10} m^3/C. This corresponds to $\sim 10^{-28}$ m^3 per singly charged ion that enters the polymer. The value of α is a function of the synthesis conditions, the ions, and the electrolyte material.

The strain rate depends on how quickly ions can be moved in and out of the polymer. The strain rate is primarily diffusion limited and so shrinking the size of the polymer actuator should provide a great increase in speed. As long as the polymer synthesis techniques and actuator assembly do not present an obstacle to miniaturization, a polymer actuator system could be shrunk to near the molecular scale (probably on the order of tens of nanometers).

Strain Gages

Conducting polymers can be used as strain gages. In a strain gage, the resistance changes as the gage is stretched. The resistance change is given by:

$$\frac{\Delta R}{R_s} = G\varepsilon ,$$

where R_s is the unstrained resistance of the gage and ε is the strain. The factor G is known as the gage factor of the sensor. A higher gage factor improves the sensitivity of the strain gauge.

While pure polypyrrole has been used to make strain gages (Madden, 2000), thus far, the best strain gages made with conducting polymers have been made by coating a flexible fabric with a layer of polypyrrole (De Rossi, Della Santa, and Mazzoldi, 1999; Spinks, Wallace, Liu, and Zhou, 2003; Spinks, G. G. Wallace and et al. 2002). The reported gage factors are around 13 although, as will be seen in this thesis, there can be large variations and gage factors as high as 60 are measured in Chapter 7.

Organic Transistors

Polymer, oligomer, and small molecule organic semiconductors can be used to create transistors. The underlying equations for organic transistors are almost the same as the equations used to describe inorganic (e.g. Si) based transistors. Organic transistors are much slower than Si based devices but the processes used to lay down the organic semiconductor material and the processes used to build organic transistors can be much cheaper and simpler, making them ideal for low-complexity low-cost applications.

Research on organic transistors began relatively recently (Tsumura, Koezuka, Tsunoda and Ando, 1986; Tsumura, Koezuka and Ando, 1986; Jones, Chyan and Wrighton, 1987). Organic materials, especially conducting polymers, can be spin coated to create thin uniform layers of semiconductor. Field effect transistor designs, such as the MISFET (Metal-Insulator-Semiconductor Field Effect Transistor[2]) use such thin films of semiconductor doped either p or n as the active regions and so are particularly suitable for thin film organic semiconductors (Horowitz, 1998).

Mobilities typical for semiconducting polymers are between 10^{-7} $m^2/V/s$ to 10^{-6} $m^2/V/s$ (0.001 to 0.01 $cm^2/V/s$) (Horowitz, 1998). For small oligomers and organic molecules higher mobilities should be attainable. These mobilities are approaching those of amorphous silicon ($\mu \approx 10^{-4}$ $m^2/V/s$ = 1 $cm^2/V/s$) but are still much lower than for crystalline silicon (μ = 0.005 to 0.1 $m^2/V/s$ or 50 to 1000 $cm^2/V/s$). Maximum currents in the transistors built to date range from microamps to a few milliamps (Horowitz, 1998; Epstein, Hsu, Chiou, and Prigodin, 2002; Nilsson, Kugler, Svensson and Berggren, 2002; Halik, Klauk, Zschieschang, Kriem, Schmid, Radlik and Wussow, 2002).

Many of the organic based devices that are being developed are being built on flexible plastic substrates. Some groups are using patterned metal (gold or platinum) to form electrical contacts while other groups have developed techniques for creating all organic integrated devices, using highly conducting polymers to form the circuit interconnects (Drury, Mutsaers, Hart, Matters and De Leeuw, 1998; Okuzaki, Ishihara,

[2] Also called an IGFET (Insulated Gate FET) or a MOSFET (Metal Oxide Semiconductor FET) if the insulator is an oxide layer, which is usually the case for Si based devices where the oxide layer ($Si0_2$) is grown by exposing the Si to oxygen.

and Ashizawa, 2003; Lodha and Singh, 2001; Sirringhaus, Kawase, Friend, Shimoda, Inbasekaran, Wu, and Woo, 2000).

Electrochemical polymer transistors have also been built (Lofton, Thackeray and Wrighton, 1986). The active polymer is immersed in an electrochemical salt solution and a counter electrode (or gate) changes the solution potential to drive positive or negative ions into or out of the polymer. The conductivity between the transistor source and drain, which is a function of the ion doping level, changes as the ions enter or leave. The switching speed of the transistors is limited by the diffusion of ions into and out of the polymer. Wrighton achieved switching speeds of up to 10 kHz with a polyaniline based electrochemical transistor by shrinking the active dimension of the polymer transistor to about 50 nm (Jones, Chyan, and Wrighton, 1987).

1.2. Muscle Like Actuator Technologies

Conducting polymers are used in this thesis because of their range of properties and the range of devices that can be fabricated with them, but there are several polymeric technologies that compete as actuators with conducting polymers. Because a large part of this thesis is devoted to improvements in conducting polymer actuators, a short overview is given here of other promising actuator materials. A more comprehensive review is given by Madden et al. (Madden, John D., Takshi, A., Madden, P. G., Anquetil, P. A., Vandesteeg, N., Zimet, R., Lafontaine, S. R. L., Wieringa, P. A. and Hunter, I. W., to be published). An earlier comparison of artificial actuator technologies with muscle is given by Hunter and Lafontaine (Hunter, I. W. and Lafontaine, S., 92).

Dielectric elastomer films expand or contract when a voltage is applied to electrodes on each surface (Pelrine, Kornbluh, Pei and Joseph, 2000). Electrostatic attraction pulls the electrodes together and, because the elastomer volume is constant, the film gets longer and wider. Peak strains of more than 100%, stresses of 2.4 MPa, and response over 1 kHz make dielectric elastomers very capable materials. The primary disadvantage of the materials as an actuator is the high voltage (~1-10 kV) that must be applied, which requires a special power supply.

Liquid crystal elastomers change dimension when liquid crystal groups attached to a polymer matrix undergo a phase transition (Selinger, Jeon and Ratna, 2002; Ahn, Roberts, Davis and Mitchell, 1997; Brand, 1989; Kremer, Lehmann, Skupin, Hartmann, Stein and Finkelmann, 1998). The most successful of the liquid crystal actuators undergo thermal phase transitions and exhibit strains up to 40% at stresses of 140 kPa. Reponse times are limited by the thermal heat transfer and can be on the order of minutes (Thomsen, Keller, Naciri, Pink, Jeon, Shenoy and Ratna, 2001). However, using a high power laser to directly heat a sample, the response time has been reduced to 1 s (Thomsen, Keller, Naciri, Pink, Jeon, Shenoy, and Ratna, 2001).

Ionic metal composites (IPMC) are made by sandwiching a thin layer of polymeric electrolyte between two very thin metal electrodes (Shahinpoor, 1996; Shahinpoor, Bar-Cohen, Simpson and Smith, 1998). When a potential is applied, the change in concentration of the ions and entrained water molecules cause a swelling of the electrolyte. Because of the way the ions are shuttled back and forth across the electrolyte, the IPMCs operate only in bending and it is therefore difficult to compare with numbers for stress and strain with other actuator technologies. Strips that are 20 mm long by 5mm wide by 200 μm thick can generate on the order of 15 mN force in bending

with a response time to an applied voltage of about 0.25 to 0.5 s (Shahinpoor and Kim, 2001).

Finally, there is a class of ferroelectric polymers which undergo active strains of up to 5% at stresses as high at 45 MPa (Xia, Cheng, Xu, Li, Zhang, Kavarnos, Ting, Abdul-Sedat and Belfield, 2002; Zhang, Bharti and Zhao, 1998; Zhang, Li, Poh, Xia, Cheng, Xu and Huang, 2002). The polymers are activated by electric fields and have typical operating voltages ~1 kV. In some newer materials the operating voltage can be 10× lower. The frequency response in the ferroelectric polymers can be as high as 100 kHz.

Each of these materials have their own disadvantages as actuators. The traditional conducting polymers such as polypyrrole have low efficiencies and driven by high currents (Madden and others, 2001). The dielectric elastomer and the ferroelectric polymers both require high voltages to be stimulated. Liquid crystal elastomers are thermally operated and are generally slow[3], while the IPMC materials operate at low voltage but can deflect only in a bending mode.

While some of the competing actuator technologies are very promising, none of the other actuator materials has the incredible range of electrical, optical and mechanical properties of conducting polymers. For the fabrication of an integrated all organic feedback loop conducting polymer actuators is the only choice of material.

1.3. Chapter Descriptions

Chapter 2: This chapter first reviews the diffusive elastic model developed by J. Madden that gives an expression for the electrical impedance of conducting polymer and relates the charge density to the polymer stress and strain (Madden, 2000). Using the model as basis, the limits on the performance of conducting polymers as an actuator are related to the material properties.

Chapter 3: When a potential is applied to one end long thin strip of conducting polymer in electrolyte, the voltage has to propagate along the length of the strip. The voltage in strips of polymer is measured for the first time as a function of position and time. A model is developed to describe the voltage, current, and charge density in the polymer. The model can be used to design conducting polymer actuators to meet performance requirements.

Chapter 4: A model is derived that relates the deflection and force of a trimorph (three layer) conducting polymer actuator to the charge density.

Chapter 5: Experiments on trimorph actuators in liquid electrolyte are described and results are compared to the model derived in Chapter 4. Experiments also show that forces of individual trimorphs can be added together by creating trimorph stacks.

Chapter 6: Using liquid salt based gels instead of liquid electrolyte, trimorph actuators that operate in air can be built. Such actuators are described in Chapter 6 and, using video measurements, the displacement of the air operated trimorphs is shown to very closely match the trimorph model derived in Chapter 4.

[3] The liquid crystal elastomers can be fast if a laser source is used but this adds to the cost and the required infrastructure for operation.

Chapter 7: A position feedback loop is created using a conducting polymer actuator and a conducting polymer strain gage. A model of the control loop described the operation well for the rejection of slow disturbance ramps. Step disturbances are not as well rejected because of poor high frequency strain gage response. The operation of the feedback loop is the first ever with a conducting polymer actuator and strain gage.

Chapter 8: The last chapter of the thesis gives a summary of the important contributions to the field and some directions for continued research.

Reference List

1. Ahn, K.H., Roberts, P.M.S., Davis, F.J. and Mitchell, G. Electric Field Induced Macroscopic Shape Changes in Liquid Crystal Elastomers. Abstracts of Papers of the American Chemical Society. 1997 Sep 7; 214:218-POLY.

2. Anquetil, P.A., Yu, H., Madden, J.D., Madden, P.G., Swager, T.M., and Hunter, I.W. Thiophene-based conducting polymer molecular actuators. Bar-Cohen, Y., ed. Smart Structures and Materials 2002: Electroactive Polymer Actuators and Devices, Proceedings of SPIE Vol. 4695.

3. Baughman, R.H., Shacklette, R.L., and Elsenbaumer, R.L. Micro electromechanical actuators based on conducting polymers. Lazarev, P.I., Editor. *Topics in Molecular Organization and Engineering, Vol.7: Molecular Electronics*. Dordrecht: Kluwer; 1991; p. 267.

4. Brand, H.R. Electromechanical Effects in Cholesteric and Chiral Smectic Liquid-Crystalline Elastomers. Makromolekulare Chemie-Rapid Communications. 1989 Sep; 10(9):441-445.

5. De Rossi, D., Della Santa, A. and Mazzoldi, A. Dressware: Wearable hardware. Materials Science and Engineering C . 1999; 7(1):31-35.

6. Della Santa, A., De Rossi, D. and Mazzoldi, A. Performance and work capacity of polypyrrole conducting polymer linear actuator. Synthetic Metals. 1997; 90:93-100.

7. Drury, C.J., Mutsaers, C.M.J., Hart, C.M., Matters, M. and De Leeuw, D.M. Low-Cost All-Polymer Integrated Circuits. Applied Physics Letters. 1998 Jul 6; 73(1):108-110.

8. Epstein, A.J., Hsu, F.C., Chiou, N.R. and Prigodin, V.N. Electric-Field Induced Ion-Leveraged Metal-Insulator Transition in Conducting Polymer-Based Field Effect Devices. Current Applied Physics . 2002 Aug; 2(4):339-343.

9. Guadarrama, A., Fernandez, J.A., Inguez, M., Souto, J. and De Saja, J.A. Discrimination of Wine Aroma Using an Array of Conducting Polymer Sensors in Conjunction With Solid-Phase Micro- Extraction (Spme) Technique. Sensors and Actuators B-Chemical. 2001 Jun 15; 77(1-2):401-408.

10. Halik, M., Klauk, H., Zschieschang, U., Kriem, T., Schmid, G., Radlik, W. and Wussow, K. Fully Patterned All-Organic Thin Film Transistors. Applied Physics Letters. 2002 Jul 8; 81(2):289-291.

11. Horowitz, G. Organic Field-Effect Transistors. Advanced Materials. 1998 Mar 23; 10(5):365-377.

12. Hunter, I.W. and Lafontaine, S. A comparison of muscle with artificial actuators. *Technical Digest IEEE Solid State Sensors and Actuators Workshop*: IEEE. 178-185.

13. Hutchison, A.S., Lewis, T.W., Moulton, S.E., Spinks, G.M. and Wallace, G.G. Development of polypyrrole-based electromechanical actuators. Synthetic Metals. 2000; 113:121-127.

14. Jones, E.T.T., Chyan, O.M. and Wrighton, M.S. Preparation and Characterization of Molecule-Based Transistors With a 50-Nm Source-Drain Separation With Use of Shadow Deposition Techniques - Toward Faster, More Sensitive Molecule- Based Devices. Journal of the American Chemical Society. 1987 Sep 2; 109(18):5526-5528.

15. Kremer, F., Lehmann, W., Skupin, H., Hartmann, L., Stein, P. and Finkelmann, H. Piezoelectricity in Ferroelectric Liquid Crystalline Elastomers. Polymers for Advanced Technologies. 1998 Oct-1998 Nov 30; 9(10-11):672-676.

16. Levi, M.D., Gofer, Y. and Aurbach, D. A Synopsis of Recent Attempts Toward Construction of Rechargeable Batteries Utilizing Conducting Polymer Cathodes and Anodes. Polymers for Advanced Technologies. 2002 Oct-2002 Dec 31; 13(10-12):697-713.

17. Lodha, A. and Singh, R. Prospects of manufacturing organic semiconductor-based integrated circuits. IEEE Transactions on Semiconductor Manufacturing. 2001 Aug; 14(3):281-296.

18. Lofton, E.P., Thackeray, J.W. and Wrighton, M.S. Amplification of Electrical Signals With Molecule-Based Transistors - Power Amplification up to a Kilohertz Frequency and Factors Limiting Higher Frequency Operation. Journal of Physical Chemistry. 1986 Nov 6; 90(23):6080-6083.

19. Luzzati, S., Panigoni, M. and Catellani, M. Spectroscopical Evidences of Photoinduced Charge Transfer in Blends of C-60 and Thiophene-Based Copolymers With a Tunable Energy Gap. Synthetic Metals . 2001 Jan 15; 116(1-3):171-174.

20. Madden, J.D. , Schmid, B., Lafontaine, S.R., Madden, P.G., Hover, F.S., McLetchi, K., and Hunter, I.W. Conducting Polymer Driven Actively Shaped Propellers and Screws. SPIE 10th Annual Symposium on Electroactive Materials and Structure. San Diego, California.

21. Madden, John D. Conducting Polymer Actuators, Ph.D. Thesis. Cambridge, MA: Massachusetts Institute of Technology; 2000.

22. Madden, J.D., Cush, R.A., Kanigan, T.S. and Hunter, I.W. Fast contracting polypyrrole actuators. Synthetic Metals. 2000 May; 113:185-193.

23. Madden, J.D., Madden, P.G., and Hunter, I.W. Characterization of polypyrrole actuators: modeling and performance. Yoseph Bar-Cohen, Editor. Proceedings of SPIE 8th Annual Symposium on Smart Structures and Materials: Electroactive Polymer Actuators and Devices. Bellingham WA: SPIE; 2001; pp. 72-83.

24. Madden, J.D. , Takshi, A., Madden, P.G., Anquetil, P.A., Vandesteeg, N., Zimet, R., Lafontaine, S.R.L., Wieringa, P.A., and Hunter, I.W. Artificial Muscle Technology: Physical Principles and Naval Prospects. UUST Conference Proceedings; Durham, NH.

25. Madden, J.D., Yu, H.-H., Anquetil, P.A., Swager, T.M. and Hunter, I.W. Large strain molecular actuators. EAP Newsletter. 2000; 2(2):9-10.

26. Marsella, M.J. and Reid, R.J. Toward molecular muscles: design and synthesis of an electrically conducting poly[cyclooctatetrathiophene]. Macromolecules. 1999; 32:5982-5984.

27. Mazzoldi, A., Della Santa, A., and De Rossi, D. Conducting polymer actuators: Properties and modeling. Osada, Y. and De Rossi, D.E., editors. Polymer Sensors and Actuators. Heidelberg: Springer Verlag; 1999.

28. Miquelino, F.L.C., Depaoli, M.A. and Genies, E.M. Photoelectrochemical Response in Conducting Polymer-Films. Synthetic Metals. 1994 Dec; 68(1):91-96.

29. Nilsson, D., Kugler, T., Svensson, P.O. and Berggren, M. An all-organic sensor-transistor based on a novel electrochemical transducer concept printed electrochemical sensors on paper. Sensors and Actuators B-Chemical. 2002 Sep 20; 86(2-3):193-197.

30. Okuzaki, H., Ishihara, M. and Ashizawa, S. Characteristics of conducting polymer transistors prepared by line patterning. Synthetic Metals. 2003 Apr 4; 137(1-3):947-948.

31. Osada, Y. and De Rossi, D.E. Polymer Sensors and Actuators. Berlin: Springer; 2000.

32. Otero, T.F. and Sansinena, J.M. Soft and Wet Conducting Polymers for Artificial Muscles. Advanced Materials. 1998 Apr 16; 10(6):491-+.

33. Pei, Q. and Inganas, O. Electrochemical Application of the bending beam method. 1. Mass transport and volume changes in polypyrrole during redox. Journal of Physical Chemistry. 1992; 96(25):10507-10514.

34. Pelrine, R., Kornbluh, R., Pei, Q. and Joseph, J. High-speed electrically actuated elastomers with strain greater than 100%. Science. 2000 Feb 4; 287:836-839 .

35. Selinger, J.V., Jeon, H.G. and Ratna, B.R. Isotropic-Nematic Transition in Liquid-Crystalline Elastomers. Physical Review Letters. 2002 Nov 25; 89(22):art. no.-225701.

36. Shahinpoor, M. Ionic Polymeric Gels as Artificial Muscles for Robotic and Medical Applications. Iranian Journal of Science and Technology. 1996; 20(1):89-136.

37. Shahinpoor, M., Bar-Cohen, Y., Simpson, J.O. and Smith, J. Ionic Polymer-Metal Composites (Ipmcs) as Biomimetic Sensors, Actuators and Artificial Muscles - a Review. Smart Materials & Structures. 1998 Dec; 7(6):R15-R30.

38. Shahinpoor, M. and Kim, K.J. Ionic Polymer-Metal Composites: I. Fundamentals. Smart Materials & Structures. 2001 Aug; 10(4):819-833.

39. Shepherd, R.L., Barisci, J.N., Collier, W.A., Hart, A.L., Partridge, A.C. and Wallace, G.G. Development of Conducting Polymer Coated Screen-Printed Sensors for Measurement of Volatile Compounds. Electroanalysis. 2002 May; 14(9):575-582.

40. Sirringhaus, H., Kawase, T., Friend, R.H., Shimoda, T., Inbasekaran, M., Wu, W. and Woo, E.P. High-Resolution Inkjet Printing of All-Polymer Transistor Circuits. Science. 2000 Dec 15; 290(5499):2123-2126.

41. Skotheim, T.A., Elsenbaumer, R.L., and Reynolds, J.R. Handbook of Conducting Polymers. Editors ed. New York: Marcel Dekker; 1998.

42. Smela, E., Kallenbach, M. and Holdenried, J. Electrochemically Driven Polypyrrole Bilayers for Moving and Positioning Bulk Micromachined Silicon Plates. Journal of Microelectromechanical Systems. 1999 Dec 1; 8(4):373.

43. Smela, E. A microfabricated moveable electrochromic "pixel" based on polypyrrole. Advanced Materials. 1999; 11(16):1343-1345.

44. Spinks, G.M. , G. G. Wallace and et al. Conducting polymers and carbon nanotubes as electromechanical actuators and strain sensors. Materials Research Society Symposium Proceedings 698 (Electroactive Polymers and Rapid Prototyping). 2002; 5-16.

45. Spinks, G.M., Wallace, G.G., Liu, L. and Zhou, D. Conducting Polymers Electromechanical Actuators and Strain Sensors. Macromolecular Symposia. 2003 Mar; 192:161-169.

46. Swager, T.M. Ultrasensitive Sensors From Self-Amplifying Electronic Polymers. Chemical Research in Toxicology. 2002 Dec; 15(12):125.

47. Swager, T.M. and Wosnick, J.H. Self-Amplifying Semiconducting Polymers for Chemical Sensors. Mrs Bulletin. 2002 Jun; 27(6):446-450.

48. Talbi, H., Just, P.E. and Dao, L.H. Electropolymerization of Aniline on Carbonized Polyacrylonitrile Aerogel Electrodes: Applications for Supercapacitors. Journal of Applied Electrochemistry . 2003 Jun; 33(6):465-473.

49. Thomsen, D.L., Keller, P., Naciri, J., Pink, R., Jeon, H., Shenoy, D. and Ratna, B.R. Liquid Crystal Elastomers With Mechanical Properties of a Muscle. Macromolecules. 2001 Aug 14; 34(17):5868-5875.

50. Tsumura, A., Koezuka, H. and Ando, T. Macromolecular Electronic Device - Field-Effect Transistor With a Polythiophene Thin-Film. Applied Physics Letters. 1986 Nov 3; 49(18):1210-1212.

51. Tsumura, A., Koezuka, H., Tsunoda, S. and Ando, T. Chemically Prepared Poly(N-Methylpyrrole) Thin-Film - Its Application to the Field-Effect Transistor. Chemistry Letters. 1986 Jun; (6):863-866.

52. Xia, F., Cheng, Z.Y., Xu, H.S., Li, H.F., Zhang, Q.M., Kavarnos, G.J., Ting, R.Y., Abdul-Sedat, G. and Belfield, K.D. High Electromechanical Responses in a Poly(Vinylidene Fluoride- Trifluoroethylene-Chlorofluoroethylene) Terpolymer. Advanced Materials. 2002 Nov 4; 14(21):1574-+.

53. Zhang, Q.M., Bharti, V. and Zhao, X. Giant Electrostriction and Relaxor Ferroelectric Behavior in Electron-Irradiated Poly(vinylidene fluoride-trifluoroethylene) Copolymer. Science. 1998; 280(26):2101-2104.

54. Zhang, Q.M., Li, H.F., Poh, M., Xia, F., Cheng, Z.Y., Xu, H.S. and Huang, C. An All-Organic Composite Actuator Material With a High Dielectric Constant. Nature. 2002 Sep 19; 419(6904):284-287.

2. Understanding of the diffusive elastic model

The diffusive elastic model of conducting polymer expansion and contraction was developed by John Madden as part of his Ph. D. thesis (Madden, 2000). In Part 1 of this chapter a qualitative description of the model as developed by J. Madden is given and the model equations are presented[1]. Once the model has been described, in Part 2 I will use the model to show which material properties limit the response of conducting polymers.

While the importance of specific material properties such as strain/charge ratio or the ionic diffusion coefficient have already been well understood (Madden, 2000; Mazzoldi, Della Santa, and De Rossi, 1999), this chapter will relate a wider range of material properties to the dynamic performance of conducting polymer actuators. The effect properties such as the stable electrochemical range of the material, the electrolyte and polymer conductivities, the double layer capacitance, and the ability of one or both ions to move within the polymer and electrolyte will be described.

Each material property affects the actuator properties such as peak strain, peak stress, or strain rate. The relations presented between material and actuator properties should help focus new material development.

2.1. The Diffusive Elastic Model (DEM)

The diffusive elastic model (DEM) describes the electrical and mechanical behavior of a thin film of conducting polymer placed in an electrolyte solution (Figure 2.1). A counter electrode (which can also be conducting polymer) is also placed in solution so that the electrochemical potential of the polymer film can be controlled. The model accurately predicts the electrical behavior of the conducting polymer polypyrrole in a liquid electrolyte at frequencies from 10^{-3} Hz up to 10^{5} Hz.

The solution itself is made up of a solvent (often water or propylene carbonate) with a dissolved salt such as tetraethylammonium hexafluorophosphate (TEAP). TEAP is made up of a large cation (tetraethylammonium) and a much smaller and more mobile anion (hexafluorophosphate). The relative size of the salt ions is important: when the polymer potential is changed, very large ions are effectively blocked from entering the polymer because they are unable to diffuse between the polymer chains but the smaller ions are able to enter or leave the polymer.

To expand or contract the polymer, a voltage is applied to the polymer film between the polymer and the counter electrode. As soon as the voltage is applied, ions at the polymer surface will begin charging the electrochemical double layer capacitance at the film surface (Figure 2.1B). In the diffusive elastic model, where the capacitance of the double layer is assumed to be independent of voltage, the charge is directly proportional to the double layer voltage.

[1] For a more detailed derivation, refer to (Madden, 2000).

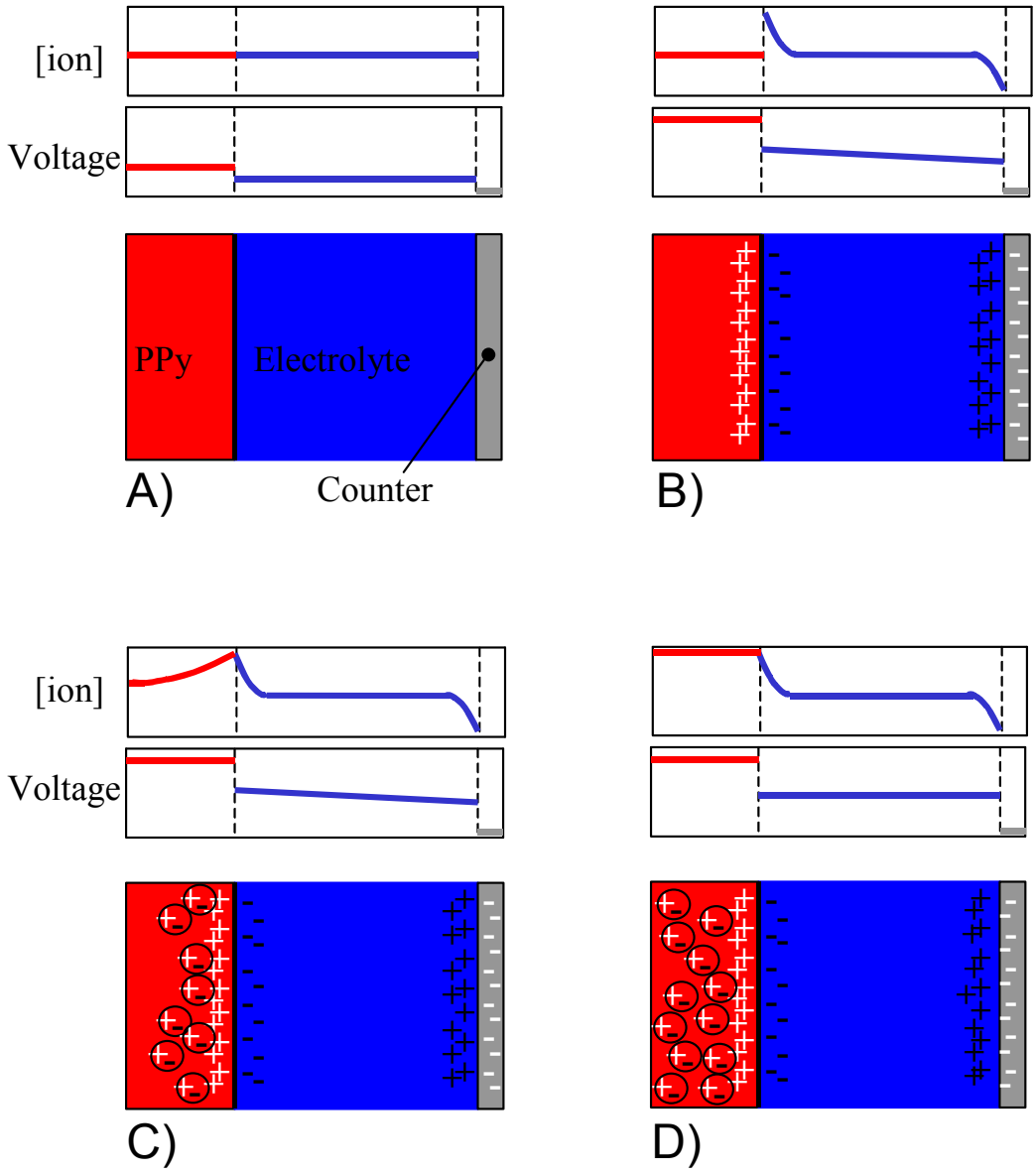

Figure 2.1 Charging of the conducting polymer. The upper two plots of each subfigure show the ion concentration and the voltage in the polymer (polypyrrole, red), in the electrolyte (blue), and in the counter electrode (gray). A) The polymer at rest. There is a voltage difference at the interface between the polymer and the electrolyte and at the interface between the electrolyte and the counter electrode. B) When a potential is applied, a current begins to flow through the electrolyte and ionic charge builds up in the double layers. C) The concentration of ions at the polymer surface drives the diffusion of ions into the polymer. Inside the polymer the ions are paired with holes or electrons to form neutral species. D) The polymer is fully charged when the concentration of ions in the polymer is equal to the concentration of ions in the double layer at the polymer electrolyte interface. The figure depicts charging for single ion (anion) movement into and out of the polymer.

As the double layer on the solution side of the polymer/solution interface charges or discharges the ion concentration at the surface changes. If the polymer voltage is negative, positive ions are attracted to the polymer and negative ions are driven away. If

the polymer is positive, negative ions are attracted and the positive ions are driven away. The resulting changes in concentration will in turn drive diffusion of ions into or out of the polymer film to cause expansion and contraction.

Typical values for the double layer capacitance are available in the literature and are generally around 0.1 to 0.4 F/m^2 (Bard, Allen J. and Faulkner, Larry R., 80). The amount of charge (and the number of moles of ions) can be estimated by using $\Delta Q = C_{dl}\Delta V$ ($N = C_{dl}\Delta V / N_A e$), where ΔQ is the change in double layer charge, C_{dl} is the double layer capacitance, and ΔV is the change in the voltage applied to the polymer film (e and N_A are the charge on the electron and Avagadro's number).

To calculate the ion concentration, the volume occupied by the ions must be known. While the concentration does vary with the distance from the electrode, an effective or average double layer thickness can be used. In the model, the double layer thickness is related to the double layer capacitance by the dielectric constant following the parallel plate or Helmholtz model: $\delta = \varepsilon A / C_{dl}$ (where δ is the double layer thickness, ε is the solvent dielectric constant, and A is the surface area). Once the double layer thickness is known or estimated, the concentration at the surface can be calculated[2].

The concentration of ions at the surface of the polymer drives ionic diffusion into or out of the polymer (Figure 2.1C). Diffusion continues until a uniform concentration is reached inside the polymer and equilibrium is reached between the ion concentration in the polymer and in the double layer (Figure 2.1D). The diffusion rates in the solid polymer are much slower than in the liquid electrolyte and so diffusion in the liquid is assumed to be instantaneous.

It should be noted that in the diffusive elastic model, movement of ions is not driven by the electric field within the polymer. Because the conductivity of the polymer is assumed to be very high, electronic charge moves quickly to shield the charges on the ions[3]. Even in the presence of an electric field within the material, migration will not occur because the ionic charge is effectively neutralized by much more mobile charge carriers in the polymer.

When the ions enter or leave the polymer, the polymer expands or contracts. If both positive and negative ions diffuse into and out of the polymer, expansion due to influx of one ion will be counteracted by contraction due to outflow of the ion with opposite charge (Pei and Inganas, 1992b; Pei and Inganas, 1992a). By choosing salts with one small and one very large ion, the influx and outflow are dominated by the smaller ion. In the salt tetraethyl ammonium hexafluorophosphate (TEAP), the negative ions (the hexafluorophosphate) are smaller and can squeeze between the polymer chains while the cations are too big to diffuse into the polymer bulk. With TEAP in propylene carbonate, the expansion and contraction of the polymer appear to be due only to the movement of the negative hexafluorophosphate ions (Madden, 2000; Lewis, Spinks, Wallace, Mazzoldi and De Rossi, 2001; Pei and Inganas, 1993).

[2] In the diffusive elastic model, the double layer thickness can also be calculated from the bulk capacitance of the polymer ((Madden, 2000), Section 10.4.1.4).

[3] If the conductivity of the polymer is not high, then electronic charge may not compensate the ionic charge. The effect of migration, which will increase the charging rate, must then be taken into account to properly model the polymer behavior.

Equations of the Diffusive Elastic Model

In the diffusive elastic model, the admittance of a polymer strip in an electrolyte solution is given by

$$Y(s) = \frac{s}{R} \cdot \frac{\frac{1}{\sqrt{\tau_{DDL}}} \cdot \tanh\left(\sqrt{s \cdot \tau_D}\right) + \sqrt{s}}{\frac{\sqrt{s}}{\tau_{RC}} + s^{3/2} + \frac{s}{\sqrt{\tau_{DDL}}} \cdot \tanh\left(\sqrt{s \cdot \tau_D}\right)}, \tag{1}$$

where

$$\tau_D = \frac{h^2}{4 \cdot D}, \tag{2}$$

$$\tau_{RC} = R \cdot C_{dl}, \tag{3}$$

$$\tau_{DDL} = \frac{\delta^2}{D}, \tag{4}$$

and *Y(s)* is the admittance as a function of the Laplace variable *s*, *h* is the thickness of the polymer strip, *D* is the diffusion coefficient of the ion within the polymer, *R* is the series resistance (which includes any wiring or contact resistance and the resistance of the electrolyte), C_{dl} is the double layer capacitance, and δ is the thickness of the double layer[4]. A full derivation of the admittance is given by J.Madden (Madden, 2000).

The admittance (or its inverse the impedance) relates the current through the polymer to the voltage ($I(s) = Y(s)\ V(s)$). A second equation relates the charge injected into the polymer to the expansion:

$$\varepsilon(s) = \alpha \frac{q(s)}{LWh} + \frac{\sigma(s)}{E(s)}, \tag{5}$$

where ε is the strain, α is the strain/charge ratio, *q* is the charge injected into the polymer bulk, *L*, *W*, and *h* are the length, width, and thickness of the polymer strip, σ is the stress applied to the strip, and *E* is the Young's modulus of the polymer. We can substitute $q(s) = I(s)/s$ to find:

$$\begin{aligned} \varepsilon(s) &= \alpha \frac{I(s)}{s \cdot LWh} + \frac{\sigma(s)}{E(s)} \\ &= \alpha \frac{Y(s) \cdot V(s)}{s \cdot LWh} + \frac{\sigma(s)}{E(s)} \end{aligned} \tag{6}$$

to relate stress and strain to the voltage or current applied to the conducting polymer film[5].

Each of the time constants in the admittance equation has a specific physical interpretation. The first, τ_D, is the time constant for the diffusion of ions into the

[4] The admittance is given for a film with both sides exposed to solution.

[5] In fact, the use of $q(s) = I(s)/s$ is an approximation. The charge that causes expansion is the charge that diffuses into the polymer bulk. The current $I(s)$ includes both the current due to charge that diffuses into the polymer and the current due to charging the double layer capacitance. In practice for polypyrrole, except at very short time scales (~1 μs) or extremely thin films (<200 nm) the charge stored in the double layer capacitance is negligible compared to the charge that has diffused into the polymer bulk (see the next section for more details).

polymer. At times longer than τ_D after a change in applied potential, the concentration of ions is essentially uniform through the thickness of the film. For times less than τ_D, the concentration of ions must be found by solving Fick's law of diffusion (Madden, 2000; Atkins, P. W., 90).

The second time constant τ_{RC} is related to the charging time of the double layer. If either the double layer capacitance or the series resistance (the electrolyte and contact resistance) increase, the time taken for the double layer to fully charge will increase. When the double layer charging time is lengthened, the concentration of ions at the surface of the polymer builds up more slowly and the rate of diffusion of ions into the polymer is also slowed. Usually, τ_{RC} is much less than τ_D and the double layer charging does not limit performance.

Finally, τ_{DDL} is the time constant for the diffusion of ions through the double layer thickness. After a step change in voltage, the diffusion of ions into the polymer is insignificant until at least τ_{DDL}. Before the time has reached τ_{DDL}, ions have not yet diffused across the double layer thickness and there cannot have been any expansion or contraction due to ion influx or outflow. τ_{DDL} is therefore a fundamental limit on the response speed of actuation for conducting polymers[6]. Ions are in essence unable to move into or out of the polymer in a time shorter than τ_{DDL}.

While there is no time constant directly associated with the series resistance and the volumetric capacitance of the polymer, these can also limit the performance. If there is a large diffusion current flowing to charge the volumetric capacitance, there can be a large current drop through the series resistance. The current drop reduces the voltage across the double layer and, as a consequence, the surface concentration of ions is reduced.

2.2. Implications of the Diffusive Elastic Model

The diffusive elastic model as developed in J. Madden's Ph.D. thesis (Madden, 2000) matches the experimental admittance of thin PF_6^- doped polypyrrole films in electrolyte solution over more than eight orders of magnitude of frequency. The equations of conducting polymer behavior given by the theory have led to a much better understanding of what limits the performance of polymer actuators but the thesis did not directly connect the specific material properties of the conducting polymer to different performance limitations. In addition, the diffusive elastic model was derived for a conducting polymer film with negligible resistive voltage drop along the film. In a real polymer, the resistance reduces the voltage and slows the contraction rates.

Below the different time constants of the diffusive elastic model that were presented above are related to material properties of both the polymer and the electrolyte. In Section 2.3, performance related issues that are not described by the diffusive elastic

[6] The double layer diffusion time constant is a limit not only for the bulk swelling model of conducting polymers where volume of the ions themselves is presumed to create expansion or contraction but also for conducting polymer actuators where a conformational change is induced by oxidation or reduction and compensated by ionic diffusion. Until the ions cross the double layer, they cannot contribute to the bulk expansion or contraction.

model (such as the resistive drop in the film) are addressed and related to material properties.

Relation of Diffusive Elastic Model Time Constants and Series Resistance to Material Properties

The time constants associated with the diffusive elastic model each have different implications for actuator performance and for what ultimately limits the actuators. The diffusive elastic model also includes a series electrolyte and contact resistance that considerably impacts the speed of the actuators.

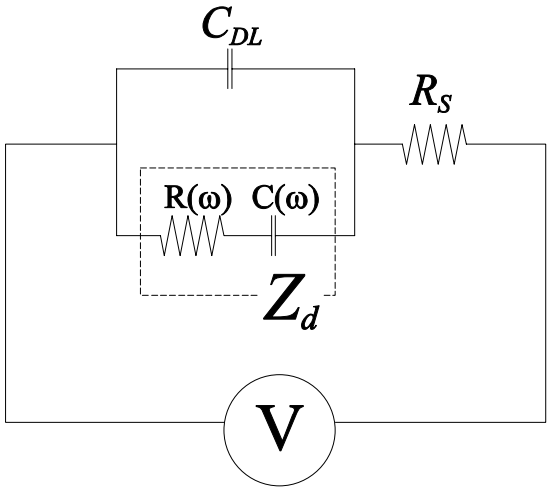

Figure 2.2 Circuit model of a conducting polymer in solution. The resistance R_s includes the resistance of the electrolyte solution and any contact resistance. C_{dl} is the capacitance of the double layer at the polymer electrolyte interface. Z_d is the impedance of ions diffusing into or out of the polymer and includes a bulk capacitance term. Charging of the bulk capacitance leads to expansion and contraction of the polymer while charging of the double layer does not.

Double Layer versus Bulk Ionic Charging

The ionic charge density within the polymer is not simply the integral of the current applied to the polymer actuator and electrolyte. Distinguishing between the ionic charge density in the polymer and the total charge passed into the actuator circuit can be important because expansion is due only to the charge density within the polymer.

Charge is stored in two capacitances (see Figure 2.2 showing the equivalent circuit for the polymer actuator). The first is a bulk capacitance of the polymer material where charges are stored in the three dimensional volume of the polymer. The bulk capacitance corresponds to the equivalent capacitance of the diffusive element Z_d in Figure 2.2. Only charge stored here causes expansion of the polymer.

The second capacitance is the double layer capacitance at the polymer surface. In almost all cases, the quantity of charge stored in the double layer capacitance on the polymer surface is negligible compared to the charge stored in the polymer bulk. Only for very thin films and at very short time scales does it become important to distinguish between the two regions. A typical double layer thickness for the conducting polymers is ~1 nm ((Madden, 2000) p. 313). When diffusion has reached equilibrium and the concentration of ions in the polymer is equal to the concentration in the double layer, the ratio of bulk charge Q_{bulk} to total charge Q_{total} will be given by the ratio of volumes:

$$\frac{Q_{bulk}}{Q_{total}} = \frac{A \cdot h_{polymer}}{A \cdot (h_{polymer} + 2\delta)} = \frac{h_{polymer}}{h_{polymer} + 2\delta}, \tag{7}$$

where $h_{polymer}$ is the thickness of the polymer film, δ is the thickness of the double layer, and A is the surface area of the film[7]. Practically, for a typical 1 nm double layer and at frequencies where the polymer bulk is fully charged, less than 1% of the charge will be in the double layer for films thicker than 200 nm.

At short time scales the ratio of double layer charge to bulk charge can be very high when the double layer charging is much faster than ion diffusion. However these time scales are very small. A rough estimate can be found by calculating the time constant for diffusion of ions into the polymer to a depth $d = \delta$:

$$\tau = \frac{d^2}{4D} = \frac{\delta^2}{4D}, \tag{8}$$

where D is the diffusion coefficient. At times greater than τ the ion concentration within the thickness δ has effectively reached equilibrium. At this equilibrium there are an equal number of ions inside the polymer as there are in the double layer. At times much longer than τ, the number of ions within the polymer bulk is much greater than the number of ions in the double layer. For typical values δ = 1 nm and $D = 10^{-12}$ m^2/s, $\tau \approx$ 0.25 μs.

The double layer charge is thus unimportant compared to the bulk charge in the polymer film except at time scales that are very short (< 1 μs)[8] or when the film is very thin (< 200 nm). As a consequence of the negligible charge in the double layer, the charge in the polymer can be calculated by integrating the external current applied rather than needing to distinguish between the double layer and the bulk currents.

Implications for Response Speed

Strategies to increase the response speed of the polymer include 1) increasing the charging rate in the polymer (increasing $\frac{\partial \rho}{\partial t}$, where ρ is the charge density) without sacrificing the strain/charge ratio 2) increasing the strain/charge ratio without sacrificing the charging rate, or 3) ensuring that the double layer is charged as quickly as possible using resistance compensation.

An important consequence of diffusion driven expansion and contraction is that strain rates depend on the difference between the polymer ion concentration and the double layer concentration. The change from minimum to maximum concentration will create the highest concentration gradients at the surface. Changing from an intermediate concentration to the maximum (or minimum) will generate lower concentration gradients and lower strain rates. When the concentration is close to the maximum, only slow rates can be achieved moving to higher concentration (and vice versa for concentrations close to the minimum). Thus the peak strain rate depends on the polymer charging level and the direction of strain.

[7] The total charge is calculated assuming there is a double layer on both sides of the film (i.e. both sides of the film are exposed to the electrolyte).

[8] Such short times are actually much faster than the typical time constants for charging of the double layer itself.

1) Increasing the Charging Rate

The charging rate of the polymer can be increased in four ways. The first three require improved material properties while the fourth relies on changes in the geometry of the polymer.

Because the charging rate is controlled by diffusion of ions into the polymer, increasing the diffusion coefficient will improve the response speed. For a given material, changing the salt ion can considerably change the diffusion coefficient (Bay, Mogensen, Skaarup, Sommer-Larsen, Jorgensen and West, 2002; Maw, Smela, Yoshida, Sommer-Larsen, and Stein, 2001; Ren and Pickup, 1995). Smaller ions usually move more quickly into the interstitial spaces than do larger ions. But changes in ion size also affect the strain/charge ratio. An expected increase in strain rate because of a higher charging rate can be offset by a decrease of the strain/charge ratio. The tradeoff between the two has not yet been well studied.

The diffusion rate can also be changed using different synthesis methods. The morphology of the synthesized polymer changes considerably depending on the electrochemical potential of the deposition, the current density, and the shape of the deposition waveform (Sadki, Schottland, Brodie and Sabourand, 2000). Typically in the past, synthesis of polypyrrole has been optimized for conductivity (Yamaura, Sato and Hagiwara, 1990; Sato, Yamaura and Hagiwara, 1991) but improvements in actuator performance might be realized by optimizing deposition for faster diffusion. The effect of deposition conditions on diffusion speed and contraction rate has also not been well studied.

The third way to increase the charging rate is to increase the concentration gradients so that diffusion is faster. Gradients within the polymer are determined by the concentration in the double layer. The maximum double layer concentration is limited by the maximum potential – the degradation potential – of the polymer or of the electrolyte. Above (or below) the degradation potential, higher (or lower) concentrations can be reached but at the expense of unwanted chemical reactions that affect long term performance. If the capacitance is linear with voltage, doubling the maximum potential applied to the polymer will double the concentration and hence the charging rate[9]. Strategies to increase the stable potential range include changing the chemical structure of the polymer or electrolyte to block reactive sites or removing oxygen and other impurities that react with the polymer. The best performance may be achieved only in pure environments within hermitically sealed packages.

Finally, the rate of charge density change can be improved by altering the geometry of the polymer and the electrolyte. If the same voltage is applied along two polymer strips of different thickness, the charge density increases faster in the thinner strip. The faster rate is a consequence of there being less volume to charge in the thinner strip. The time constant $\tau_D = h^2/4D$ (the diffusion time constant) relates the strip thickness h to the charging time. Halving the thickness can reduce the charging time by a factor of four.

One other limit to the change in concentration in the double layer occurs if the ion concentration is driven to zero. A very positive potential could make the cation

[9] If the charge in the double layer is proportional to the voltage, doubling the maximum potential should double the concentration at the polymer surface.

concentration zero. Likewise, a very negative potential could make the anion concentration zero. If the concentration of one ion reaches zero, further charging can only occur via concentration changes of the oppositely charged ion.

Reaching zero concentration has two interesting effects: if the ion at zero concentration is the mobile ion and is diffusing *out* of the polymer, the maximum gradient is set not by the material degradation potential but rather is reached at the voltage at which zero concentration is reached. On the other hand, if the non-diffusing ion reaches zero concentration, further increases in double layer voltage will result in twice the increase in concentration of the mobile ion. The charging rate for diffusion *into* the polymer is expected to increase.

2) Increasing the Strain/charge Ratio

Increasing the strain/charge ratio can also increase the polymer contraction rate. While it may be that the strain/charge ratio generally increases as ion size increases, this has yet to be proven. Part of the difficulty is that the strain/charge ratio is also solvent dependent with some solvent molecules (in particular water) getting entrained with the ions (Bay, Jacobsen, Skaarup and West, 2001). However, as mentioned in the discussion of diffusion speed, even if ion size does raise the strain/charge ratio, increased ion size can slow diffusion and so mitigate the potential improvements.

While in polypyrrole, the strain observed is due to the intercalation of ions between the polymer chains, new polymer structures are being developed that use hinging mechanisms along the polymer backbone to boost the strain/charge ratio dramatically (Marsella and Reid, 1999; Anquetil, P. A., Yu, H., Madden, J. D., Madden, P. G., Swager, T. M. and Hunter, I. W., 2002; Madden, Yu, Anquetil, Swager and Hunter, 2000). With hinging backbones, it is likely that diffusion will play a much smaller role in contraction and expansion as far fewer ions will be needed. The amount of contraction and expansion is also expected to be far less dependent on ion size since ion influx will not be directly responsible for volume change but will only trigger the conformational change. Smaller faster ions should therefore be used to trigger volume changes.

3) Resistance Compensation

While diffusion of the ions into the polymer poses a fundamental limit, the charging of the double layer can be a practical limit to actuator rates. If the series resistance for charging the double layer is significant, the double layer voltage and hence the double layer concentration increase can be slow enough that ionic diffusion has time to equilibrate. For the fastest rate, the maximum double layer voltage must be reached as quickly as possible. This can be done by eliminating the effect of series resistance using resistance compensation (Madden, Cush, Kanigan and Hunter, 2000).

When current is flowing in the circuit shown in Figure 2.2, there is a voltage drop $V_R = iR_s$ across the series resistance R_s. At very high currents, the voltage across the double layer can be considerably less than the voltage applied to the entire circuit. Resistance compensation increases the voltage applied to the circuit by iR_s ($V_{applied} = V + iR_s$) so that the controlled voltage is the voltage across the double layer[10].

[10] In practice, the series resistance can be measured by applying a very fast voltage pulse to the circuit and measuring the current. For a short pulse, most of the voltage drop is across the resistor and $R_s = V/i$. When

Without resistance compensation, every effort should be made to reduce the series resistance. Lowering the series resistance by reducing contact resistance, by improving the electrolyte conductivity or by changing the electrolyte geometry will improve the double layer charging time. Even without resistance compensation, reducing the series resistance will improve the actuator by increasing the efficiency.

2.3. Beyond the Model: Creep, Conductivity, and Transference Numbers

There are three specific properties that can have a large effect on performance but are not included or described by the diffusive elastic model. The first, creep, comes into play at high stresses or over long times. Creep is also important at lower stresses if the polymer weakens by electrochemical degradation because of too extreme a potential. The second property is the conductivity of the polymer itself. In the derivation of the diffusive elastic model it is assumed that the entire conducting polymer is at the same potential. However, for either low conductivity polymers or for geometries with long current paths (such as long strips with voltage applied at one end) there can be considerable potential drop due to resistance. Finally, the transference number of the ions within the polymer or within the electrolyte also affects the strain and the strain rate that can be achieved.

Creep

Creep and the modeling of creep in polypyrrole are discussed in Chapter 7 (Passive Linear Stress Strain Measurements). With the limited strain (typically ~2-4%) of conducting polymer actuators based on polypyrrole, creep of a few percent can render the actuator incapable of generating force. To compensate for the lengthening due to creep, mechanisms can be designed to adjust muscle attachment points but these are cumbersome. A ratchet muscle mechanism similar to natural muscle actin myosin cross bridges could be designed with polypyrrole but the manufacturing will be complicated. Solutions based on better design of materials are more desirable. Increased crosslinking of the polymer or construction of composite materials can reduce creep.

Conductivity

The conductivity of the polymer begins to affect the polymer potential if there are high currents or long electronic current paths through the polymer bulk. In Chapter 4 the voltage drop due to current (ohmic potential drop) in long polymer strips is directly measured. Voltage drops along the length of the polymer slow the polymer actuation because the average concentration of ions in the double layer is lowered.

There are three ways of minimizing the ohmic potential drop. The first is to improve the conductivity of the material itself. Conductivity can be increased by better material processing (e.g. (Yamaura, Hagiwara and Iwata, 1988; Hagiwara, Hirasaka, Sato and Yamaura, 1990; Sato, Yamaura, and Hagiwara, 1991)) or by coating or blending with another material of higher conductivity. For example gold ($\sigma = 4.5 \times 10^7$ S/m) on polypyrrole ($\sigma = 10^4$ S/m) will increase the conductivity of polypyrrole or a layered

---

resistance compensation is being used, the measured current is multiplied by the resistance to give $V = V_{double\ layer} + iR_s$.

blending of polypyrrole ($\sigma = 10^4$ S/m) and polyquarterthiophene ($\sigma = 10$ S/m) will boost the conductivity of polyquarterthiophene (Spinks et al., for example, grow conducting polymer tubes which incorporate a coiled gold wire (Spinks, Wallace, Liu and Zhou, 2003)). Coating or blending also affect other averaged properties such as the Young's modulus and the overall strain/charge ratio so care must be exercised to balance the different effects.

The second method to reduce potential drop is to reduce the amount of current. To achieve the same strain rate with less current requires an increase in the strain/charge ratio (lower current gives a lower rate of charging and hence a lower strain rate unless the strain/charge ratio is increased).

Finally, the third way to lower the potential drop is to reduce the length of the current paths. Making electrical contact at both ends or at multiple points along a strip will result in faster actuation (see Chapter 4).

Resistance compensation might be though of as a method of eliminating the effect of the polymer resistance on the polymer potential. However only the potential where the external circuit is connected can be resistance compensated in a long polymer strip. To avoid any degradation of the polymer or electrolyte, the highest (or lowest) potential must not stray outside the potential limits. The potential at the electrical contact points can be set to the maximum (or minimum) but the rest of the polymer strip will be at less than the maximum (or greater than the minimum) because of ohmic drop.

If the polymer electronic conductivity becomes very low, conductivity also affects the rate of diffusion (and the DEM model no longer applies). At low conductivity, the assumption of the diffusive elastic model that the electronic conductivity is much higher than the ionic conductivity in the polymer breaks down. With reduced shielding of ions in the bulk, ionic charge in the polymer will generate an electric field that opposes diffusion of ions into the material and slows the strain rate.

Transference Numbers

For the best strain and strain rate, only one ion species should move into and out of the polymer. If two ions are moving in the polymer bulk, the expansion due to one ion is countered by the contraction of the other.

In a polymer actuator system, ions can be mobile in the conducting polymer and in the electrolyte. In the electrolyte, the transference number of an ion is the fraction of electric field driven current carried by that ion. If the electrolyte has a single current carrying ion (transference number of 1) with a second stationary ion (transference number of 0), the double layer is charged (or discharged) only by the mobile ion. Concentration gradients created by the double layer will only drive diffusion of the electrolyte's mobile ion into and out of the polymer. Thus having a transference number for one ion close to zero can ensure that there is only a single ion moving into or out of the polymer.

In the polymer bulk, ions are very quickly paired with electronic charge and their motion is not driven by electric fields. The concept of a transference number as it is used for an electrolyte is not directly applicable. However, there is a net current in the polymer that is due to influx and outflow of ions. In the polymer bulk then, the transference number of one ion species should be defined as one ion's proportion of the total ion flow. Note that if the electrolyte transference number is 1, the polymer transference number has to be 1 as there is only one ion species in the double layer.

The polymer transference number of a species is expected to be related to the ratio of ion sizes. For tetraethylammonium hexafluorophosphate, the tetraethylammonium ion is very large and is unable to diffuse or diffuses very slowly into or out of the polymer. The smaller hexafluorophosphate ion does diffuse into the bulk to change the volume.

2.4. Material Properties and Actuator Performance

One of the goals of this chapter has been to use the diffusive elastic model of conducting polymer actuators to relate bulk actuator properties to specific material properties. The relationships introduced in the preceding sections are summarized in Figure 2.3 (peak strain and peak stress) and Figure 2.4 (strain and stress rate). Many of the specific material properties affect all of the bulk actuator properties.

Ion Size

The ion sizes in the electrolyte affect the peak strain, the peak stress, and the strain and stress rates. In polymer actuators that operate by ion intercalation, large ions are expected to have a larger strain/charge ratio and hence larger peak strains and stresses. Ions that are too bulky are not able to diffuse into and out of the polymer at all.

It is better to have only one ion that can diffuse in and out of the polymer. Otherwise expansion due to one ion is counteracted by contraction due to the other. Ideally, one ion cannot diffuse (with a transference number in either the polymer or the electrolyte of zero) while the other ion is mobile. Larger ions generally have slower diffusion.

Ion Solvent Interaction

In some cases, ions may entrain solvent molecules as they diffuse into and out of the polymer. The extra volume of the solvent molecules leads to a greater strain/charge ratio (Bay, Jacobsen, Skaarup, and West, 2001; Grande, Otero and Cantero, 1998; Otero, Cantero and Grande, 1999).

Conformational Changes

During the process of oxidation and reduction of conducting polymers, there is a conformational change along the backbone of the polymer. In traditional actuator materials (polypyrrole, polyaniline), calculations suggest that the change in chain length due to conformational change is small (< 1%). Newer materials such as the calixarene based molecules being developed by the Swager and Hunter groups at MIT could have chain length contractions of up to 88% (Anquetil, Patrick A., Yu, Hsiao-hua, Madden, John D., Madden, Peter G., Swager, T. M. and Hunter, Ian W., 2002).

Anisotropy and Ordering

In conducting polymer actuators, there is evidence that there are direction dependent effects during the expansion and contraction. Herod and Schlenoff found that stretched films of polyaniline showed greater contraction and expansion perpendicular to the direction of stretching than in the direction of stretching (11.1% perpendicular vs. 1.6% parallel to the stretch with chemical doping) (Herod and Schlenoff, 1993). Smela and Gadegaard found expansions perpendicular to the plane of thin polypyrrole films of as much as 30% of the film thickness (Smela and Gadegaard, 1999). The authors suggested that the very large expansions observed are likely due to the structuring of the

polymer film in the plane of the substrate. It will be possible to reproduce such ordering effects on a larger scale when techniques can be found to better orient the polymer chains.

Polymer Transference Number

When both the positive and negative ion species in the electrolyte are able to diffuse into and out of the polymer, expansion due to one ion is counteracted by contraction due to the other ion. Preventing one of the ion species from diffusing into the polymer will result in greater expansion and contraction (larger strain/charge ratio and higher strain/stress rates). Ideally, the transference number of one ion species will be very close to one while the transference number of the oppositely charged species will be effectively zero. The transference number is closely tied to ion size.

Degradation Voltage

The degradation voltage of the polymer or of the electrolyte is a practical limit on the peak concentrations of ions in the double layer. Because the peak double layer concentrations determine the peak ion concentrations in the polymer, degradation limits the maximum strain or stress inside the polymer.

The maximum concentration in the double layer also determines the maximum ionic gradient and hence the maximum ion diffusion rate into or out of the polymer. The maximum diffusion rate in turn determines the maximum stress and strain rates.

Electrolyte Concentration

The concentration of ions in the electrolyte determines the conductivity of the electrolyte. Higher electrolyte conductivity will shorten the double layer charging time and will also increase efficiency by reducing resistive loss.

Electrolyte Transference Number

If the transference numbers of the ions in the electrolyte are 1 and 0, then only one ion will charge and discharge the double layer. If only one ion charges and discharges the double layer, that ion in turn will be the only one that diffuses into and out of the polymer causing expansion and contraction. Single ion flow is desirable so that expansion from one ion entering isn't counteracted by contraction from the other ion leaving the polymer volume.

Polymer Bulk Capacitance

The maximum expansion and contraction of the polymer actuator depends on the maximum number of ions that can be inserted and removed. At the maximum voltages that can be applied, the polymer bulk capacitance is a measure of the total charge that can be exchanged. The maximum strain is

$$\varepsilon_{\max} = \int_{V_{\min}}^{V_{\max}} \alpha \cdot C_{vol} \cdot dV \,, \tag{9}$$

where V_{max} and V_{min} are the maximum and minimum voltages that can be applied, α is the strain/charge ratio, and C_{vol} is the capacitance per unit volume of the polymer. If the polymer is being driven by a voltage source rather than a current source, the polymer bulk capacitance also determines the ratio of strain to voltage:

$$\frac{d\varepsilon}{dV} = \alpha \cdot \frac{d\rho}{dV} = \alpha \cdot C_{vol} \,, \tag{10}$$

where α is the strain/charge ratio, C_{vol} is the bulk capacitance per unit volume, and V is the applied voltage. The bulk capacitance is closely related to the double layer capacitance since it is the double layer concentration that determines the bulk ion concentration.

Double Layer Capacitance

The double layer capacitance determines the voltage needed to create a given concentration at the polymer surface. If the double layer capacitance increases without changing the double layer thickness, there will be more charge per volt in the double layer and the concentration of ions per volt will also be greater. The greater ionic concentration will in turn drive diffusion faster so that the actuator will contract or expand faster. If there is more charge in the double layer at the maximum voltages (just within the degradation voltages) the maximum expansion of the polymer should also be greater.

Elastic Modulus

If the elastic modulus is low, large displacements will result from changes in the actuator load. A high elastic modulus on the other hand will reject such disturbances more easily.

In the diffusive elastic model the displacement per charge inserted does not depend on the elastic modulus.

The stress generated does depend on the Young's modulus:

$$\sigma = E\varepsilon + \alpha E\rho , \tag{11}$$

where E is the Young's modulus, ε is the strain, α is the strain/charge ratio, and ρ is the charge density. Increasing the Young's modulus increases the stress that can be generated per unit charge.

Electrolyte Resistance

Reducing the electrolyte resistance will result in faster charging of the double layer at the surface and will also reduce ohmic energy losses to increase actuator efficiency.

Polymer Resistance

The resistance in the polymer actuator itself affects performance in two ways. First, as current flows through the polymer, energy is lost through resistive heating. Second, voltage drops due to current flow reduce the voltage across the double layer. A lower voltage across the double layer reduces the concentration of ions in the polymer and the contraction or expansion of the polymer is slower. Polymer closest to the point where current is delivered will contract the fastest while polymer further from the current delivery point which is at a lower voltage will contract more slowly.

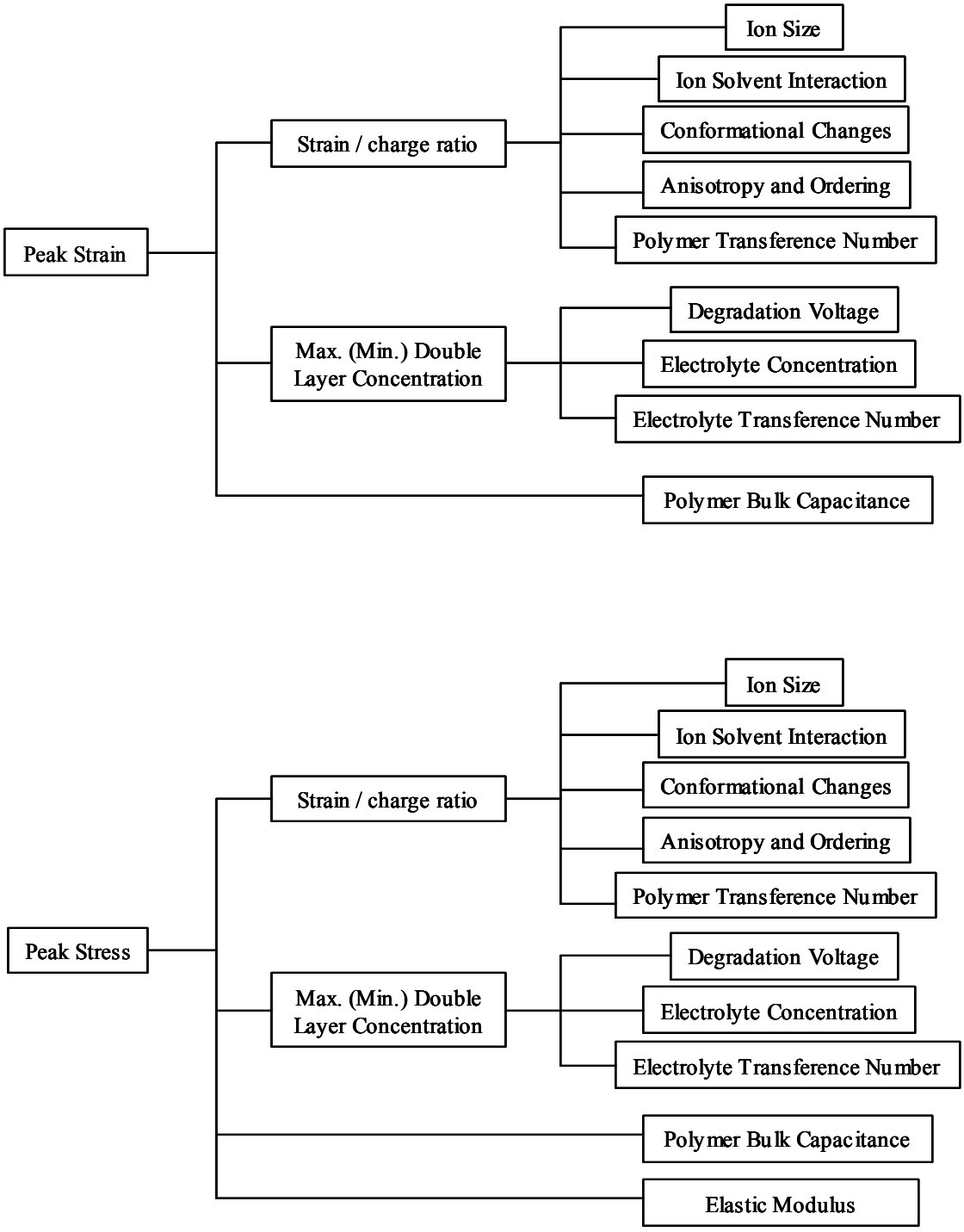

Figure 2.3 Relationship of Peak Strain and Peak Stress to Material Properties of Conducting Polymer Actuators.

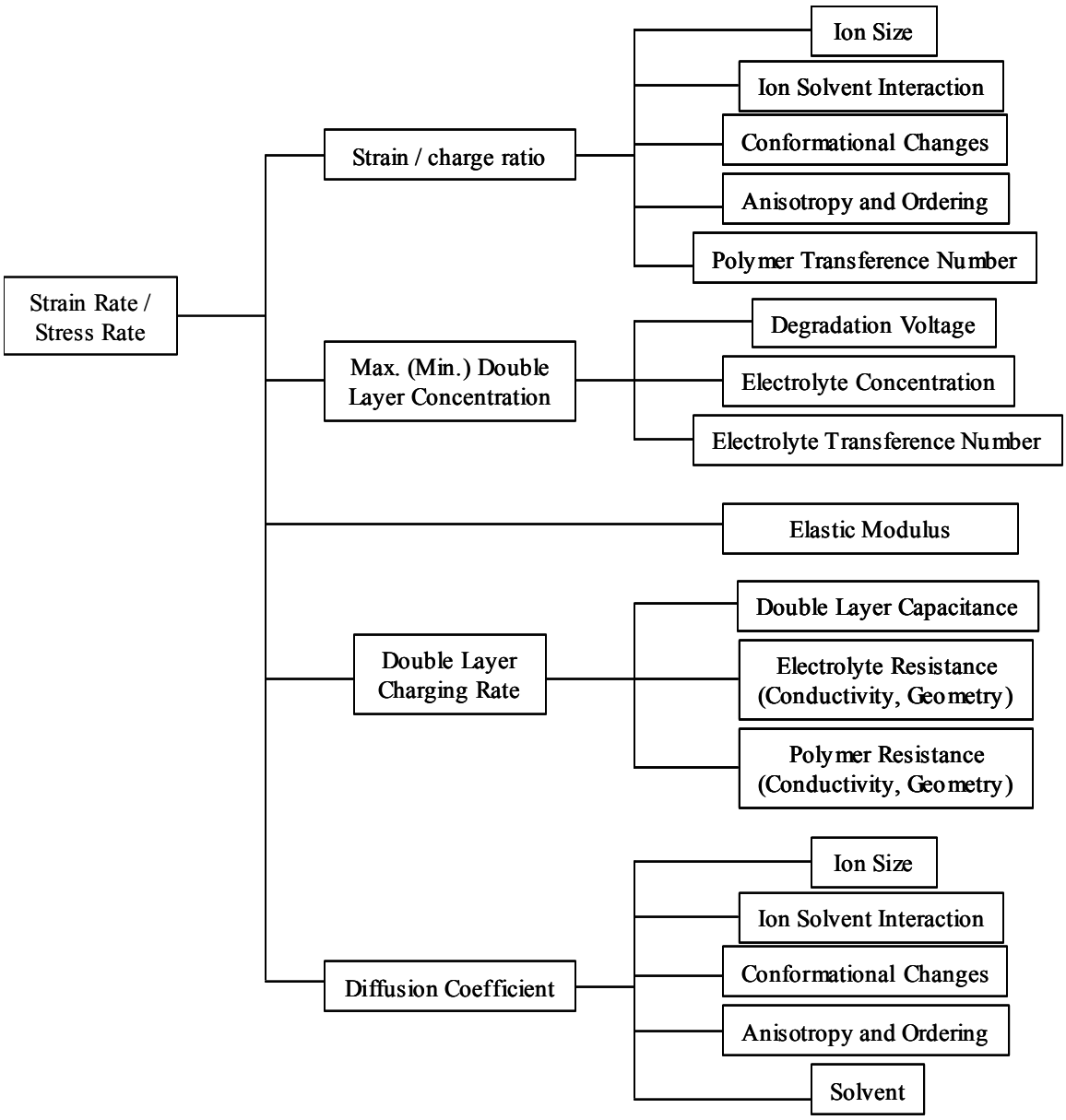

Figure 2.4 Relationship of Strain Rate and Stress Rate to Material Properties of Conducting Polymer Actuators.

Reference List

1. Anquetil, P.A., Yu, H., Madden, J.D., Madden, P.G., Swager, T.M., and Hunter, I.W. Thiophene Based Molecular Actuators. SPIE 9th Annual Symposium on Electroactive Materials and Structures; San Diego, CA. pp. 424-434.

2. Anquetil, P.A., Yu, H., Madden, J.D., Madden, P.G., Swager, T.M., and Hunter, I.W. Thiophene-based conducting polymer molecular actuators. Bar-Cohen, Y., ed. Smart Structures and Materials 2002: Electroactive Polymer Actuators and Devices, Proceedings of SPIE Vol. 4695.

3. Atkins, P.W. Physical Chemistry. 4 ed. New York: W.H. Freeman; 1990.

4. Bard, A.J. and Faulkner, L.R. Electrochemical Methods, Fundamentals and Applications. 1 ed. New York: Wiley; 1980.

5. Bay, L., Jacobsen, T., Skaarup, S. and West, K. Mechanism of Actuation in Conducting Polymers: Osmotic Expansion. Journal of Physical Chemistry B. 2001 Sep 13; 105(36):8492-8497.

6. Bay, L., Mogensen, N., Skaarup, S., Sommer-Larsen, P., Jorgensen, M. and West, K. Polypyrrole Doped With Alkyl Benzenesulfonates. Macromolecules. 2002 Dec 3; 35(25):9345-9351.

7. Grande, H., Otero, T.F. and Cantero, I. Conformational Relaxation in Conducting Polymers: Effect of Polymer-Solvent Interactions. Journal of Non-Crystalline Solids. 1998 Aug; 235:619-622.

8. Hagiwara, T., Hirasaka, M., Sato, K. and Yamaura, M. Enhancement of the electrical conductivity of polypyrrole film by stretching: influence of the polymerization conditions. Synthetic Metals. 1990; 36:241-252.

9. Herod, T.E. and Schlenoff, J.B. Doping induced strain in polyaniline: stretchoelectrochemistry. Chemistry of Materials. 1993; 5:951-955.

10. Lewis, T.W., Spinks, G.M., Wallace, G.G., Mazzoldi, A. and De Rossi, D. Investigation of the Applied Potential Limits for Polypyrrole When Employed as the Active Components of a Two-Electrode Device. Synthetic Metals. 2001 Jun 1; 122(2):379-385.

11. Madden, John D. Conducting Polymer Actuators, Ph.D. Thesis. Cambridge, MA: Massachusetts Institute of Technology; 2000.

12. Madden, J.D., Cush, R.A., Kanigan, T.S. and Hunter, I.W. Fast contracting polypyrrole actuators. Synthetic Metals. 2000 May; 113:185-193.

13. Madden, J.D., Yu, H.-H., Anquetil, P.A., Swager, T.M. and Hunter, I.W. Large strain molecular actuators. EAP Newsletter. 2000; 2(2):9-10.

14. Marsella, M.J. and Reid, R.J. Toward molecular muscles: design and synthesis of an electrically conducting poly[cyclooctatetrathiophene]. Macromolecules. 1999; 32:5982-5984.

15. Maw, S.,Smela, E.,Yoshida, K.,Sommer-Larsen, P., and Stein, R.B. The effects of varying deposition current on bending behavior in PPy(DBS)-actuated bending beams. 2001; 89, 175-184.

16. Mazzoldi, A., Della Santa, A., and De Rossi, D. Conducting polymer actuators: Properties and modeling. Osada, Y. and De Rossi, D.E., editors. Polymer Sensors and Actuators. Heidelberg: Springer Verlag; 1999.

17. Otero, T.F., Cantero, I. and Grande, H. Solvent Effects on the Charge Storage Ability in Polypyrrole. Electrochimica Acta. 1999; 44(12): 2053-2059.

18. Pei, Q. and Inganas, O. Conjugated polymers and the bending cantilever method: electrical muscles and smart devices. Advanced Materials. 1992a; 4(4):277-278.

19. Pei, Q. and Inganas, O. Electrochemical Application of the bending beam method. 1. Mass transport and volume changes in polypyrrole during redox. Journal of Physical Chemistry. 1992b; 96(25):10507-10514.

20. Pei, Q. and Inganas, O. Electrochemical applications of the beam bending method; a novel way to study ion transport in electroactive polymers. Solid State Ionics. 1993; 60:161-166.

21. Ren, X.M. and Pickup, P.G. Impedance Measurements of Ionic Conductivity as a Probe of Structure in Electrochemically Deposited Polypyrrole Films. Journal of Electroanalytical Chemistry . 1995 Oct 31; 396(1-2):359-364 .

22. Sadki, S., Schottland, P., Brodie, N. and Sabourand, G. The mechanisms of pyrrole electropolymerization. Chemical Society Review. 2000; 29:289-293.

23. Sato, K., Yamaura, M. and Hagiwara, T. Study on the electrical conduction mechanism of polypyrrole films. Synthetic Metals. 1991; 40:35-48.

24. Smela, E. and Gadegaard, N. Surprising volume change in PPy(DBS): An atomic force microscopy study. Advanced Materials. 1999; 11(11):953-957.

25. Spinks, G.M., Wallace, G.G., Liu, L. and Zhou, D. Conducting Polymers Electromechanical Actuators and Strain Sensors. Macromolecular Symposia. 2003 Mar; 192:161-169.

26. Yamaura, M., Hagiwara, T. and Iwata, K. Enhancement of electrical conductivity of polypyrrole film by stretching: counter ion effect. Synthetic Metals. 1988 ; 26:209-224.

27. Yamaura, M., Sato, K. and Hagiwara, T. Effect of counter-anion exchange on electrical conductivity of polypyrrole films. Synthetic Metals. 1990; 39:43-60.

3. Finite Conductivity Effects in Long Actuators

For conducting polymer actuators to move from the laboratory into products, descriptions of the material behavior must not only be accurate but must also guide the choice of design parameters.

In Chapter 2, the diffusive elastic model derived by J. Madden was presented (Madden, 2000). An assumption of the model is that the entire conducting polymer is at the same electrical potential but for long strips with voltage applied at one end the assumption no longer holds. Experiments presented in this chapter directly measure the voltage change along the length of a polymer strip for the first time.

A model is then developed that describes the current, voltage, and charge density in the strip. The model accurately describes the behavior of the polymer at short and long times and can be used to choose actuator length and the number of electrical contact points if a required strain is specified at a particular frequency.

For every ion that diffuses into a polypyrrole actuator, an electron is carried through the polymer to or from the external charging circuit to balance and to shield the charge of the ion. The flow of electrons causes an ohmic voltage drop V in the polypyrrole

$$V = \int I(x)/\left(A \cdot \sigma\right)\mathrm{d}x\,, \tag{1}$$

where I is the current density, σ is the conductivity, A is the area through which the current flows, and x is the distance along the path of the current flow. If a voltage is applied at one end of a polypyrrole strip, the other end of the strip will always be at a lower potential because of the flowing current.

The drop in voltage affects the ionic charging rate because it reduces the electrochemical double layer concentration. In Chapter 2, it was explained that a fast polymer charging rate depends on getting the voltage across the double layer as high as possible to increase the surface concentration of ions. For maximum charging rate throughout the length of a long polymer strip, the ohmic voltage drop should be made small so the double layer is kept uniformly charged.

From Equation (1), the ohmic voltage drop can be reduced either by increasing the conductivity, by increasing the area through which the current flows, or by decreasing the path length along which the current flows. There are inevitable tradeoffs. For example, making a polypyrrole strip thicker to reduce the voltage drop can slow the contraction because even if the actual charging rate is faster, the charging rate per unit volume can be slower.

In some cases, the voltage drop will not be significant. If the actuator is operated at low rates, the required current is low[1]. If the current paths are short and the cross-sectional area is large, the voltage drop can be small even for large currents.

In other cases however, the voltage drop can be a large fraction of the applied potential. In long strips with small cross-sectional area, only a fraction of the strip may contract. In experiments with strips of polypyrrole, Della Santa et al. found that only the first 30 mm actively contracted during electrochemical stimulation, quite likely because

[1] Even at low actuation rates, parasitic currents can cause potential drops in the films (West et al. SPIE proceedings).

the potential of the rest of the strip hardly changed (Della Santa, DeRossi and Mazzoldi, 1997; Della Santa, De Rossi and Mazzoldi, 1997).

To design engineering systems that make use of conducting polymer actuators, the qualitative understanding of the impact of voltage drop on performance must be shown experimentally and must be modeled. In this chapter, the voltage along polypyrrole strips during charging is directly measured for the first time. On short time scales (~ ms), the resistances in the polypyrrole strip and through the electrolyte act as a voltage divider circuit. At longer times, the double layer capacitance and the capacitance of the polymer bulk begin to charge and the applied voltage begins to propagate along the strip. (Typical measured voltage response to a step in voltage plotted versus position and time in Figure 3.3 and Figure 3.4).

In Sections 3.2 and 3.3 of this chapter, the experimental measurements of the charging of a polypyrrole strip are presented. In the following section (Section 3.4), a model is developed that describes the changes in voltage through position and time and the model is compared to the experiments.

3.1. Synthesis

Polypyrrole was synthesized at –20 to –40 °C in a 0.05 M tetraethylammonium hexafluorophosphate, 0.05 M pyrrole, 1% H_2O solution in propylene carbonate. The polymer was grown on a glassy carbon crucible masked with Kapton tape at a current density of 1.25 A/m^2 (0.125 mA/cm^2).

3.2. Results

To measure the rate at which the polymer charges along its length, a strip of polymer is immersed in an electrolyte bath (Figure 3.1). Every 20 mm, thin pieces of the strip are cut and folded up out of the solution so that electrical contact can be made in the air. There are seven electrical contacts in total and the length of the strips is 120 mm.

During experiments, a voltage is applied between one end of the polymer strip and the stainless steel bath. The other six electrodes are used to measure the potential of

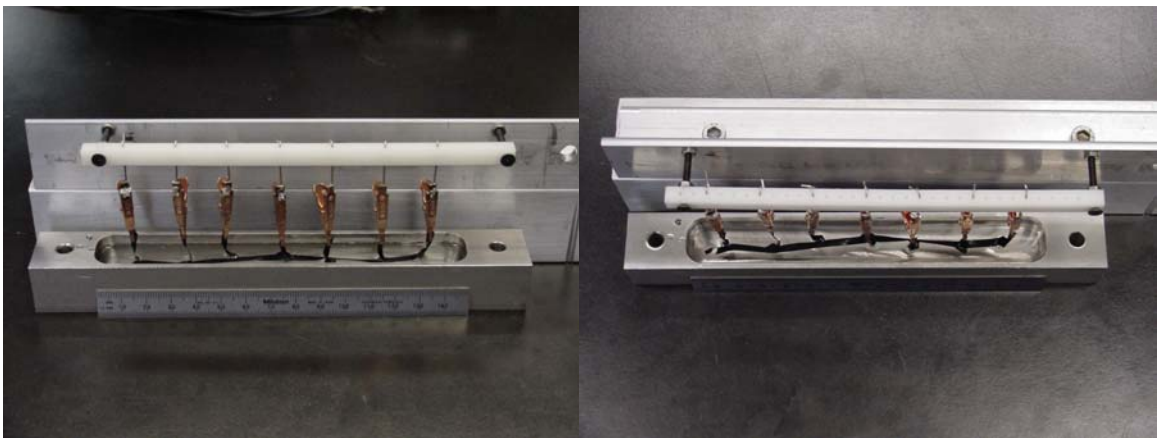

Figure 3.1: Front and top views of the multiple tap experimental setup. The polymer strip (black) is held in the electrolyte solution by 7 alligator clips spaced 20 mm apart. Voltage and current are applied to the polymer strip at one end or both ends. The stainless steel bath is used as a counter electrode and a reference electrode is also inserted into solution.

the polymer strip as the voltage and current propagate (Figure 3.2).

Resistances between connections 1 and 2 and between connections 6 and 7 include contact resistances between the external circuit and the polymer. In the models presented in Section 3.4, the effect of the contact resistance must be included when comparing the experimental results with the models derived above.

The geometry and properties of the two polymer strips used for the results presented in this chapter are shown in Table 3-1.

Table 3-1: Parameters for the model of the charging of a long conducting polymer strip.

Parameter	Value	Source
Diffusion coefficient (D)	10^{-12} m^2/s	(Madden, 2000)
Double layer capacitance	0.1 to 0.4 F/m^2	(Madden, 2000)
Bulk polymer capacitance	10^8 F/m^3	(Madden, 2000)
Strip length	120 mm	measured
LOW RESISTANCE STRIP		
Thickness	30 μm	measured
Width	10 mm	measured
Total resistance	57.8 Ω	measured
Conductivity	6920 S/m	calculated
HIGH RESISTANCE STRIP		
Thickness	7-8 μm	measured
Width	8 mm	measured
Resistance	3780 Ω	measured
Conductivity	496 S/m	calculated

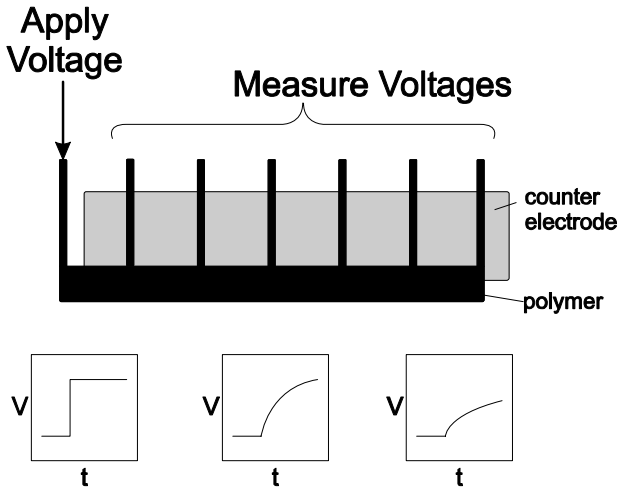

Figure 3.2: Diagram of experimental setup. When a voltage is applied at one end of the polymer, it propagates along the length of the strip. The voltage is measured every 20 mm along the 120 mm long strip.

3.2.1 Voltage as a Function of Position and Time

Plots of the voltage as a function of position and time are shown in Figure 3.3 and Figure 3.4. One strip has a low resistance (Figure 3.3, 58 Ω end to end) while the other strip has a much higher resistance (Figure 3.4, 3780 Ω end to end). The geometry and conductivity of the electrolyte is identical in both cases.

Figure 3.5 and Figure 3.6 plot the voltage data as a function of time and show the current versus time for the two strips. Each of the lines in the voltage plots is a measurement of the voltage at one of the clips attached along the polymer strip. As time increases the voltage of the entire polymer strip approaches the step voltage applied at one end, with the furthest clip lagging the furthest behind. The currents are high when the step is applied and gradually decrease as the strip is charged. As is expected, the voltage charges more slowly and current is lower in the strip with the higher polymer resistance.

The plots of the current (in Figure 3.5 and Figure 3.6) show that the lower resistance strip has a higher current. But the ratio of currents in the two strips is not given by the ratio of strip resistances. Immediately after the step, the ratio of currents is at its maximum of ~8 while the ratio of strip resistances is 65 (see Table 3-1). What might seem to be an unexpected difference in current ratios turns out to be well described by the model developed in Section 3.4.

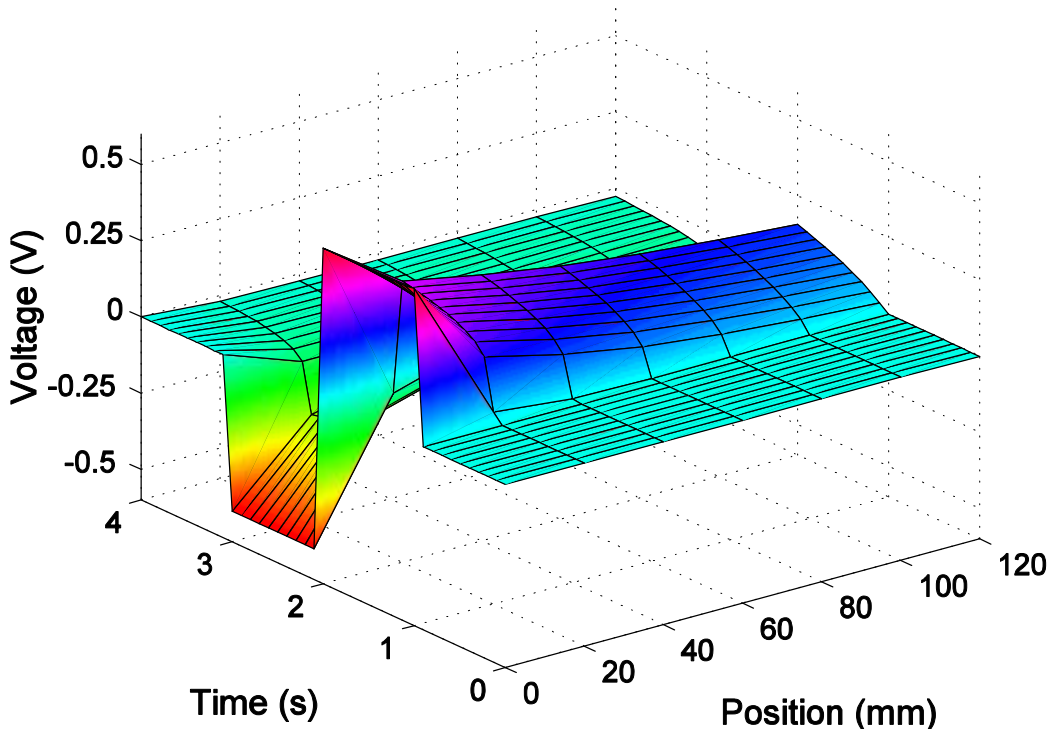

Figure 3.3: Voltage versus Position and Time for the high resistance strip of polypyrrole.

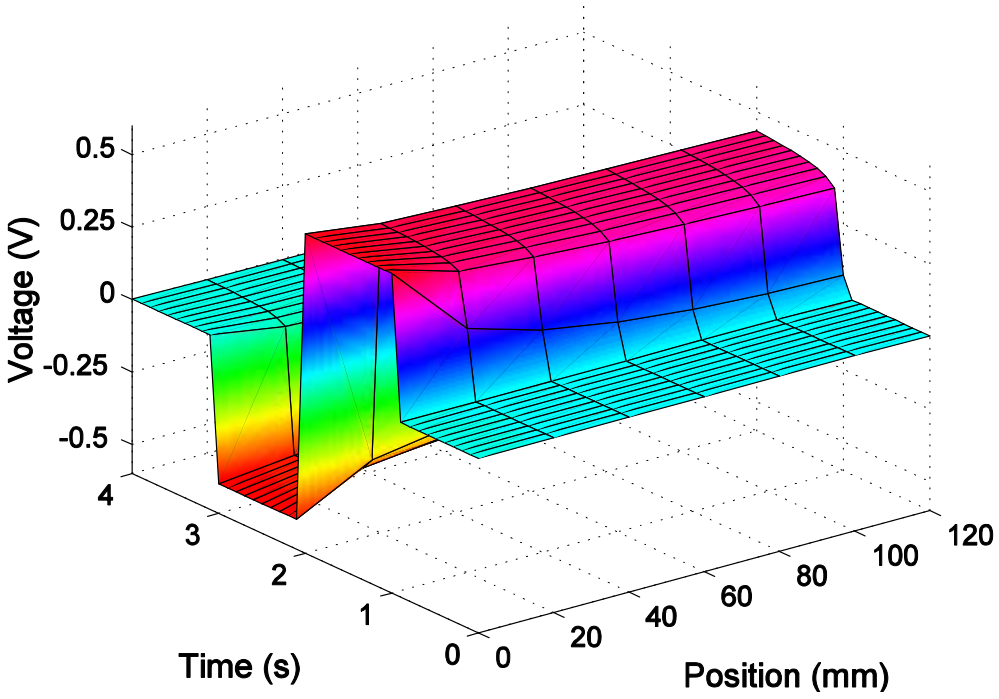

Figure 3.4: Voltage versus Position and Time for the low resistance strip of polypyrrole. The voltage equilibrates much faster in the low resistance strip than in the high resistance strip.

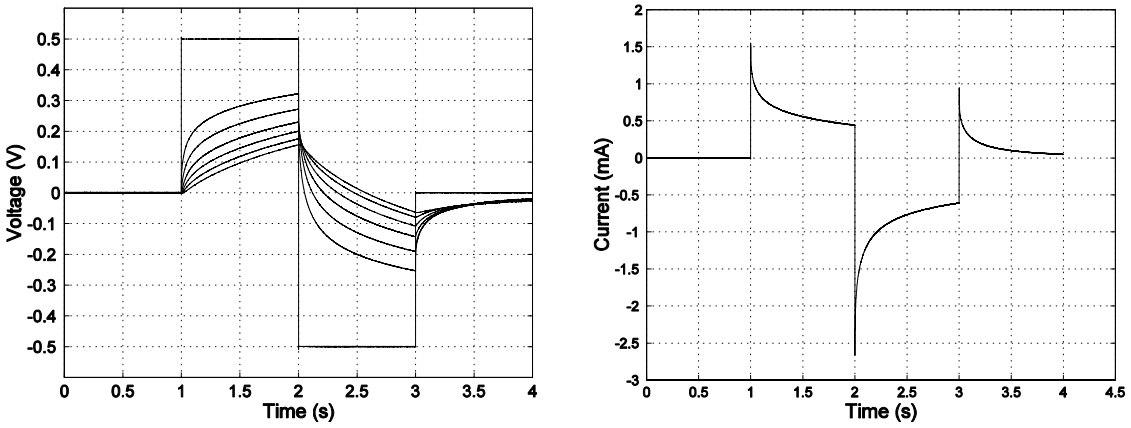

Figure 3.5: Voltage and Current versus Time for a high resistance polymer strip. Each curve in the voltage versus time plot (left) is a measurement of the voltage at one of the 20 mm increments.

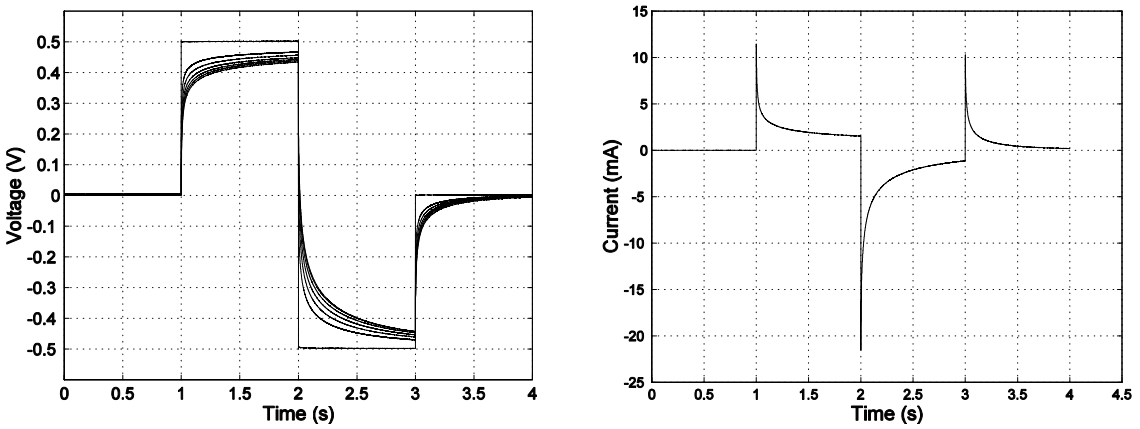

Figure 3.6: Voltage and Current versus Time for low resistance polymer strip. Each curve in the voltage versus time plot (left) is a measurement of the voltage at one of the 20 mm increments.

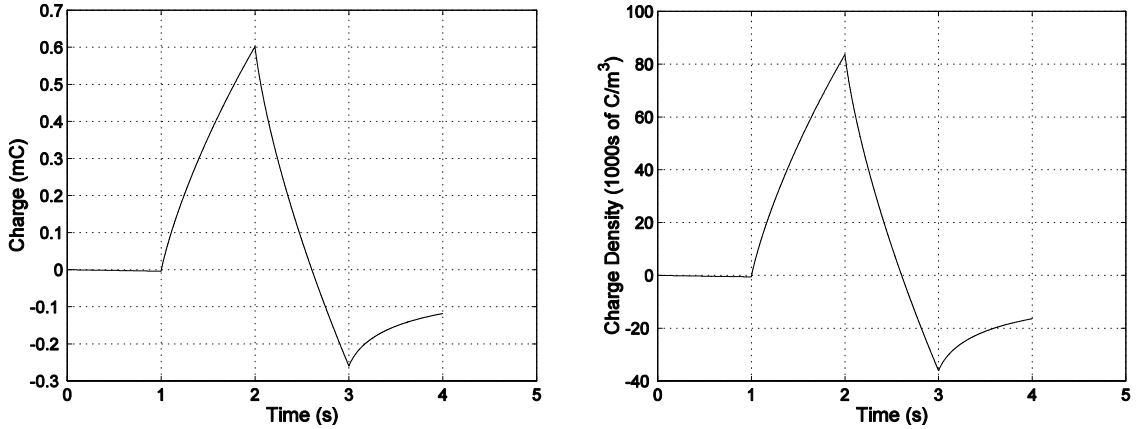

Figure 3.7: Charge versus Time (left) and Charge Density versus Time (right) for the high resistance strip of polypyrrole. After 1 s, the peak charge density is 84000 C/m^3.

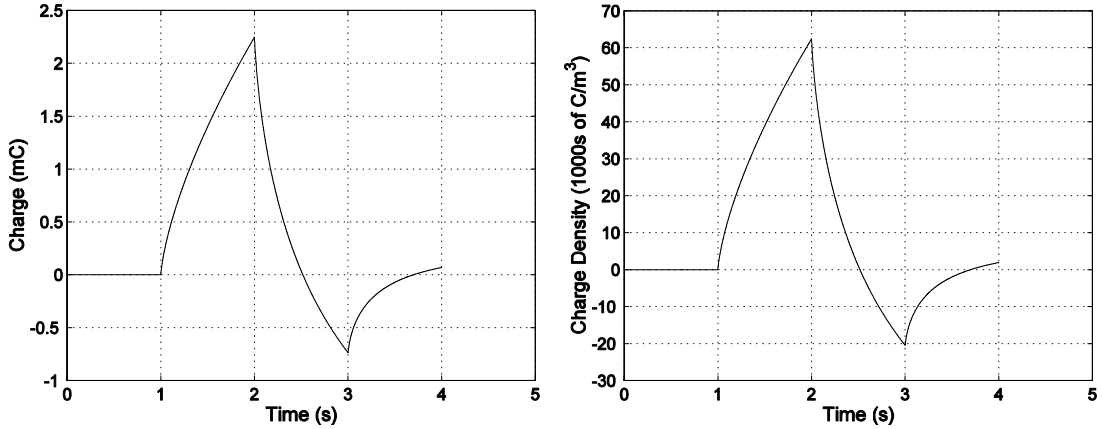

Figure 3.8: Charge versus Time (left) and Charge Density versus Time (right) for the low resistance strip of polypyrrole. After 1 s, the peak charge density is 62000 C/m^3.

3.2.2 Charge and Average Charge Density as a Function of Time

The strain ε of a strip of polypyrrole under constant load is proportional to the charge density ρ

$$\varepsilon = \alpha \cdot \rho , \qquad (2)$$

where α is the strain / charge density ratio. The charge density is therefore an indirect measure of the polymer strain. Figure 3.7 shows the charge (integrated current) and the charge density for the high conductivity strip while Figure 3.8 shows the same plots for the low conductivity strip.

Even though the currents in the higher resistance strip are considerably smaller, the peak charge density is actually slightly higher than that for the low resistance strip. The greater charge density is a consequence of the smaller volume of the high resistance strip. If the resistances of the two strips is the same, the charge density transferred to the thinner strip should clearly be higher. If the resistivity of the two strips were the same, the thinner strip's higher resistance (smaller cross-sectional area) will reduce the expected increase. In the strips used, the higher resistance strip is both thinner and has a higher resistivity, which both reduce the charge transfer rate. Surprisingly though, the charge density of the higher resistance strip still increases faster (81000 C/m^3/s, Figure 3.7 versus 70000 C/m^3/s, Figure 3.8). In this case, the impact of the volume of the strip and of the thickness in particular turns out to be more important than the effect of the resistance.

The results underline the importance of modeling so that the behavior can be calculated in terms of the geometry and the conductivities of the materials. The results also demonstrate the importance of the strip geometry on performance.

3.3. Double Ended Current Injection

As the length of the polymer strip increases and the current must travel further to reach the end, the voltage at the end of the strip takes longer to be affected by the applied potential. To increase the rate of charging, the far end of the strip can also be connected to the applied potential.

At short times, if the distance between the contact points is large enough, the voltage applied at one end of a strip will not affect the voltage at the other end (see for example Figure 3.3 in the last section) and the two contact points will appear (initially) to charge independently. At these short times, using two contact points can double the strip charging rate. For shorter length strips, an applied voltage at one end does immediately affect the voltage at the other end (see Figure 3.4 in the last section, low resistance strip); as a result, two contact points will increase the charging rate by less than 2×.

Figure 3.9 shows the voltage as a function of position for the two strips when a step potential is applied at both ends. For the high resistance strip (upper plot) the voltage in the center of the strip is almost unaffected by the applied potential at the shortest times plotted (0.01 s, see also Figure 3.14, page 59). For the low resistance strip (lower plot), even at the shortest time (0.2 ms, see also Figure 3.14, page 59) the voltage at the middle of the strip has jumped to almost 0.2 V.

Figure 3.10 shows the charge density plotted versus time for the two strips. The

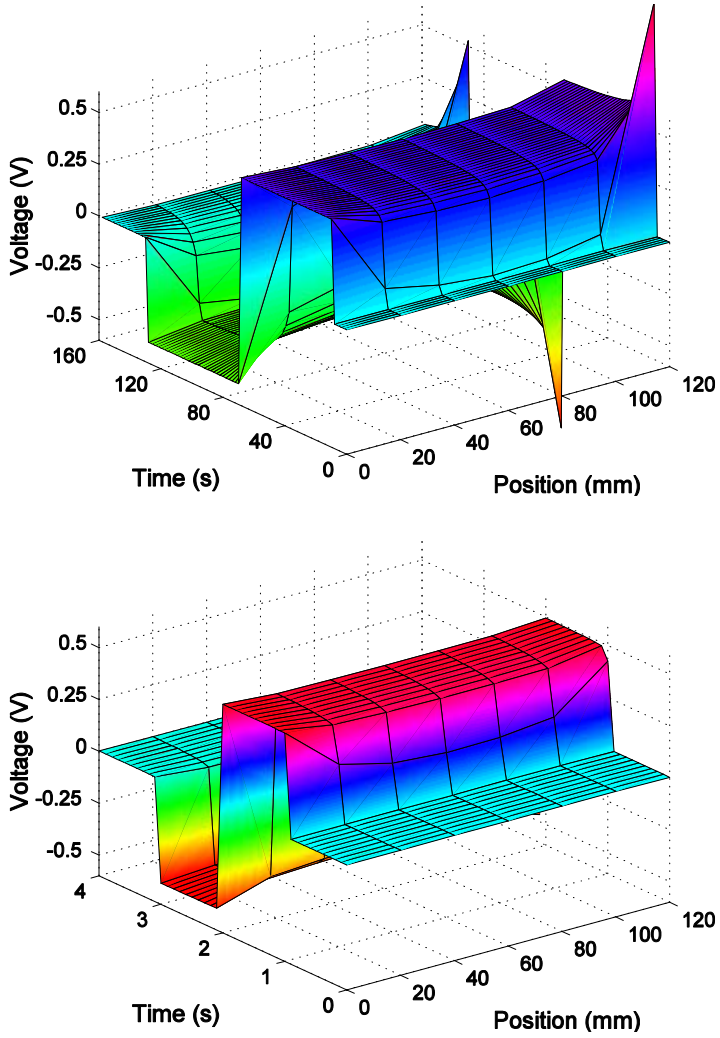

Figure 3.9: Double Ended Voltage versus Time and Position. Top: high resistance strip (t = 0 to 160 s); Bottom: low resistance strip (t = 0 to 4 s). The spike in the high resistance strip is an experimental artifact due to different electrical contact resistance at each end of the strip.

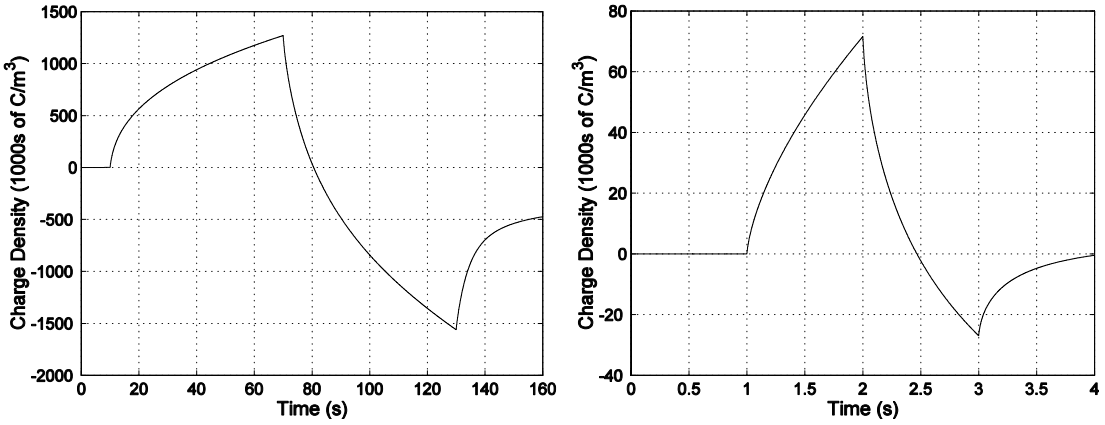

Figure 3.10: Charge Density versus Time for Double Injection. Left: high resistance polypyrrole strip; right: low resistance polypyrrole strip. Note that the time scales are different.

ratios of the charge density when voltage is applied at two ends / the charge density when voltage is applied at one end is plotted versus time in Figure 3.11.

For the high resistance strip, where an applied voltage at one end does not immediately reach the other end, the charge density ratio starts close to 2 and drops asymptotically towards 1. For the low resistance strip, the ratio starts at 1.5 and drops towards 1. After a long time (as $t \to \infty$), the ratio of charge densities always approaches 1.

From the standpoint of designing a long polymer strip actuator, any number of attachment points could be used to apply voltage. The number of actuator points that should be used will depend on the contraction rates that are needed. Fastest contraction will be achieved if the voltage is applied uniformly along the strip (an infinite number of attachment points). Practically however, a small number of contact points desirable. In the next section it will be shown that for a given frequency there is a characteristic length that determines how far an applied voltage waveform will propagate. The characteristic

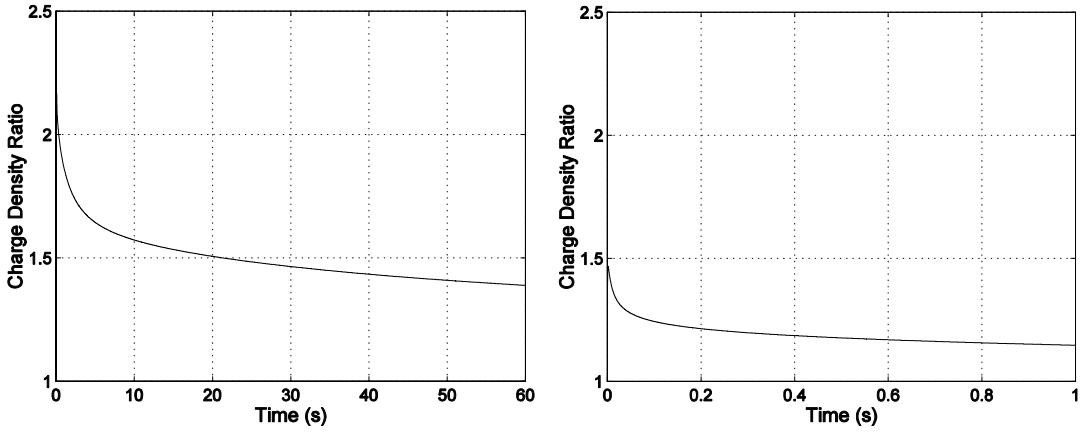

Figure 3.11: Ratio of Charge Densities versus Time for the high resistance (left) and low resistance (right) strips. The ratio is the charge density of the double ended experiment over the charge density of the single ended experiment. Note the different time scales in the left and right hand plots.

length depends on the relative impedance of the polymer strip and of the electrolyte and can be used to calculate the improvement in response with an added contact point. At low frequencies, contact points can be further apart. Even at very high frequencies, making the contact point separation much less than the characteristic length won't improve performance very much.

3.4. Modeling of the Finite Conductivity Effects

In this section, a model is derived to describe the behaviour of long polymer strips as they are charged. In Sections 3.4.1 through 3.4.3, expressions are found for the voltage and for the current in the strips as a function of position and the Laplace variable[2] s.

In Section 3.4.4, the expressions for current are integrated to find an equation for the charge density along the strip and the average charge density of the entire strip. Because the strain is proportional to the charge density, this equation can be used to predict the displacement of the polymer.

Section 3.4.5 compares the model to the measured results at very short time scales (or equivalently, high frequencies). Section 3.4.6 also shows that the model accurately predicts the steady state behavior of the voltage and current in the strip.

The difficulties of finding a complete time domain equivalent to the Laplace domain description that has been derived are discussed in Section 3.4.7. No analytic inverse Laplace transform has been found for the model and attempts to invert the model transfer functions numerically run into trouble because of singularities. However, the model is found to match the experimental results very nicely at high and low frequencies.

Finally, Section 3.4.8 discusses how the model can be used to help engineer conducting polymer actuator systems to meet performance requirements using two or more electrical contact points. An expression for the strain as a function of frequency and the number of contact points is presented that can help the engineer design the configuration of a strip actuator.

3.4.1 Derivation of the equations describing the behavior of the long strip

The behaviour of a long strip of conducting polymer in electrolyte can be described by breaking up the length of the strip and electrolyte into very thin (infinitesimal) thin sheets as shown in Figure 3.12.

In the derivation that follows, it is assumed that the electric field in the polymer is much larger in parallel to the strip than in the direction perpendicular while the electric field in the electrolyte is much smaller parallel to the strip than in the direction perpendicular. Currents are thus assumed to flow only along the strip in the polymer and only perpendicular to the strip in the electrolyte. At high frequencies of excitation or for electrolyte conductivities that are roughly equal to or larger than the polymer conductivity, currents in the electrolyte parallel to the polymer can become significant. The assumptions are kept nonetheless as they greatly simplify the model.

[2] The Laplace domain is more convenient for the derivation as it simplifies the differential equations into ordinary differential equations. The derivation also makes use of the expression derived by J. Madden for the admittance of a polymer in electrolyte that is in the Laplace domain.

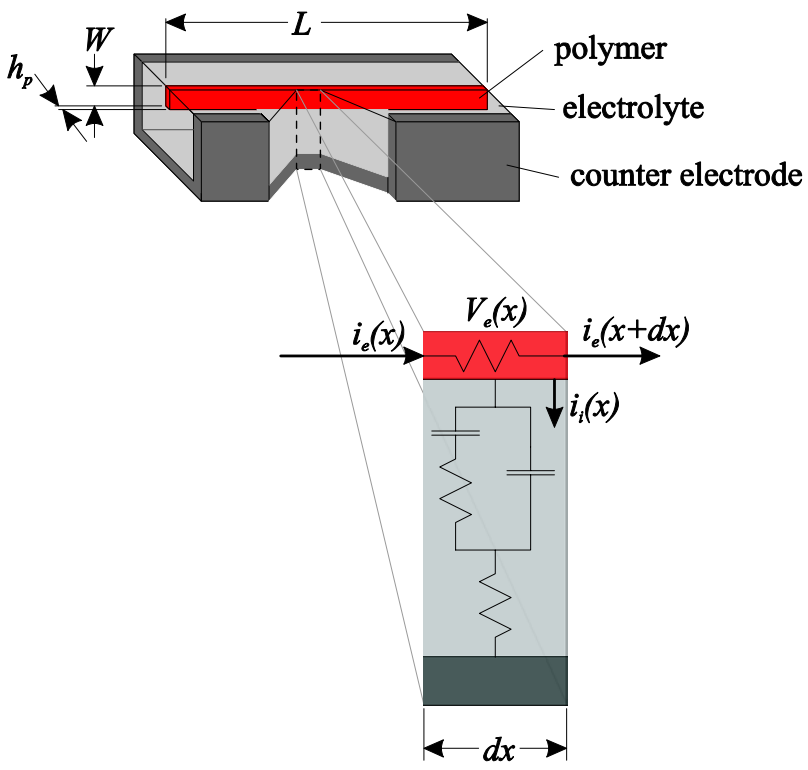

Figure 3.12: Geometry of the polymer strip and of the element of length *dx* used in the derivation of the model equations. The strip has length *L*, width *W*, and thickness h_p. The electron current is $i_e(x)$, the ion current is $i_i(x)$, and the voltage in the polymer strip is $V_e(x)$.

The impedance along the polymer through the thin sheet is denoted Z_e and the impedance perpendicular to the polymer through the electrolyte is denoted Z_i where the subscripts *e* and *i* refer to regions of electron and ion flow. The derivation is simplified somewhat by using the admittance $Y_i = 1/Z_i$.

For the thin sheet, the relationships between the electron current i_e, the ion current i_i, and the voltage in the polymer strip V_e are found using Kirchoff's and Ohm's Laws

$$i_e(x) - i_e(x+dx) = i_i(x), \tag{3}$$

$$V_e(x) - V_e(x+dx) = i_e Z_e, \tag{4}$$

$$i_i(x) = Y_i V_e(x), \tag{5}$$

and then substituting for Z_e and Y_i

$$Z_e(s) = \frac{Z_e^{total}(s)\cdot dx}{L}, \tag{6}$$

$$Y_i(s) = \frac{Y_i^{total}(s)\cdot dx}{L}, \tag{7}$$

where Y_i^{total} is the total impedance between the polymer strip through the electrolyte to the counter electrode, Z_e^{total} is the total impedance through the polymer strip, and *L* is the

length of the polymer strip and electrolyte (x is the position along the length of the strip). The current and voltage in the polymer are described by the differential equations:

$$\frac{\partial i_e}{\partial x} = -\frac{Y_i^{total}(s)}{L} V_e(x,s), \tag{8}$$

and

$$\frac{\partial V_e}{\partial x} = -\frac{Z_e^{total}(s)}{L} i_e(x,s). \tag{9}$$

These equations can be combined to give two second order differential equations:

$$\frac{\partial^2 V_e(x,s)}{\partial x^2} = \left(\frac{Z_e^{total}(s) \cdot Y_i^{total}(s)}{L^2} \right) V_e(x,s), \tag{10}$$

and

$$\frac{\partial^2 i_e(x,s)}{\partial x^2} = \left(\frac{Z_e^{total}(s) \cdot Y_i^{total}(s)}{L^2} \right) i_e(x,s). \tag{11}$$

The form of the solution for both cases is

$$u(x,s) = A(s) e^{\kappa(s)x} + B(s) e^{-\kappa(s)x}, \tag{12}$$

where

$$\kappa(s) = \sqrt{\frac{Z_e^{total}(s) Y_i^{total}(s)}{L^2}}, \tag{13}$$

and where u can be either i_e or V_e. $\kappa(s)$ has units of length^{-1}. As such, the inverse of κ can be considered a characteristic length. The value of κ is, despite appearance in Equation (13), independent of the strip length L because the total impedance and admittance can be expressed as impedance and admittance per unit length.

The coefficients $A(s)$ and $B(s)$ can be found by matching the boundary conditions. For the current equation, the boundary conditions are

$$i_e(0,s) = I_o(s), \tag{14}$$

$$i_e(L,s) = 0, \tag{15}$$

where I_o is the current applied at $x = 0$. The boundary conditions for the voltage equation are:

$$V_e(0,s) = V_o(s), \tag{16}$$

$$V_e(0,s) = \frac{i_i(0,s)}{Z_e(s)} = \frac{1}{Z_e^{total}(s)} \frac{\partial i_e(0,s)}{\partial x}, \tag{17}$$

where V_o is the voltage applied at $x = 0$ (a relationship between V_o and I_o will be derived shortly that can be used to find the current response to an applied voltage or the voltage response to an applied current). When the differential equations are solved with the boundary conditions, the solutions are:

$$i_e(x,s) = I_o(s) \frac{\sinh(\kappa(s)(L-x))}{\sinh(\kappa(s)L)}, \tag{18}$$

and

$$V_e(x,s) = V_o(s)\frac{\cosh(\kappa(s)(L-x))}{\cosh(\kappa(s)L)}. \tag{19}$$

3.4.2 Expressions for the Impedance and Admittance

Expressions for the admittance and impedance of the polymer strip are needed to complete the solutions derived in the previous section. The impedance of the polymer strip to electron flow is purely resistive:

$$Z_e^{total} = \frac{L}{\sigma_{polymer} \cdot W \cdot a}. \tag{20}$$

The admittance of the polymer and electrolyte to ion flow is more complicated as it involves the transfer of charge through the electrolyte, the charging of the double layer between the electrolyte and the polymer, and the diffusion of ions into the polymer bulk. The expression for the admittance is given in Chapter 2 and was derived in J. Madden's thesis (Madden, 2000):

$$Y_i^{total}(s) = \frac{s}{R} \cdot \frac{\frac{\sqrt{D}}{\delta}\tanh\left(\frac{a}{2}\sqrt{\frac{s}{D}}\right) + \sqrt{s}}{\frac{\sqrt{s}}{RC} + s^{\frac{3}{2}} + \frac{\sqrt{D}}{\delta}s \cdot \tanh\left(\frac{a}{2}\sqrt{\frac{s}{D}}\right)}, \tag{21}$$

where D is the diffusion coefficient for the ions in the polymer bulk, δ is the thickness of the double layer, R is the resistance through the electrolyte, and C is the double layer capacitance. The variables C, and δ can be re-expressed in terms of the double layer capacitance per unit area, the capacitance per unit volume of the polymer, the conductivity of the electrolyte, and the geometry[3]:

$$C = 2 \cdot C_{DL_{area}} \cdot L \cdot W, \tag{22}$$

$$\delta = \frac{C_{A_{DL}}}{C_{V_{bulk}}}, \tag{23}$$

where $C_{DL_{area}}$ is the double layer capacitance per unit area, $C_{V_{bulk}}$ is the capacitance per unit volume of the polymer, L is the length of the strip, and W is the width of the strip.

Almost all of the parameters in the equations (21) to (23) are known (the values are listed in Table 3-1 on page 43). The resistance for the electrolyte geometry used in the experiments is not trivial to calculate (although the conductivity of the electrolyte has been measured experimentally[4]). Instead, the resistance of the electrolyte can be found

[3] The relationship between the double layer thickness δ and the double layer and bulk capacitances is based on the assumption that the capacitance per unit volume in the double layer (C_A/δ) is equal to the capacitance per unit volume (C_V) in the bulk (Madden, 2000).

[4] The conductivity of the electrolyte is ~0.1 S/m for 0.05 M tetraethylammonium hexafluorophosphate in propylene carbonate. (J. Madden, unpublished data).

by fitting to the equations. The latter approach is used in Section 3.4.5 where experimental results are compared to the model.

3.4.3 Relationship Between I_o and V_o

Knowing only the current, it should be possible to calculate the voltage. Likewise, knowing only the voltage, it should be possible to calculate the current. Using the relationship

$$\frac{\partial V_e}{\partial x} = -\frac{Z_e^{total}}{L} i_e(x,s), \tag{24}$$

and substituting the solutions for i_e and V_e (Equations (18) and (19)) yields

$$V_o(s) = I_o(s)\sqrt{\frac{Z_e^{total}}{Y_i^{total}}}\coth(\kappa(s)L), \tag{25}$$

or

$$I_o(s) = V_o(s)\sqrt{\frac{Y_i^{total}}{Z_e^{total}}}\tanh(\kappa(s)L), \tag{26}$$

and so both the current and voltage can be found if only one of the two is known at the end of the strip.

3.4.4 Expression for Ionic Charge Density in the Polymer

Since the strain and stress generated are proportional to the ionic charge density ($\varepsilon = \alpha\rho + \sigma / E$) it is important to find an equation for the charge density through the length of the polymer. The ionic charge is the integral of the ionic current and the density of charge is found by dividing charge by the volume.

For the volume of polymer in the thin sheet (Figure 3.12), the charge entering the strip is given by

$$Q(x,t) = \int i_i(x,t)dt\,, \tag{27}$$

or

$$\rho(x,t) = \frac{Q(x,t)}{a\cdot W\cdot dx} = \frac{1}{a\cdot W}\int \frac{i_u(x,t)}{dx}dt = \frac{1}{a\cdot W}\int \frac{i_e(x,t) - i_e(x+dx,t)}{dx}dt\,, \tag{28}$$

which can be transformed into the Laplace domain:

$$\begin{aligned}\rho(x,s) &= \frac{1}{a\cdot W}\frac{1}{s}\left(-\frac{\partial i_e(x,s)}{\partial x}\right),\\ &= \frac{1}{a\cdot W}\frac{1}{s}\left(V_o(s)\sqrt{\frac{Y_i^{total}(s)}{Z_e^{total}(s)}}\tanh(\kappa(s)L)\right)\kappa(s)\frac{\cosh(\kappa(s)(L-x))}{\sinh(\kappa(s)L)},\end{aligned} \tag{29}$$

and finally, simplifying by using the definition of κ(s) we find

$$\rho(x,s) = \frac{1}{a\cdot W\cdot L}\left(V_o(s)\sqrt{\frac{Z_e^{total}(s)}{Y_i^{total}(s)}}\right)\frac{1}{s}\frac{\cosh(\kappa(s)(L-x))}{\cosh(\kappa(s)L)}\,. \tag{30}$$

This expression gives the charge density distribution along the length of the strip as a function of frequency.

The average strain of the entire strip depends on the average charge density. Average charge density in the entire strip can be found by integrating the electronic current at $x = 0$ through time or by integrating Equation (30) with respect to x and dividing by the length. The average charge density in the strip $\bar{\rho}(s)$ is:

$$\bar{\rho}(s) = \frac{Q(s)}{L \cdot W \cdot a} = \frac{1}{L \cdot W \cdot a} \frac{1}{s} V_o(s) \sqrt{\frac{Y_i^{total}}{Z_e^{total}}} \tanh\left(\kappa(s) \cdot L\right). \tag{31}$$

This equation for the average charge density can be used to predict the displacement of the polymer at any chosen frequency and can also help in the selection of distance between attachment points. A typical engineering specification for the performance of an actuator might include a magnitude of strain achievable at a certain frequency. By calculating the strain at a particular frequency

$$\varepsilon(s) = \alpha \cdot \bar{\rho}(s) = \frac{\alpha \cdot Q(s)}{L \cdot W \cdot a} = \frac{\alpha}{L \cdot W \cdot a} \frac{1}{s} V_o(s) \sqrt{\frac{Y_i^{total}}{Z_e^{total}}} \tanh\left(\kappa(s) \cdot L\right), \tag{32}$$

(where α is the strain to charge ratio) for different lengths L, the maximum distance between voltage contact points can be found (this is discussed at greater length in the Subsection 3.4.8).

3.4.5 High Frequency or Short Time Response

At very high frequencies, the impedance to electron flow Z_e^{total} and the admittance function for ion flow Y_i^{total} simplify to:

$$Z_e^{total}\left(s \to \infty\right) = R_e^{total}, \tag{33}$$

and

$$Y_i^{total}\left(s \to \infty\right) = \frac{1}{R_{electrolyte}^{total}}, \tag{34}$$

where R_e^{total} and $R_{electrolyte}^{total}$ are the end to end resistance of the polymer (electron flow) and the resistance through the electrolyte (ion flow). The equation for κ(s) simplifies to:

$$\kappa^2 = \frac{1}{L^2} \frac{R_e^{total}}{R_{electrolyte}^{total}}, \tag{35}$$

which is now independent of s. In the time domain, the high frequency limit corresponds to very short times. At these very short times, the model double layer capacitance and bulk capacitance have very low impedance and the polymer and electrolyte behave as resistors.

The response of the two strips at $t = 0.2$ ms (the first sample taken after the step voltage is applied) is shown in Figure 3.13 as a function of position. In the high resistance polymer, the resistance along the polymer film is so great that at 60 mm and further from the end the voltage rise is below the noise level (below a few mV). On the

other hand, in the low resistance strip there is an immediate jump in voltage even at a position of 120 mm (at the far end).

The dashed lines in Figure 3.13 are the fit of the model in the limit of high frequency (with $\kappa^2 = R_e^{total} / \left(L^2 \cdot R_{electrolyte}^{total}\right)$). The parameters for the model are all taken from Table 3-1 with the exception of $R_{electrolyte}^{total}$.

Using results from the low resistance strip, the calculation of $R_{electrolyte}^{total}$ was complicated somewhat by contact resistance which affects the voltage difference between 0 mm and 20 mm. The value for $R_{electrolyte}^{total}$ is found using the following procedure:

1) By combining Equations (19) and (26), I_o at t = 0 can be written as a function of the voltage at t = 0 at any position x:

$$I_o(x) = V_x(x)\sqrt{\frac{1}{R_{electrolyte}^{total} R_e^{total}}}\,\frac{\sinh(\kappa L)}{\cosh(\kappa(L-x))}, \qquad (36)$$

and where from Equation (35) it is known that κ is a function of the electrolyte resistance.

2) I_o is measured experimentally and the only unknown in Equation (36) is the electrolyte resistance. The equation is solved for $R_{electrolyte}^{total}$ using the measured current and the measured voltage at any position.

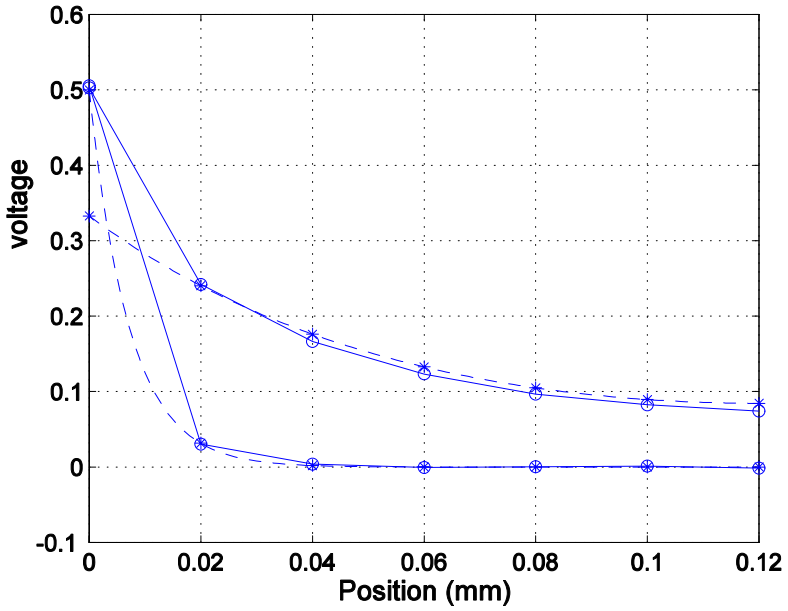

Figure 3.13: Voltage versus position measured immediately after the application of a voltage step at position = 0 mm. The solid lines and circles are the voltages measured every 20 mm. The dashed lines are the voltages calculated using the model. ($R_{solution}$ = 13.8 Ω, $R_{polymer}$ = 57.6 Ω and $R_{polymer}$ = 3780 Ω). The curve for the low resistance strip was found by fitting the electrolyte resistance so the model voltage matches the measured voltage at x = 20 mm (fit with one free parameter). The model for the high resistance strip is calculated using the same electrolyte resistance as the low resistance strip (no free parameters).

The value of $R_{electrolyte}^{total}$ = 13.8 Ω was found using results from the low resistance strip at the point x = 20 mm (R_e^{total} = 57 Ω, I_o = 11.5 mA, L = 120 mm, and V(x=20 mm) = 0.24 V). . The voltage at x = 20 mm was used instead of the voltage at x = 0 mm because the contact resistance at x = 0 mm causes an unmodeled change in the voltage[5]. The calculated κ = 17 m^{-1} (κ = (59 mm)$^{-1}$) for the low resistance strip and κ = 138 m^{-1} (κ = (7.2 mm)$^{-1}$) for the high resistance strip.

In Figure 3.13, the model predictions are shown as dashed lines. The electrolyte resistance calculated for the low resistance strip is also used to calculate the dashed line for the high resistance strip. Thus, the model for the high resistance strip at t = 0 s has no free parameters. The model describes the measured data at t = 0 s very well for both strips.

3.4.6 Low Frequency and Long Time Response

At very low frequencies ($s \to 0$ or $t \to \infty$) the response of the polymer tends to zero current and a uniformly distributed voltage along the entire length of the strip. The admittance of the diffusive elastic model is purely capacitive as $s \to 0$:

$$Y(s) = sC\left(\frac{a}{2\cdot\delta}+1\right), \tag{37}$$

where as before, C is the capacitance of the double layer, a is the thickness of the polymer strip, and δ is the double layer thickness. Substituting into the voltage equation we find:

$$\kappa(s)^2 = s\frac{R_{polymer}C\left(\frac{a}{2\delta}+1\right)}{L^2}, \tag{38}$$

and so as $s \to 0$, $\kappa(s) \to 0$ as well. The voltage simplifies to:

$$V(x, s\to 0) = V_o(s\to 0)\frac{\cosh(0\cdot(L-x))}{\cosh(0\cdot L)} = V_o(s\to 0)$$

The low frequency response of the strip at arbitrary x is therefore given by the low frequency response at x = 0 (i.e. V_o).

3.4.7 Response as a Function of Time

Unfortunately, the model developed does not have an analytical inverse Laplace transform and so has not been expressed in the time domain. Attempts to use a numerical inversion failed to give meaningful results[6] because of singularities in the Laplace

---

[5] Once the electrolyte resistance is known, the voltage that is predicted by the model can be found for x = 0 mm and can be compared to the actual experimental value. The voltage difference is caused by current flowing through the contact resistance $R_{series} = \frac{V_{measured} - V_{predicted}}{I} = \frac{0.5V - 0.33V}{11.5mA} = 14.8\Omega$.

[6] Methods for the numeric calculation of the inverse Laplace transform rely on the Bromwich integral $f(t) = \frac{1}{2\pi i}\int_{c-i\infty}^{c+i\infty} F(y)e^{iy}dy$, where $F(s)$ is the Laplace transform of $f(t)$ and $c > c_o$ with c_o the most positive real part of any singularities of $F(s)$ (Davies and Martin, 1979). The hyberbolic functions in the

representation. As the model stands, the low frequency (long time) and high frequency (short time) limits have been demonstrated to match the experimental results but there has not yet been experimental verification at all other frequencies.

Two different approaches can lead to verification of the model at these intermediate frequencies. If the verification is to be done in the Laplace domain, the frequency domain transfer function of the applied voltage should be measured. One way to measure the transfer function is the apply a swept sine and measure the voltage as a function of position. On the other hand, to carry out the verification in the time domain, the solution to the differential equations in the time domain can be found numerically and matched to the experimental data.

Despite the lack of verification at intermediate frequencies, the excellent fit at high frequencies gives confidence that the model is correct.

3.4.8 Two or More Electrical Contact Points

If electrical contact is made at both ends of the polymer, the equations for the voltage, current, and average charge density need to be changed to reflect the different boundary conditions. Using symmetry, the same equations can be used but with slightly modified variables.

For a strip of length L with contact at both ends the current, the boundary condition at $x = \frac{1}{2}L$ are identical to the boundary condition of a strip of total length $\frac{1}{2}L$ with only a single contact point. The voltage, current, and charge density between $x = 0$ and $x = \frac{1}{2}L$ are therefore given by the equations derived above but with $L \to \frac{1}{2}L$:

$$i_e(x,s) = I_o(s)\frac{\sinh\left(\kappa(s)\left(\frac{1}{2}L - x\right)\right)}{\sinh\left(\kappa(s)\frac{1}{2}L\right)}, \tag{39}$$

$$V_e(x,s) = V_o(s)\frac{\cosh\left(\kappa(s)\left(\frac{1}{2}L - x\right)\right)}{\cosh\left(\kappa(s)\frac{1}{2}L\right)}, \tag{40}$$

$$\rho(x,s) = \frac{2}{a \cdot W \cdot L}\left(V_o(s)\sqrt{\frac{Z_e^{total}(s)}{Y_i^{total}(s)}}\right)\frac{1}{s}\frac{\cosh\left(\kappa(s)\left(\frac{1}{2}L - x\right)\right)}{\cosh\left(\kappa(s)\frac{1}{2}L\right)}. \tag{41}$$

The solution must be symmetric around $x = \frac{1}{2}L$ and so:

$$i_e(x,s) = -i_e(L - x, s), \tag{42}$$

$$V_e(x,s) = V_e(L - x, s), \tag{43}$$

$$\rho(x,s) = \rho(L - x, s), \tag{44}$$

and with a bit of algebra it can be shown that Equations (39) to (41) are in fact general.

Taking the limit of high frequencies (as was done in Section 3.4.5), we can compare equation (40) to the short time response for the two contact point experiments. The short time data[7] and the model (with no fitted parameters[8]) are plotted in Figure 3.14.

---

expressions for voltage and current in the Laplace domain have poles in the right half plane that stretch out to $+\infty$. As a consequence, the Bromwich integral cannot be used to invert the model.

[7] For the low resistance strip, the data is plotted for $t = 0.2$ ms. The data for the high resistance strip was taken at 10 ms intervals. Because the change in voltage over 10 ms is significant, to get a value

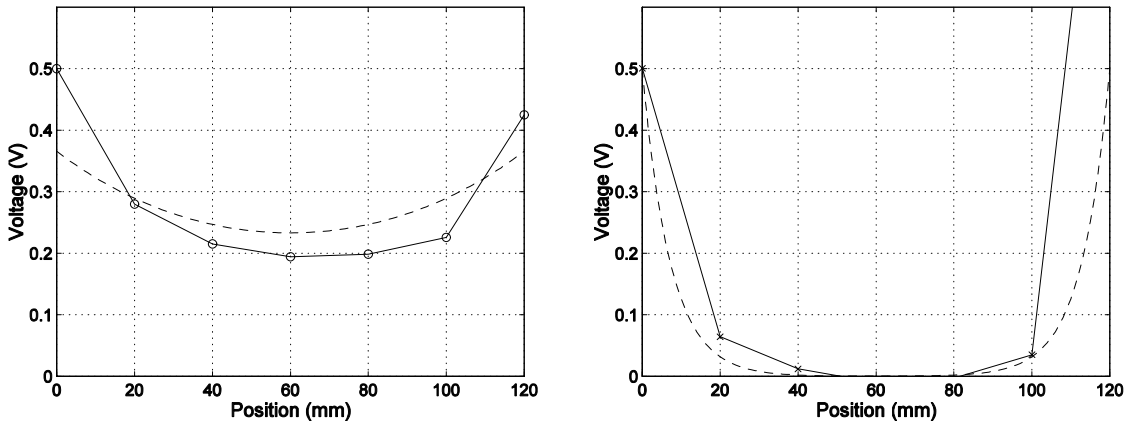

Figure 3.14: Experimental and modeled results for two contact points. Left plot: low resistance strip (data from t = 0.2 ms). Right plot: high resistance strip (data extrapolated to t = 0 s from the samples at 10, 20 and 30 ms). In the model the voltage applied at both ends of the strips is the same but (due to experimental limitations discussed in the text) the actual voltages applied were not the same at both ends.

The model describes the data pretty well but the match is not as good as the match for the single contact experiments.

There are a couple of experimental problems that could explain the greater difference between experimental results and the model curve. As discussed in Section 3.4.5, there is contact resistance to the polymer. In the low resistance strip model, the contact resistance is assumed to be the same at both ends but based on the asymmetrical voltage, the two ends of the strip must have different contact resistances. A second experimental issue relates to the use of a potentiostat to compensate for part of the contact resistance. Because only one potentiostat was used, resistance compensation could only be done for one end of the polymer strip and so different voltages ended up being applied to the two ends. Future experiments would be better performed using two potentiostats.

Finally, for the purpose of actuator design, it is of interest to see how the total current and the average charge density are affected by electrical contact at both ends instead of only one end of the strip. The total current I_o(s) for an applied voltage is twice the current that would result for a strip of length $\frac{1}{2}L$:

$$I_o(s) = 2 \cdot V_o(s) \sqrt{\frac{Y_i^{total}}{Z_e^{total}}} \tanh\left(\kappa(s) \tfrac{1}{2} L\right), \tag{45}$$

and the average charge density is:

$$\bar{\rho}(s) = \frac{2}{L \cdot W \cdot a} \frac{1}{s} V_o(s) \sqrt{\frac{Y_i^{total}}{Z_e^{total}}} \tanh\left(\kappa(s) \cdot \tfrac{1}{2} L\right). \tag{46}$$

---

representative of $t \approx 0$ s, the data from t = 10, 20, and 30 ms were used generate a quadratic extrapolation back to t = 0 s.

[8] Values for the model are taken from Table 3-1 with the exception of the electrolyte resistance. The value used for the electrolyte resistance was found in Section 3.4.5 and is 13.8 Ω.

It should be pointed out that $\kappa(s)$ and the ratio $\frac{Y_i^{total}}{Z_e^{total}}$ are both independent of the length of the strip ($Y_i^{total} = Y_{i/length} \cdot L$, $Z_e^{total} = Z_{e/length} \cdot L$, and $\kappa(s) = \sqrt{Z_{e/length} \cdot Y_{i/length}}$, where $Z_{e/length}$ and $Y_{i/length}$ are the impedance and admittance per unit length).

While experiments have yet to be done with more than two contact points, the above equations (Equations (45) and (46)) can be generalized to an arbitrary number of equally spaced contact points. For *N* contacts and a total strip length *L,*

$$I_o(s) = 2(N-1) \cdot V_o(s) \sqrt{\frac{Y_i^{total}}{Z_e^{total}}} \tanh\left(\kappa(s) \frac{L}{2(N-1)} \right), \tag{47}$$

and

$$\bar{\rho}(s) = \frac{2(N-1)}{L \cdot W \cdot a} \frac{1}{s} V_o(s) \sqrt{\frac{Y_i^{total}}{Z_e^{total}}} \tanh\left(\kappa(s) \cdot \frac{L}{2(N-1)} \right). \tag{48}$$

Finally, the strain as a function of frequency can be expressed as

$$\varepsilon(s) = \alpha \frac{2(N-1)}{L \cdot W \cdot a} \frac{1}{s} V_o(s) \sqrt{\frac{Y_i^{total}}{Z_e^{total}}} \tanh\left(\kappa(s) \cdot \frac{L}{2(N-1)} \right), \tag{49}$$

where α is the strain to charge ratio of the conducting polymer. Equation (49) can be used to guide the selection of strip length and number of electrical contact points given a required strain at a given frequency.

3.5. Conclusions

The results and model in this chapter bring conducting polymer actuators another step towards being well modeled engineering materials. The first measurements of the voltage along the length of a conducting polymer strip demonstrate that the conductivity and geometry play an important role in the charging rate of long actuators in electrolyte.

At high frequencies or very short times, the applied voltage propagates faster along a strip with low resistance than a strip with high resistance. At these short times the double layer capacitance of the actuator system is effectively short circuited and the potential distribution depends on the relative resistance of the polymer and of the electrolyte. At low frequencies or very long times, the strip equilibrates to the applied voltage.

The model developed describes the voltage, current, and charge density along the strip as a function of both position and the Laplace frequency variable *s*. The model matches the experimental results beautifully at very short times for strips with a single contact point and correctly predicts the steady state behaviour. The behavior of strips with two contact points is also is reasonably well modeled, with errors that are probably due to experimental setup limitations. Future work must be directed towards validating the model at intermediate frequencies either by developing a time domain representation of the model or by experimentally measuring the polymer transfer function.

Finally, the model can be used as a design tool for conducting polymer actuators. With the extended model that describes a strip with an arbitrary number of electrical

contact points, the designer can calculate how the strain will vary as a function of both the frequency and as a function of the number of attachment points.

Reference List

1. Davies, B. and Martin, B. Numerical inversion of the Laplace transform: a survey and comparison of methods. Journal of Computational Physics. 1979; 33:1-32.

2. Della Santa, A., De Rossi, D. and Mazzoldi, A. Performance and work capacity of polypyrrole conducting polymer linear actuator. Synthetic Metals. 1997; 90:93-100.

3. Della Santa, A., DeRossi, D. and Mazzoldi, A. Characterization and modeling of a conducting polymer mucle-like linear actuator. Smart Materials and Structures. 1997; 6:23-34.

4. Madden, John D. Conducting Polymer Actuators, Ph.D. Thesis. Cambridge, MA: Massachusetts Institute of Technology; 2000.

4. Derivation of Trimorph Equations

Conducting polymer actuators are generally operated in a liquid electrolyte solution. In the diffusive elastic model, ions from the solution are driven into or out of the polymer by creating a high or low concentration in the surface double layer. In many cases, bimorph deflection is used to amplify the fairly small active polymer strains (~1-2%) (Pei and Inganas, 1992a; Smela, Inganas, Pei and Lundstrom, 1993; Smela, Inganas and Lundstrom, 1995; Jager, Smela and Inganas, 1999; Smela, 1999; Della Santa, Mazzoldi, Tonci and De Rossi, 1997; Mazzoldi, Della Santa, and De Rossi, 1999; Otero, Rodriguez, Angulo and Santamaria, 1993; Otero and Sansinena, 1995; Kaneto, Min, and MacDiarmid, 1996; Pei and Inganas, 1992b).

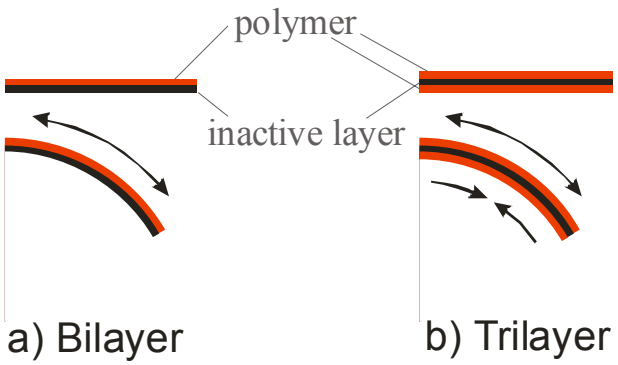

Figure 4.1: Structure of (a) bilayers and (b) trilayers. In a typical bilayer, one layer actively expands and contracts while the second layer does not change dimension. The expanding and contracting layer causes a bending of the device. In a typical trilayer device, the middle layer does not chance dimension while the upper and lower layers undergo opposing motions; if the upper layer expands, the lower layer contracts and vice versa. Arrows indicate the direction of expansion or contraction.

Motion in bimorphs is caused by the expansion or contraction of a thin polymer layer relative to a second thin inactive layer (Figure 4.1). Trimorphs or trilayer devices[1] (with one polymer layer expanding, a central inactive layer, and another polymer layer contracting, Figure 4.1b) have also been built for operation in liquid electrolyte (Otero and Sansinena, 1995; Otero and Huerta, 2000; Otero and Cortes, 2003; Mazzoldi and others, 1999) or for operation in air using a central ionically conducting gel layer (Madden, Cush, Kanigan, Brenan and Hunter, 1999; Wallace, G. G., Ding, J., Zhou, D. and Spinks, G. M., 2002; Kaneto and others, 1996; Sansinena, Olazabal, Otero, Fonseca and De Paoli, 1997; Lewis, Spinks, Wallace, De Rossi and Pachetti, 1997).

For a bimorph, a separate electrode, typically stainless steel or platinum, must be used to complete the electrochemical circuit. The two polymer electrodes in the trilayer devices remove the need for a mechanically inactive electrochemical counter electrode. Also, because the polymer electrodes act as ion reservoirs, the electrolyte is only needed to transport ions and not to store ions and hence it can be made extremely thin. Therefore, the overall actuator volume can also be made smaller.

Equations that relate the deflection of bimorph strips to the geometry and expansion of the polymer layer were derived by Pei and Inganas in 1992 (Pei and Inganas, 1992a; Pei and Inganas, 1992b). No papers have yet been published presenting equations for conducting polymer trimorph deflection. Furthermore, no equations

[1] The term trimorph and trilayer are used interchangeably in this thesis.

relating bimorph or trimorph force to the charge in the conducting polymer have been published.

This short chapter presents for the first time derivation for equations of deflection and force for a trimorph conducting polymer actuator. The equations in this chapter are used to model the trimorphs built in Chapter 5 and Chapter 6.

Derivation of Trimorph Deflection and Force Equation

We begin with a flat beam of uniform cross-sectional area along its entire length (Figure 4.2). The beam is made up of three layers: the top and bottom layer are made of a conducting polymer material that expands or contracts when ions enter or leave. The middle layer can be either a solid or a gel electrolyte (that is ionically conducting but electronically insulating).

For the purposes of the derivation, we will assume that the ion flux into the beam is uniform along its length. In particular, non-uniform charging effects due to any resistive drops in potential (such as those discussed in Chapter 3) along the length of the beam are ignored.

The beam has a length L and width W. The center layer has a total thickness of $2h_g$ and a Young's modulus of E_g. Each polymer layer (the two polymer layers form the outer layers of the beam) has a thickness of h_p and a Young's modulus of E_p (the total thickness of the beam is $2h_p + 2h_g$).

Following the assumptions made for bimorph deflection (Pei and Inganas, 1992b), we assume that the beam bends with uniform curvature so the strain is given by:

$$\varepsilon(y) = K \cdot y \,, \tag{1}$$

where ε is the strain, K is the curvature of the trimorph, and y is the distance from the line of zero strain in the direction normal to the surface. As a result of the beam symmetry, the y origin ($y = 0$) is at the center and so the beam thickness goes from $y = -(h_p + h_g)$ to $y = +(h_p + h_g)$.

The sum of the torques on the beam must always balance to zero and so we write:

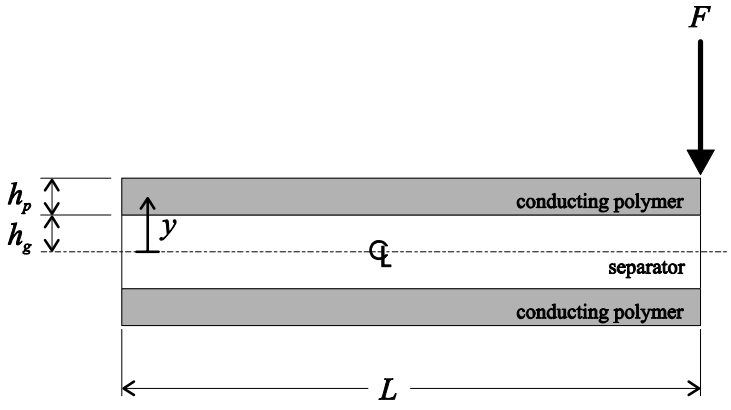

Figure 4.2: Geometry of the trimorph. A force F is applied at the end of the trimorph. The conducting polymer layers each have a thickness of h_p and the separator has a total thickness of $2h_g$. The trimorph has a length L and a width W (into the page). y is the distance from the center line.

$$\sum_i \tau_i = 0\,, \tag{2}$$

where the τ_i are the torques applied to the beam either by internal stress or by external forces. At small curvatures, for a two dimensional elastically deformed beam with a force F applied at its end,

$$\sum_i \tau_i = \int \sigma(y)\cdot W \cdot y \cdot dy + F \cdot L = 0\,, \tag{3}$$

where σ is the internal stress due to the elastic deformation. The material properties

$$\sigma_g(y) = E_g \varepsilon_g(y), \tag{4}$$

and

$$\sigma_p(y) = E_p \varepsilon_p(y) + E_p \alpha \rho\,, \tag{5}$$

can be substituted, where E_p and E_g are the elastic moduli of the polymer and center layer, ε_p and ε_g are the local strain of the polymer and center layer, α is the strain to charge ratio, and ρ is the charge density in the polymer[2]. The dimensions for the gel and polymer layers can also be substituted and the torque balance equation (3) is written

$$0 = \int_{-h_p-h_g}^{-h_g} \left[E_p K y^2 - E_p \alpha \rho y\right] dy + \int_{-h_g}^{h_g} E_g K y^2 dy + \int_{h_g}^{h_p+h_g} \left[E_p K y^2 + E_p \alpha \rho y\right] dy - F \cdot L\,, \tag{6}$$

where we have substituted the constitutive equation $\sigma = E_p(\varepsilon + \alpha\rho)$ for the stress strain relationship of the conducting polymer (α is the strain to charge ratio and ρ is the volume charge density). The substitution $\rho = \rho_{upper\_layer} = -\rho_{lower\_layer}$ has been made[3] because the charge densities in the upper and lower polymer layers are equal and opposite[4] ($\rho_{upper\_layer} = -\rho_{lower\_layer}$).

Integrating equation (6) and solving for the force we find

$$F = C_{spring} \cdot K + C_{charge} \cdot \rho\,, \tag{7}$$

where

$$C_{spring} = \frac{2WE_p}{3L} h_g^3 \left[\left(1 + \frac{h_p}{h_g}\right)^3 - 1 + \frac{E_g}{E_p}\right], \tag{8}$$

[2] The assumption is being made for the polymer layer in equation (5) that the charge density does not vary across the thickness of the material.

[3] Because of the substitution, the charge density term in the first integral has a minus sign while the charge density term in the third integral has a positive sign.

[4] In fact the charge density used is really a change in charge density. As derived, a charge density of zero is the charge density at which the beam is straight (and both conducting polymer layers have the same absolute charge density).

and

$$C_{charge} = \frac{E_p \alpha}{L} W h_g^2 \left[\left(1 + \frac{h_p}{h_g} \right)^2 - 1 \right]. \tag{9}$$

Two special cases are of interest: first, the case of zero force being applied at the end of the beam (free deflection) determines the maximum electrochemical deflection and second, the case of zero displacement at the end of the beam (the beam is clamped at both ends) determines the maximum electrochemically induced force.

For zero force ($F = 0$), the curvature / (charge density) ratio is:

$$\frac{K}{\rho} = -\frac{C_{charge}}{C_{spring}} = -\frac{3\alpha}{2h_g} \left[\frac{\left(1 + \frac{h_p}{h_g} \right)^2 - 1}{\left(1 + \frac{h_p}{h_g} \right)^3 + \left(\frac{E_g}{E_p} - 1 \right)} \right], \tag{10}$$

or making the substitutions $e = \frac{E_p}{E_g}$ and $\gamma = \frac{h_p}{h_g}$ to simplify the equations we find the curvature / (charge density) ratio to be

$$\frac{K}{\rho} = \frac{3\alpha}{2h_g} \left[\frac{(1+\gamma)^2 - 1}{(1+\gamma)^3 + (1/e - 1)} \right]. \tag{11}$$

We can likewise calculate the expected force for the case of zero deflection by setting the curvature to zero and solving for the force / (charge density):

$$\frac{F}{\rho} = C_{charge} = \frac{E_p \alpha}{L} W h_g^2 \left[(1+\gamma)^2 - 1 \right], \tag{12}$$

where we have again made the substitutions $e = \frac{E_p}{E_g}$ and $\gamma = \frac{h_p}{h_g}$.

As will be seen in Chapter 5 and Chapter 6, the trimorph equations describe the experimental results well and can serve as a tool for the design of new actuators that meet specific force and displacement requirements.

Reference List

1. Della Santa, A., Mazzoldi, A., Tonci, C. and De Rossi, D. Passive mechanical properties of polypyrrole films: a continuum poroelastic model. Materials Science and Engineering C. 1997; 5:101-109.

2. Jager, E.W.H., Smela, E. and Inganas, O. On-chip microelectrodes for electrochemisty with moveable PPy bilayer acutators as working electrodes. Sensors and Actuators B. 1999; 56:73-78.

3. Kaneto, Keiichi, Min, Yonggang, and MacDiarmid, Alan G., inventors. Conductive polyaniline laminates. US5556700. 1996 Sep 17.

4. Lewis, T.W., Spinks, G.M., Wallace, G.G., De Rossi, D. and Pachetti, M. Development of an all polymer electromechanical actuator. Polymer Preprints. 1997; 38:520-521.

5. Madden, J.D., Cush, R.A., Kanigan, T.S., Brenan, C.J. and Hunter, I.W. Encapsulated polypyrrole actuators. Synthetic Metals. 1999; 105:61-64.

6. Mazzoldi, A., Della Santa, A., and De Rossi, D. Conducting polymer actuators: Properties and modeling. Osada, Y. and De Rossi, D.E., editors. Polymer Sensors and Actuators. Heidelberg: Springer Verlag; 1999.

7. Otero, T.F. and Cortes, M.T. Artificial Muscles With Tactile Sensitivity. Advanced Materials. 2003 Feb 17; 15(4):279-282.

8. Otero, T.F. and Huerta, P. Electrochemistry and Conducting Polymers: Soft, Wet, Multifunctional, and Biomimetic Materials. Abstracts of Papers of the American Chemical Society. 2000 Mar 26; 219:372-COLL.

9. Otero, T.F., Rodriguez, J., Angulo, E. and Santamaria, C. Arificial muscles from bilayer structures. Synthetic Metals. 1993; 55-57:3713-3717.

10. Otero, T.F. and Sansinena, J.M. Artificial Muscles Based on Conducting Polymers. Bioelectrochemistry and Bioenergetics. 1995 Oct; 38(2):411-414.

11. Pei, Q. and Inganas, O. Conjugated polymers and the bending cantilever method: electrical muscles and smart devices. Advanced Materials. 1992a; 4(4):277-278.

12. Pei, Q. and Inganas, O. Electrochemical Application of the bending beam method. 1. Mass transport and volume changes in polypyrrole during redox. Journal of Physical Chemistry. 1992b; 96(25):10507-10514.

13. Sansinena, J.M., Olazabal, V., Otero, T.F., Fonseca, N.P. and De Paoli, M. A solid state artificial muscle based on polypyrrole and a solid polymeric electrolyte working in air. Chemical Communications. 1997; 7:2217-2219.

14. Smela, E., Inganas, O., Pei, Q. and Lundstrom, I. Electrochemical Muscles:Micromachining fingers and corkscrews. Advanced Materials. 1993; 5(9):630-632.

15. Smela, E., Inganas, O. and Lundstrom, I. Controlled folding of micrometer-size structures. Science. 1995 Jun 23; 268:1735-1738.

16. Smela, E. A microfabricated moveable electrochromic "pixel" based on polypyrrole. Advanced Materials. 1999; 11(16):1343-1345.

17. Wallace, G.G., Ding, J., Zhou, D., and Spinks, G.M. Ionic Liquids: An Elixir for Inherently Conducting Polymer Based Artificial Muscles. World Congress on Bioartificial Muscles 2002; Albuquerque, New Mexico.

5. Trimorphs in Liquid Electrolyte

The experiments in this chapter describe trimorph structures (Figure 5.1) that operate in liquid electrolyte[1]. A variety of design ideas were tried which improve the understanding of trimorph actuators and of conducting polymer actuators in general. The model presented in Chapter 4 is found to match nicely the experimental results presented. Combined with results from trimorphs operating in air (Chapter 6), the results in this chapter show that the model is valid and can be used in the designing these actuators. An overview of bimorph and trimorph structures built by other groups is also given in Chapter 4.

Of particular novelty in this chapter is the initial development of stacked trimorph actuators. Borrowing on Nature's muscle design with many actuators acting in parallel, test devices were built with three and with eight trimorphs moving in parallel. As expected, force increases when trimorphs are stacked. Stacking is thus a good tool for scaling up forces without sacrificing the large trimorph displacement.

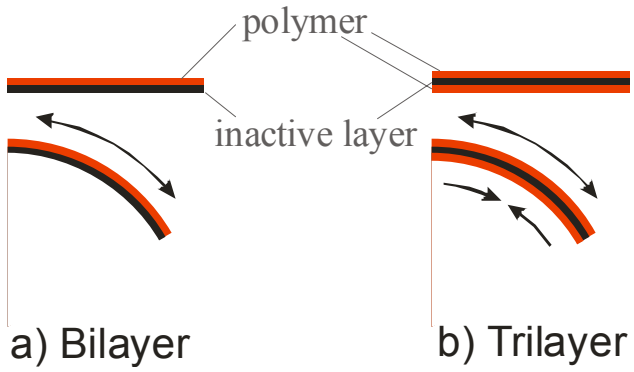

Figure 5.1 Structure of (a) bilayers and (b) trilayers. In a typical bilayer, one layer actively expands and contracts while the second layer does not change dimension. The expanding and contracting layer causes a bending of the device. In a typical trilayer device, the middle layer does not chance dimension while the upper and lower layers undergo opposing motions; if the upper layer expands, the lower layer contracts and vice versa. Arrows indicate the direction of expansion or contraction.

In the development of the stacked actuators, one advantage and one potential pitfall were noticed. The stacked actuators have lower resistance than an equal number of trimorphs operating independently. As will be described, the short distance through the electrolyte between the polymer in adjacent trimorphs reduces the resistance and should increase the response rate to an applied voltage. The potential pitfall to avoid is the construction of stacked trimorphs without fully independent trimorph motion. If care is not taken, trimorphs that are too rigidly coupled interfere mechanically with each other and reduce force and displacement.

The lessons learned in the chapter about manufacturing are applied in the next chapter for the more careful construction and analysis of trimorphs that operate in air. The initial experiments on stacking of actuators presented here are not pursued further in this thesis but are now the subject of ongoing research by another student in the Bioinstrumentation Laboratory.

[1] Through this chapter the words trimorph and trilayer and the words bimorph and bilayer are used interchangeably.

5.1. Experimental

Polypyrrole was electrochemically deposited onto a glassy carbon cylinder from a 0.05 M tetraethylammonium hexafluorophosphate 0.05 M pyrrole solution in propylene carbonate. Deposition was done at –40 °C at a current density of around 1.25 A/m^2 (0.125 mA/cm^2). The thin films (8 to 50 μm) were peeled from the beaker. The glassy carbon cylinder was masked to make films of a variety of lengths and widths. Typical sizes for films are 20-25 mm wide by 210 mm long.

Trilayers were fabricated using a flexible two part polyurethane adhesive[2] to attach sheets of polypyrrole to a central inactive layer. The inactive layer is either a thin sheet of polyethylene teraphthalate[3], a thin porous paper[4], or a nylon mesh[5]. The polyurethane adhesive was spread into a thin uniform layer to coat the central layer and polypyrrole sheets were adhered to each side. The assembly is typically clamped to give uniform thickness. Once the polyurethane cures, strips can be cut from the large (typically 25 mm by 210 mm) sheet to make the smaller trilayers for testing or for construction of stacks of trilayers. A schematic showing some of the dimensions of the trimorphs is drawn in Figure 5.2.

5.2. Trimorphs with a central adhesive only

The first and the simplest trilayers built consisted of two layers of conducting polymer film separated by a layer of polyurethane. To make them, a polypyrrole film was laid out on a flat surface and a flat blade was used to apply as uniform as possible a layer of two component polyurethane. While these trilayers showed good displacement the radius of curvature of the trilayers was non-uniform because of the varying thickness of the central polyurethane layer. The thickness usually varied by several hundred micrometers. Several different types of adhesive were also tried but with little improvement in uniformity.

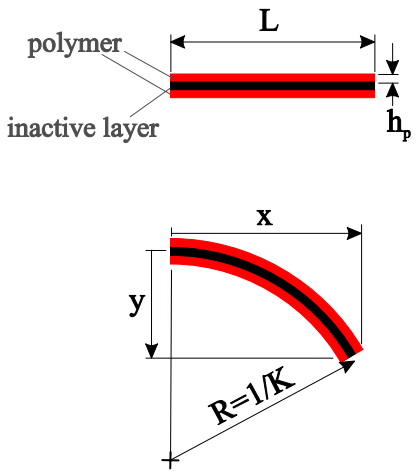

Figure 5.2: Dimensions of trilayer and trilayer deflection.

It was clear from the first set of trilayers that were fabricated that an improved method was required to give reproducible and consistent results. In particular, to ensure uniform curvature, the central inactive layer needs to be of consistent thickness. The curvature uniformity also depends on an even polypyrrole thickness but this is well controlled by the electrochemical synthesis process.

There are several possible routes to better thickness control. First, the

[2] Kalex Polyurethane, Elementis, Belleville, NJ, Part number 04022.
[3] Mylar sheet 0.9 μm to 25 μm thick, Goodfellow.
[4] Kodak lens paper cleaner, 40-50 μm thick, Kodak.
[5] Nylon mesh 67 μm thick, Hanes.

uniformity of the adhesive layered could be much improved by spreading the adhesive with a mechanized instrument rather than by hand. A spray coating could also be used (and was investigated) but the thickness of the spray coating must be great enough to prevent electrical contact between the two conducting polymer layers. Sufficient thickness could either be achieved by using a spray that creates a consistent thick layer or by applying multiple thin layers. If the conducting polymer layer is flat, the adhesive layer could also be spin coated.

5.3. Trimorphs with a central separator sheet

Another alternative for manufacturing films is to use a thin insulating film between the layers of conducting polymer. The assembly can the be clamped with flat plates to achieve more uniform thickness without risk of short circuiting the two polymer films.

The first of these trimorphs were made with polyethylene teraphthalate (PET) films[6] with thicknesses between 0.9 μm to 25 μm. The polymer was attached with adhesive to both sides of the PET films (Figure 5.3). While the adhesive cured, the layered assembly was clamped between two flat plates. Such clamping did not work without a separator (adhesive only) because it pushed the polymers films together. DV (digital video) tape was also tried as a central layer because it is thin (4 μm) and has good mechanical properties. When finished the total trimorph thickness includes the thickness of the polymer films, the insulating film, and usually between 40 and 60 μm of adhesive.

Yet another fabrication sequence uses a porous material as the separation layer (Figure 5.4). One layer of conducting polymer film is laid down on a flat teflon surface. Tissue paper or a nylon mesh is laid on top of the film as the separator and polyurethane adhesive was spread over the mesh. A layer of conducting polymer was placed on top and the entire assembly was clamped between two flat teflon plates to spread the polyurethane evenly. The porous middle layer improves the thickness uniformity by allowing the adhesive to redistribute more easily before curing.

Photographs of some trilayer actuators and a stack of trilayers (discussed in Section 5.5) that were built are shown in Figure 5.5.

Measures of total angular deflection, deflection rate, and curvature to charge ratio are made using deflections over half cycles or complete cycles. Such measures allow comparison of different actuator designs in spite of changes in geometry. The curvature

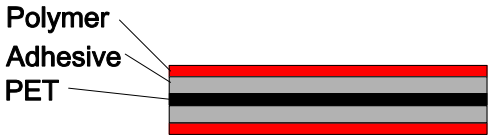

Figure 5.3: PPy / polyurethane / PET / polyurethane / PPy trilayer construction. Typical thickness for the layers are: polymer (PPy) = 10-20 μm, PET = 25 μm, Adhesive = 25-50 μm.

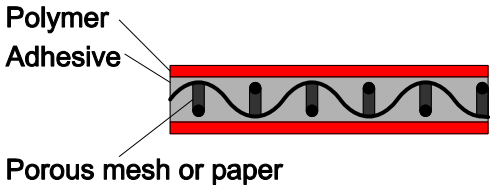

Figure 5.4: PPy / polyurethane and porous separator / PPy trilayer construction.

[6] From Goodfellow, Cambridge, England. The tradename is Mylar.

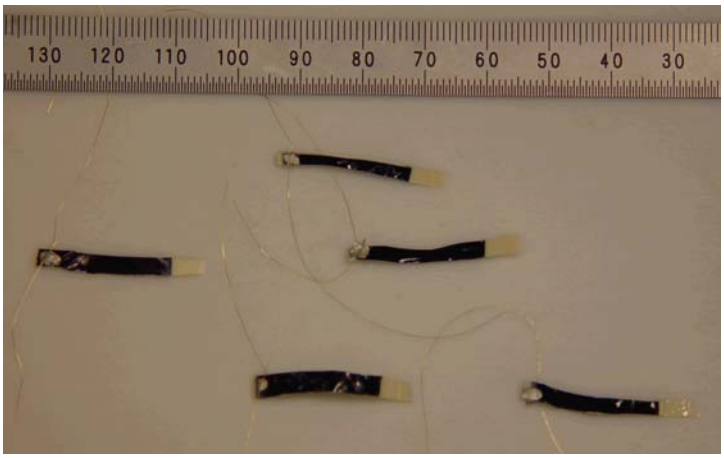

A)

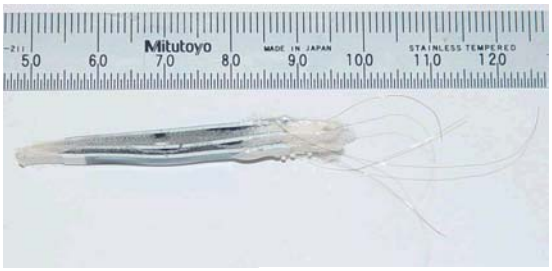

B)

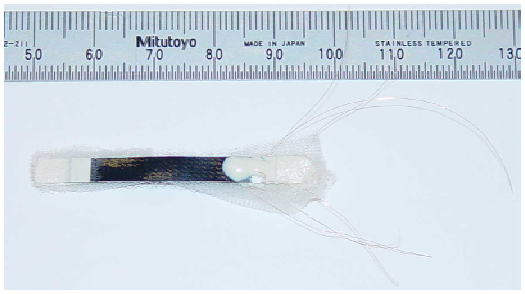

C)

Figure 5.5: Photographs of trilayers. A) Polyurethane cneters. B) and C) Three trilayer stack with mylar and polyurethane centers (rulers in mm).

to charge ratio of the actuator trilayers is particularly important as it gives a normalized measure of the ability to deflect. A larger curvature to charge means more displacement per unit of charge and faster displacement for a given current.

5.4. Displacement Results for Typical Trimorphs

Table 5-1 lists the properties of the samples from the two best designs using (1) a tissue paper separator or (2) a DV tape (PET) separator. Curvatures were calculated using measured angles and the length of the bending strips[7]. It can be seen from the error bounds on the total thickness (±12 μm and ±1 μm) that the thickness uniformity has been much improved.

The results in the table are both for 1 V waveforms applied to the trimorphs. In 5s, the tissue trimorph deflected by 45°. In 10s the DV tape trimorph deflected by 90°. While the deflection is large for the DV tape, the charge transferred is considerably larger

[7] Curvature is given by $K=\Theta/L$, *where* Θ is the angle of deflection, and L is the length of the trilayer.

for the tissue trimorph. As a result, the curvature to charge ratio of the tissue trimorph is smaller than for the DV tape.

A model for the deflection of conducting polymer trimorphs is derived in Chapter 4. The expected curvature to charge density ratio is given by:

$$\frac{K}{\rho} = \frac{3\alpha}{2h_g}\left[\frac{(1+\gamma)^2 - 1}{(1+\gamma)^3 + (1/e - 1)}\right], \qquad \textbf{(1)}$$

where K is the curvature, ρ is the ionic charge density, α is the strain/charge ratio of the polypyrrole[8], γ is the ratio $\frac{h_p}{h_g}$ with h_p and $2h_g$ the thickness of the polymer and center layers, and e is the ratio of the polymer to gel Young's moduli. The equation for deflection is cast as the ratio of curvature to charge density so that comparisons between triilayers with different geometries can be made more easily.

According to equation (1), the thinner film (DV tape) should give larger deflections per unit charge. The larger γ (h_p/h_g) combined with a considerably thinner center layer gives a better mechanical advantage.

Measurement Errors and Model Validity

For both films however, the measured curvature to charge ratio is only barely within the error bounds of the ratio predicted by equation (1) (for the tissue trimorph, the error in the experimental measurement overlaps with the error in the predicted value). The large variation in film thickness is the major contributor of the prediction error for the tissue trimorph. Even with clamping, measured film thickness differed by up to 23 μm. Some small wrinkles in the films made accurate measurement difficult because the micrometer used has a diameter of ~6 mm. Within the 6 mm diameter, the measured film thickness is maximum thickness rather than the average thickness. Thicknesses are therefore an upper bound rather than an estimate of mean value and the curvature to charge ratios calculated with equation (1) will tend to err on the low side as is observed.

The difference between the predicted and measured curvature to charge ratios underlines the importance of developing a uniform manufacturing technique to produce predictable bending. In spite of the large errors, the model is close to agreeing with the experimental results. It should be emphasized that no free parameters were used to fit the model. All the variables used in the calculations are either direct geometrical measurements or are taken from other independent experiments. If the model and experiment are to be compared properly, the trimorph dimensions must be consistent along the entire length. Much more consistent results which strongly support the model are achieved in the next chapter using liquid salt based gel electrolytes.

[8] $\alpha = 1 \times 10^{-10}\ m^3C^{-1}$ for polypyrrole in a tetraethylammonium hexafluorophosphate in propylene carbonate electrolyte (Madden, John, 2000).

	Tissue Trimorph	DV Tape Trimorph
Total trilayer thickness	<161-184 μm	<96±1 μm
PPy film thickness (h_p)	26±6 μm	14±1 μm
Center thickness ($2h_g$)	<109-132 μm	<68±2 μm
Immersed Length (L)	23±1.0 mm	17±1.0 mm
Width (W)	4.0±0.2 mm	3.7±0.2 mm
PPy Volume	2.4×10^{-9} m^3 ±13%	0.88×10^{-9} m^3 ±18%
Max deflection (and average rate)	45° (9°/s)	90° (9°/s)
Maximum curvature	34 m^{-1}±10% (5 s @ 1 V)	90 m^{-1}±10% (10 s @ 1 V)
Charge to reach max curvature	0.029 C	0.0194 C
Curvature / charge ratio	**1170 C^{-1}m^{-1}**±10%	**4640 C^{-1}m^{-1}**±10%
Predicted curvature / charge*	**700 C^{-1}m^{-1}** (424 to 1140 C^{-1}m^{-1})	**3380 C^{-1}m^{-1}** (2210 to 4670 C^{-1}m^{-1})
Calculated using the trilayer equation derived in Chapter 4 with $\alpha = 1.3\pm0.3 \times 10^{-10}$ m^3/C, $E_{separator} \approx E_{polyurethane} \approx 10$ MPa, and $E_{ppy} = 100$ MPa (in propylene carbonate).		

Table 5-1: Comparison of trimorphs made using tissue and DV tape separators. The curvature to charge ratio and the measured curvature to charge ratio for both trimorphs are only just within the error bounds using the measured experimental parameters. Total trilayer thickness is given as an upper bound because the surfaces were sometimes wrinkled and the calipers measured only the maximum thickness at several locationson the trimorphs. Errors are calculated using uncertainties in the measurement but do not include the possibility that the strips are in fact thinner due to wrinkling.

5.5. Forces from Stacked Actuators

The stress/charge ratio must be also be considered in the design of trimorph actuators. Where the strain/charge ratio gives the displacement under constant load (isotonic), the stress/charge ratio gives the force when there is no displacement (isometric). The modeled stress/charge ratio is given by[9]:

$$\frac{F}{\rho} = \frac{E_p \alpha}{L} W h_g^2 \left[(1+\gamma)^2 - 1 \right], \qquad \textbf{(2)}$$

where F is the force, ρ is the charge density, α is the strain/charge ratio, E_p is the conducting polymer modulus, L is the length of the strip, h_g is the thickness of the gel layer, and γ is the ratio h_p/h_g. Very crude measurements of force under constant load (using small weights) showed that individual trimorphs ($W \approx 5$ mm, $L \approx 25$ mm) exert forces of about 1 mN. To build devices that apply larger forces, strategies are needed to scale up the maximum loads.

An arrangement of many trimorphs pushing or pulling in parallel increases the force without sacrificing displacement (a photograph of a 3 trimorph stack is shown in Figure 5.5, page 72). To prove that parallel stacks of trimorphs do generate more force, one stack of three trimorphs and another stack of eight trimorphs were built.

[9] See Chapter 4, Derivation of the Trimorph Equations.

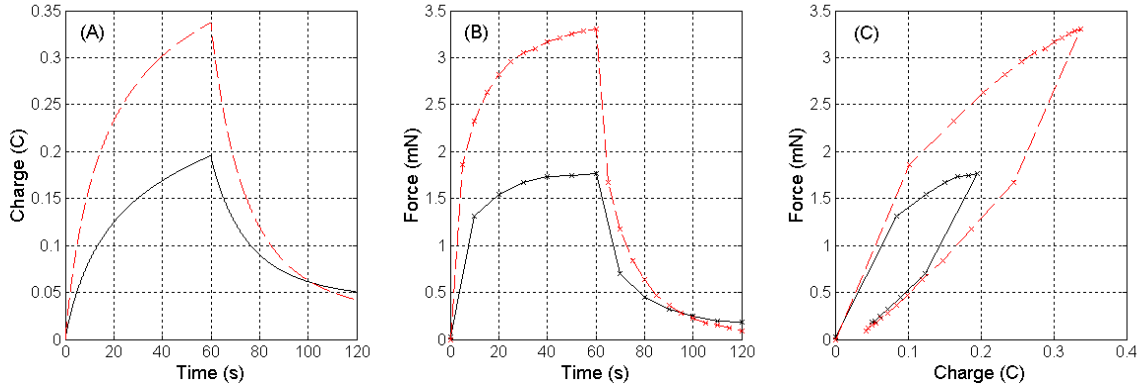

Figure 5.6: Plot of (A) Charge vs. Time, (B) Force vs Time, and (C) Force vs. Charge for a three level (triplet) stacked trilayer assembly. Upper (dashed) line: 1V square wave. Lower (solid) line: 0.5V square wave. Three trilayers were arranged mechanically in parallel. The hysteresis observed in the force vs. charge plot is due in part to the motion of the bilayer during the tests.

Experiments measured force and charge through time so the force to charge ratio can be compared to the model.

Figure 5.6 shows charge and force for the three layer (triplet) stack at applied voltages of 0.5 V and 1.0 V. The force is plotted vs. charge in Figure 5.6C. Force reaches 3.3 mN at 0.34 C after 60 s which gives an average force to charge ratio of 9.7 mN/C.

According to the model, the force versus charge relationship should be linear. The considerable hysteresis in the plot is due at least in part to motion of the trimorphs during activation. While both ends of the actuator were immobilized in clamps, the trimorphs did bend slightly during charging and discharging. Such bending will reduce the force generated as the force gets balanced between the external load and internal stress.

In Figure 5.7, the charge and force are shown for an eight layer (octet) stack at ±2 V. The average change in force over several cycles is 8.2 mN with an average change

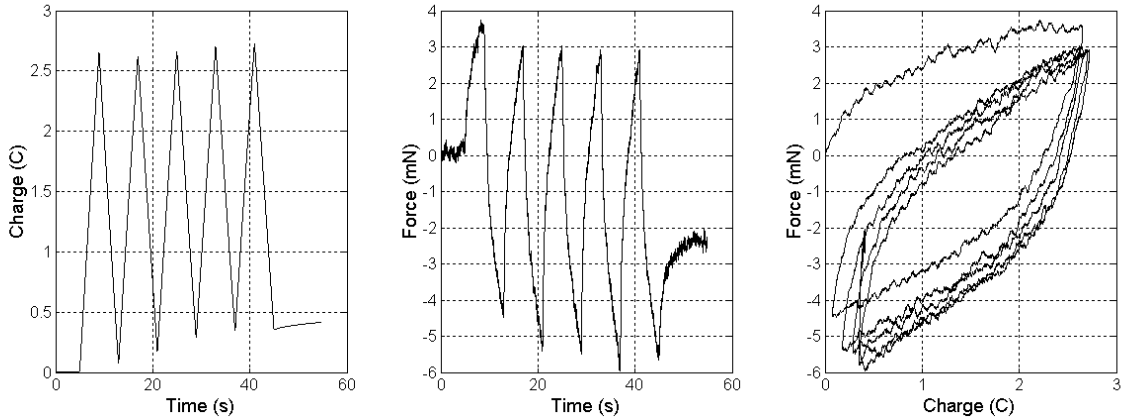

Figure 5.7 Plot of (A) Charge vs. Time, (B) Force vs Time, and (C) Force vs. Charge for a eight level (octet) stacked trilayer assembly. Eight trilayers were arranged mechanically in parallel. The considerable hysteresis observed in the force vs. charge plot is due in part to the motion of the bilayer during the tests.

in amount of charge of 2.47 C. The force to charge ratio of 3.3 mN/C is much lower than the force to charge ratio of the stacked triplet even though the maximum force is higher, which helps to explain why the octet force is not 8/3 times the triplet force.

The octet's lower force to charge ratio is a consequence of the thinner insulating layer. According to the model, force increases with the insulating layer thickness and the triplet insulating thickness is more than twice the octet insulating thickness (dimensions of the trimorphs are given in Table 5-2).

Comparison of Experiment to the Model

To check the model validity, the experimental and the model force to charge ratios are presented in Table 5-2. The model ratios are calculated using the dimensions of the single trimorphs from which the stacks were built. Values for the strain/charge ratio and the modulus of the polymer were measured in independent experiments.

The increase in peak force from 3.3 mN for the triplet to 8.5 mN for the octet suggests that the stacking of trimorphs is increasing the force. However, because of the different trimorph geometries and different amount of charge transferred, the force from the two different stacks should not scale with the number of trimorphs in each stack.

But if the force a given stack does scale with the number of trimorphs, the force to charge ratio of the stack should equal the ratio for the individual trimorph. The measured force to charge ratios of the stacks do fall within the error bounds of the model trimorph ratios. Admittedly, the error bounds are large but the numbers are in the right ballpark.

The large range for the calculated model ratios (due to large variations in trimorph thickness) and the considerable hysteresis in the experimental force versus charge curve leave some uncertainty about the model validity. If the model is to be useful, the manufacturing tolerances must be improved to give more predictable results. Both the force and the curvature to charge ratios are very sensitive to variation in trimorph thickness. Improvements in manufacturing do give results that more closely match the trimorph response and are presented in the next chapter.

	Stacked Triplet	Stacked Octet
Active length	21±0.5 mm	23±0.5 mm
Width	5±0.2 mm	4±0.2 mm
Polymer thickness	20±2 μm	20±2 μm
Trilayer total thickness	190±40 μm	100±6 μm
Change in charge	0.2 C	2.47 C
Change in force	1.8 mN	8.23 mN
Measured Force to Charge	**8.8 mN/C**	**3.3 mN/C**
Model Force to Charge (error bounds)	**5.0 mN/C (1.3 to 14.4 mN/C)**	**1.95 mN/C (0.7 to 4.4 mN/C)**
For the model calculations, $\alpha = 1.3 \pm 0.3 \times 10^{-10}$ m^3/C; $E_p = 100$ MPa.		

Table 5-2: Force to Charge Ratios of Trilayers and Trilayer Stacks. The dimensions of the triplet and octet stacks are given for reference.

Validity of the Model

With the experimental results presented in this section, there is good reason to believe that the model is valid and that increasing force by stacking of actuators is an effective method for scaling the actuator load. But the results are not yet conclusive. Further experiments on bilayers operating in air (Chapter 6) agree with the model within better tolerance and give more solid evidence that the model is valid.

5.6. Reduced Resistance in Stacked Configurations

The resistance of a stacked configuration is lower than that expected for the same number of isolated trilayers connected electrically in parallel. If the resistance of the stacked trilayers is the parallel impedance of isolated trilayers, the total resistance should be:

$$R_{total} = \frac{1}{\sum \frac{1}{R_{singlet}}} = \frac{R_{singlet}}{N} \qquad \textbf{(3)}$$

where R_{total} is the total resistance, $R_{singlet}$ is the resistance of a single trilayer, and N is the number of stacked trilayers. The single trilayer resistance is 174 Ω. The total resistance of a five stack should then be 35 Ω, more than double the measured resistance of 14 Ω.

Figure 5.8 illustrates why the resistance is lower than might be expected for a stacked assembly. The predominant resistance for a single trilayer is the resistance through the surrounding electrolyte. In a stacked arrangement, there is a second ionic current pathway through the electrolyte between the stacks. Because the current path is shorter, the resistance is reduced. If the resistance along the current path between adjacent stacked layers is R_i the total stack resistance is given by:

$$R_{total} = \frac{1}{\frac{1}{R_{ext}} + \frac{N-1}{R_i}}. \qquad \textbf{(4)}$$

The equation can be solved for R_i to find the internal resistance between the trilayers. If R_{ext} is taken to the same for the five layer stack as it is for the single trilayer (174 Ω above), the internal resistance R_i is found to be[10] 61 Ω.

Reduction of the resistance speeds polymer actuator charging when a voltage is applied. Even if the double layer charging is very fast, the diffusion current that flows generates a voltage drop across the resistance. If the resistance is lower, the voltage drop is lower and the voltage applied at the polymer double layer is increased. With higher double layer voltage, there is greater concentration change and so higher concentration gradients at the polymer surface. The result is faster strain rates. At this point, no good quantitative studies have been conducted to prove that the strain rates are faster. Currents are however higher for a stack of trimorphs than for an equal number of independent

[10] Actually, the resistance of the system is due to the electrolyte resistance, the contact resistance of electrodes to the polymer, and the series resistance of the leads. To properly model the resistance the contact and series resistances should also be measured and taken into account.

trimorphs. There is good incentive then to minimize the resistance between trimorphs by stacking the layers as closely as possible.

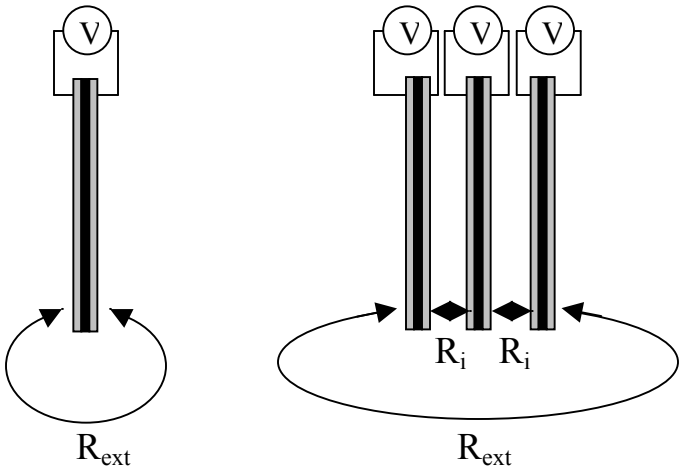

Figure 5.8 Electrolyte resistance path for a single trialyer and for stacked trilayers. In the stakced trilayers, the resistance through the electrolyte between the stacked trilayers is very small because the path length is very short.

5.7. Mechanical Interference

In the first few stacked actuators that were made, movement of the whole actuator was reduced because the trimorphs were not able to move freely. The importance of flexible hinge points at one end of the stacked arrangement is shown in Figure 5.9. If the ends of the bilayers do not have flexible attachment points, the trilayers must change shape and in some cases buckle to accommodate any motion. The reshaping of the actuators reduces the force and the displacement that can be generated.

To maximize force and displacement in parallel actuator arrangements, short uncoated segments of nylon mesh were left between the ends of the actuators and the lower attachment "bar".

The perfect attachment points would allow unhindered rotation at the joint and no translation. Side to side translation of the joints leads to hysteresis in both the position and the force (as shown in Figure 5.10) which makes control of position or of force more

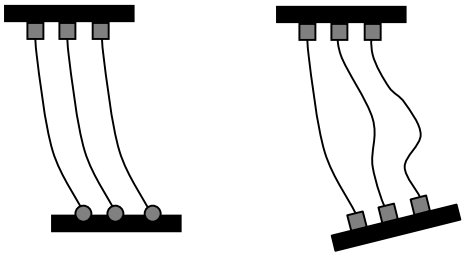

Figure 5.9 The effect of flexible vs. inflexible attachments for stacked trilayers. With flexible hinge points (left, hinges shown as circles) at one end, all of the trilayers bend at the same time. With inflexible attachment points (right, attachment points shown as squares) at both ends, some of the trilayers buckle to accommodate the motion.

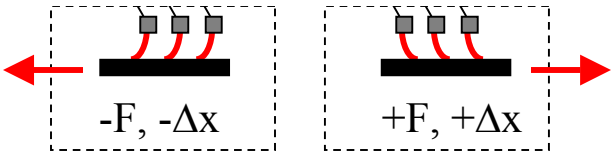

Figure 5.10 Hysteresis in Motion Caused by Translation in the stacked trilayer attachment points. If the attachments allow translation as well as rotation, then a change in direction of the force will create a hysteresis in the position.

difficult. If there is hysteresis, the displacement and the force generated by the addition or removal of charge can be accurately described by the trilayer force and displacement equation derived in Chapter 4.

5.8. Recruitment

In nature, individual bundles of muscle fibers within a muscle can be fired. The amount of force can be tailored by simultaneously activating fewer or more of the bundles. A similar strategy can be used for parallel arrangement of stacked trilayers. By controlling the potential on individual trilayers in the stack or on groups of trilayers within the stack, the force and displacement can be varied considerably.

Unlike nature's muscle, the stiffness of a stacked trilayer actuator cannot be changed. In individual natural muscle fibers, there is a considerable change in stiffness from the relaxed (unstimulated) state to the activated state. There is no similar change in stiffness that can be achieved with the individual trilayers. The large change in stiffness around joints achieved using antagonistic muscle co-contraction is also not reproducible with stacked actuators.

5.9. Conclusions

This chapter has begun to explore the design and fabrication of trimorph devices, tracing the development of trimorph actuators that were built to be used in a liquid electrolyte.

The results of position and force measurements are compared to the model equations described in Chapter 4 and, while the error bounds are admittedly large, the results do match the model without the use of any free parameters. The large errors in the model predictions reveal a need for more uniform manufacturing techniques if the engineering of trimorphs is to be predictable.

The comparison of the experimental results with the model is the first for a trimorph mode that I have seen. Of greater importance, the model is the first to predict not only position but also forces. As discussed in Chapter 4, the bimorph equations presented by Pei (Pei and Inganas, 1992; Pei and Inganas, 1993) did not include a term for a force at the free end of the beam.

While the trimorphs themselves tradeoff the force generated by a linear actuator for the greater displacement of the bending beam the stacking of actuators presented here demonstrates a method for increasing the force from the trimorph actuators without compromising the displacement. A benefit of the stacked geometry is a lower resistance because of shortened distance that ions travel through the electrolyte. However, to get maximum benefit, care must be taken to reduce mechanical interference between the motions within the stack.

In the next chapter, the discussion of trimorphs continues and describes trimorphs operating in air instead of liquid.

Reference List

1. Madden, J. Conducting Polymer Actuators. Cambridge, MA: MIT; 2000 Sep.Hardbound.

2. Pei, Q. and Inganas, O. Electrochemical Application of the bending beam method. 1. Mass transport and volume changes in polypyrrole during redox. Journal of Physical Chemistry. 1992; 96(25):10507-10514.

3. Pei, Q. and Inganas, O. Electrochemical applications of the beam bending method; a novel way to study ion transport in electroactive polymers. Solid State Ionics. 1993; 60:161-166.

6. Fabrication and Analysis of Three Layer Polymer Actuators Operating in Air

Introduction

An actuator is most versatile as an engineering tool if it can be adapted to meet varying requirements. Tailoring of an actuator for a given application is made simpler if there are good models to describe its behavior. Fabrication and packaging of the actuators should also be relatively easy if the actuator technology is to have maximum impact. This chapter describes the manufacture, testing, and modeling of trimorph (three layers: polymer, gel electrolyte, polymer) polypyrrole actuators that operate in air. A relatively simple construction procedure is demonstrated, and models are shown to predict response. These advances represent fundamental steps in demonstrating the effectiveness of conducting polymer actuators as general purpose, low voltage actuation materials.

A design by Wallace et al. was the starting point for the results presented in this chapter (Wallace, G. G., Ding, J., Zhou, D. and Spinks, G. M., 2002). Wallace et al. have manufactured a trilayer device with liquid salt gel electrolyte sandwiched between two conducting polymer layers. Wallace et al. fabricate their devices by electrochemically growing polypyrrole onto a gold coated solid electrolyte gel. Here, three layer trimorph devices were fabricated with a liquid salt gel electrolyte but without the need for gold coating. Computer video analysis synchronized with electrochemical data acquisition calculates the trilayer curvature. Plots of the curvature as function of charge show a strong correlation.

Predictions of the model for the displacement of the trimorphs developed in Chapter 4 compare very well with the experimental results. The good agreement between the experimental results and the model makes the fabrication of conducting polymer trilayer actuators much better understood.

Experimental

The conducting polymer polypyrrole was synthesized in a 0.05 M tetraethylammonium hexafluorophosphate, 0.06 M distilled pyrrole, and 1% by volume H_2O in propylene carbonate solution. Chemicals were used as received from Aldrich with the exception of pyrrole which was distilled before use. Nitrogen was bubbled through the solution as it was stirred for at least 30 minutes before use. The films were galvanostatically grown at 0.05 to 1.25 A/m^2 (0.125 mA/cm^2) onto a polished glassy carbon substrate (HTW Hochtemperatur-Werkstoffe GmbH, Gemeindewald, Germany) at –40 °C. Films were peeled from the glassy carbon using a razor blade and cut to size.

A liquid salt gel electrolyte was synthesized based on synthesis procedures described in Noda et al (Noda and Watanabe, 2000). Instead of 1-ethyl-3-methylimidazolium tetrafluoroborate liquid salt used by Noda et al., we used 1-butyl-3-methylimidazolium tetrafluoroborate ($BMIBF_4$). Equal molar parts of $BMIBF_4$ and 2-hydroxyethyl methacrylate were mixed. 2 mol % of the crosslinking agent ethylene glycol dimethacrylate and 2 mol % azo bis isobutyronitrile were added. The gel crosslinks when heated to 80 °C in an oven for 12 h. Gel conductivity was measured by

crosslinking the gel between two gold coated glass slides and was found to be 1.65 ± 0.2 × 10^{-4} S/m (impedance measurements of the gel are shown in Appendix A).

To construct the air operated trimorphs, a conducting polymer film was laid out on a 25 mm by 75 mm glass slide. A nylon mesh (60 μm thick, Hanes) was laid down on top and the liquid (non-crosslinked) gel mixture was poured over the mesh. Finally, a second layer of conducting polymer was laid down on top of the mesh and covered by a second glass slide. The two slides were clamped and placed for 12 h in an oven at 80 °C to crosslink the gel.

The operation of trimorphs in air was monitored and recorded using a Canon XL1S Digital Video Recorder so that motion could be compared to the model presented in Chapter 4. The camera was operated in a full field (non-interlaced) mode at 30 frames per second (resolution 720 by 480 pixels and between 0.15 and 0.2 mm/pixel at the actuator). The videos were transferred to computer and saved as uncompressed AVI files.

The silhouette of the trimorph was extracted from the videos and converted into an array of coordinate data points using the Matlab Image Processing Toolkit (Matlab code written to do the analysis is contained in Appendix C). A typical frame from a video is shown in Figure 6.1. The trimorph film is edge on to the camera and bends right and left during actuation. The rulers (units of millimeters) were included to allow easy calibration of the length scale. On the right hand side, there are two red LEDs that are alternately lit for each current or voltage waveform half cycle during experiments to simplify synchronization of the video images with electrochemical data.

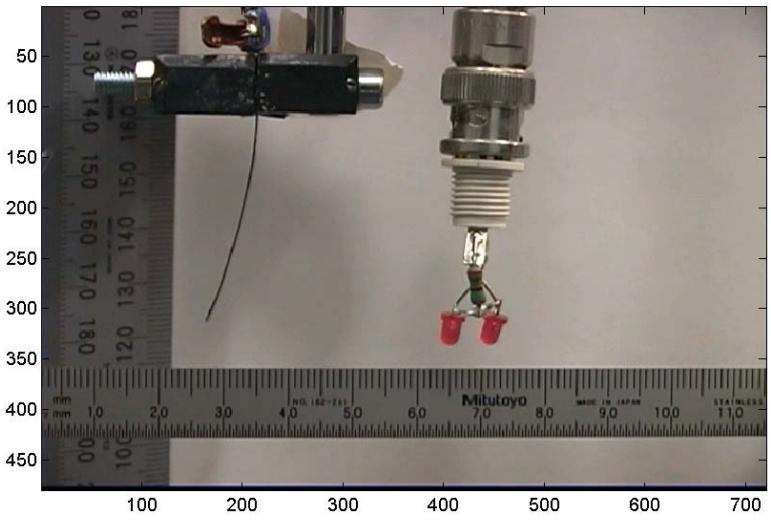

Figure 6.1: Single frame from the video of a deflecting trimorph in air. The two LEDs are used to signal the polarity of the applied potential. Rulers are marked in mm. Numbers along the outside edge of the image are scaled in pixels.

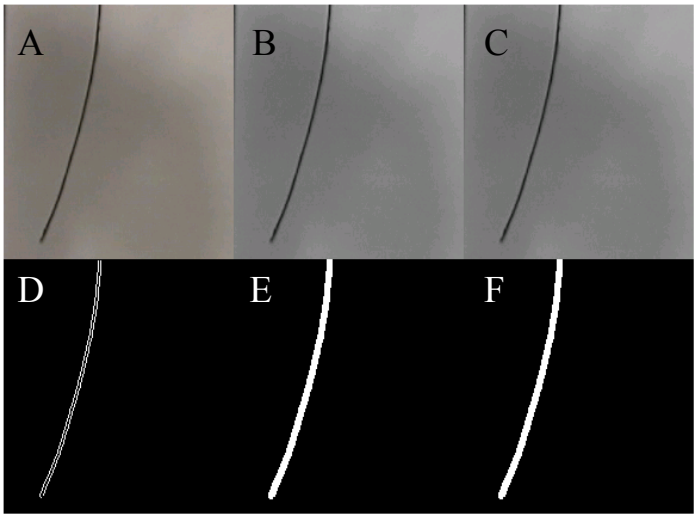

Figure 6.2: Series of images used to extract curvature from video of the deflecting trimorph. A) a subsection of the image is extracted to remove unwanted background. B) The image is converted to grayscale and C) the image is normalized in preparation for the gradient operation. Because the original image was primarily black and white already, there is little difference between the images A, B, and C. D) The gradient of the image is taken to find the edges of the trimorph strip and E) the edge points are dilated by a 3 pixel by 3 pixel square matrix to ensure that there are no gaps in the boundary. F) Any unfilled points in the interior of the bimorph are filled (in the image sequence shown, all the interior points were filled by the edge dilation and as a consequence images E) and F) are identical).

The original image has very little color and has good contrast between the background and the trimorph which simplifies extraction of the actuator location. For image processing, a smaller image is extracted (Figure 6.2A) and converted to grayscale to simplify and speed extraction of the trimorph (Figure 6.2B). Prior to edge detection, the image color map is rescaled (Figure 6.2C). Edge detection uses the Sobel method of approximating the gradient. The results of applying the edge detection algorithm are shown in Figure 6.2D. A threshold for edge detection was chosen so that the trimorph edge was detected while the variations in background (shadows) were not. After edge detection a dilation algorithm expands the points found to remove any gaps in the boundary of the trimorph (Figure 6.2E). In all the frames that were looked at manually, the expansion algorithm also filled in the region inside the edges because the trimorph is so thin. To be thorough, a filling algorithm searches for any points that may not have been filled (shown in Figure 6.2F, where because the points are all filled by the dilation (Figure 6.2E), the filled and unfilled images are identical).

The x and y coordinates of the strip in the final filled image are fit to the equation of a circle using a non-linear least squares minimization algorithm[1]. Curvatures that can

[1] The algorithm uses the Levenberg-Marquardt-Gauss-Newton method, see H.B. Nielsen: "Damping Parameter in Marquardt's Method", IMM-REP-1999-05, available on the web at: http://www.imm.dtu.dk/documents/ftp/tr99/tr05_99.pdf.

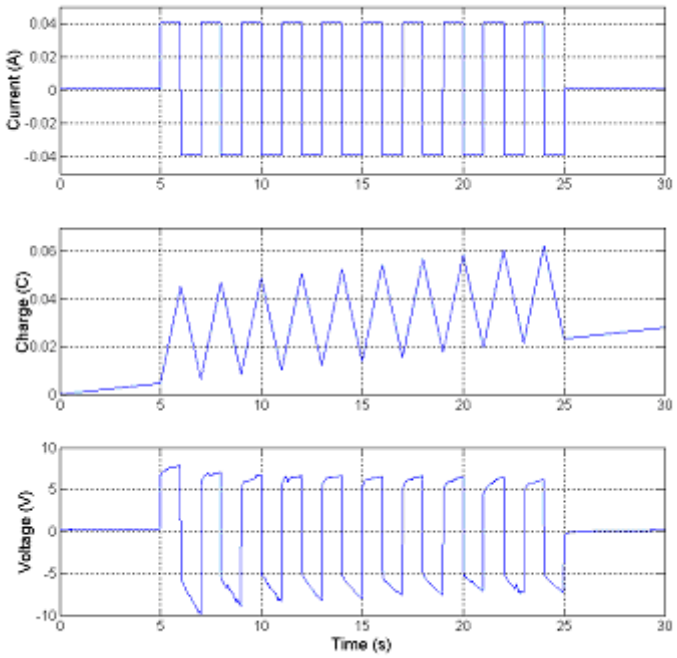

Figure 6.3: Current applied, charge (integrated current), and voltage measured during a trimorph beam bending test.

be compared to the theoretical bending equations presented in the next section of this chapter are calculated by inverting the radius[2].

For the data set presented here, the minimization algorithm did not converge for some radii larger than 2000 mm or for any radii[3] larger than 6000 mm. The very large radii correspond to frames in which the beam is very nearly straight and as a consequence an arc does not fit well to the extracted coordinates. Frames in which the radii did not converge are not thrown out as the curvature values (very close to zero) can still be used to calculate polymer actuator strains. Circles fit to the (x,y) coordinates of the bimorphs are shown in Figure 6.5 and Figure 6.6 (Figure 6.6 is an expanded view of Figure 6.5). Figure 6.7 shows the curvature (1/radius with units of m^{-1}) calculated by the image analysis plotted through time as the beam oscillates back and forth.

During testing, current square waves of different amplitudes were applied between the two outer polymer layers. Ions flow out of one layer (causing it to contract)

[2] The minimization algorithm uses a gradient descent method and it is therefore very important to start the algorithm with a guess that will descend to the true minimum. If the initial guess for the curve center is on the wrong side of the curve (for example if the initial guess for the center is placed on the convex rather than the concave side of the arc the algorithm will not converge to the proper value: the radius will tend to infinity as the origin moves further away from the curve). To aid in choosing the correct side of the strip for the placement of the curve center, the extracted data points are fit to a second order polynomial $y = a + bx + cx^2$, where a, b, and c are constant. The sign of c gives the sign of the curvature and so determines on which side of the arc the initial guess for the arc center should be placed. Once the bending beam coordinates have been extracted and an initial guess has been made for the center location, the minimization algorithm is used to find a best estimate of the center and radius.

[3] The number of iterations was limited to 100.

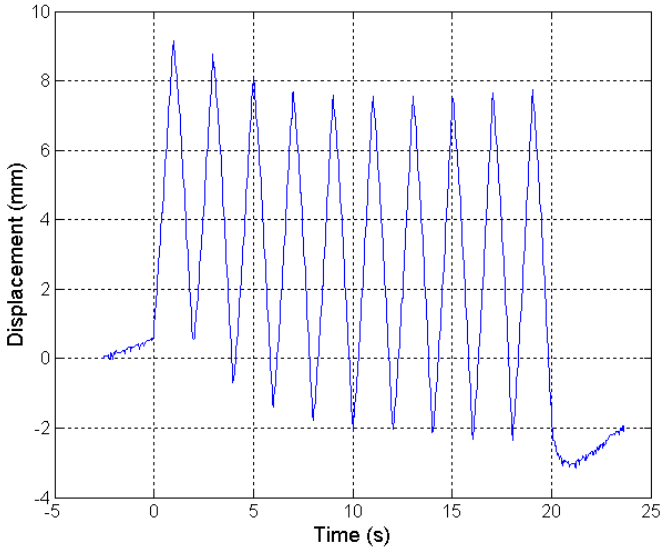

Figure 6.4: Displacement of the trimorph tip versus time for a bending trilayer polymer actuator in air. A 40 mA current square wave with a two second period is applied to the polymer electrodes as shown in Figure 6.3.

and into the other layer (causing it to expand). Typical experimental waveforms are shown in Figure 6.3. The measured displacement of the end of a 38 mm long strip is shown in Figure 6.4.

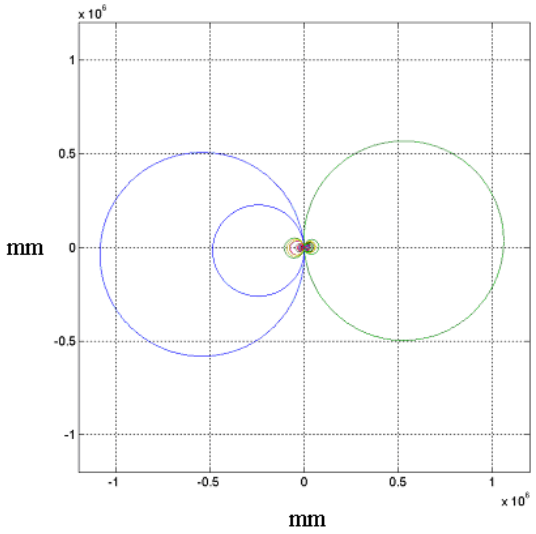

Figure 6.5: Large scale circles fit to the sequence of images of a deflecting trimorph strip (50 mA square wave). The maximum radius of curvature found in this image is 0.53×10^6 mm or 530 m. Note that the axes are marked at 10^6 mm increments.

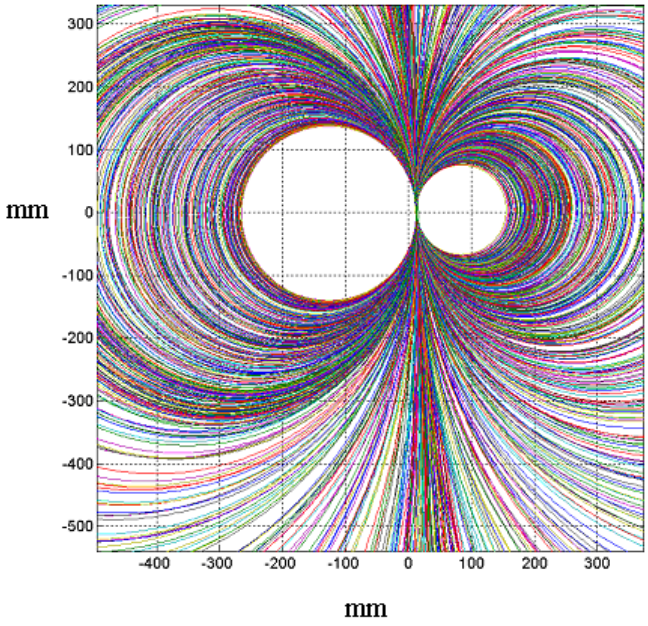

Figure 6.6: Expanded view of circles fit to the sequence of images for a deflecting bimorph. The time between adjacent circles is 1/30 s (the video frame rate). The minimum radius of the circles on the right of the image is 71.3 mm and of the circles on the left is 138.8 mm.

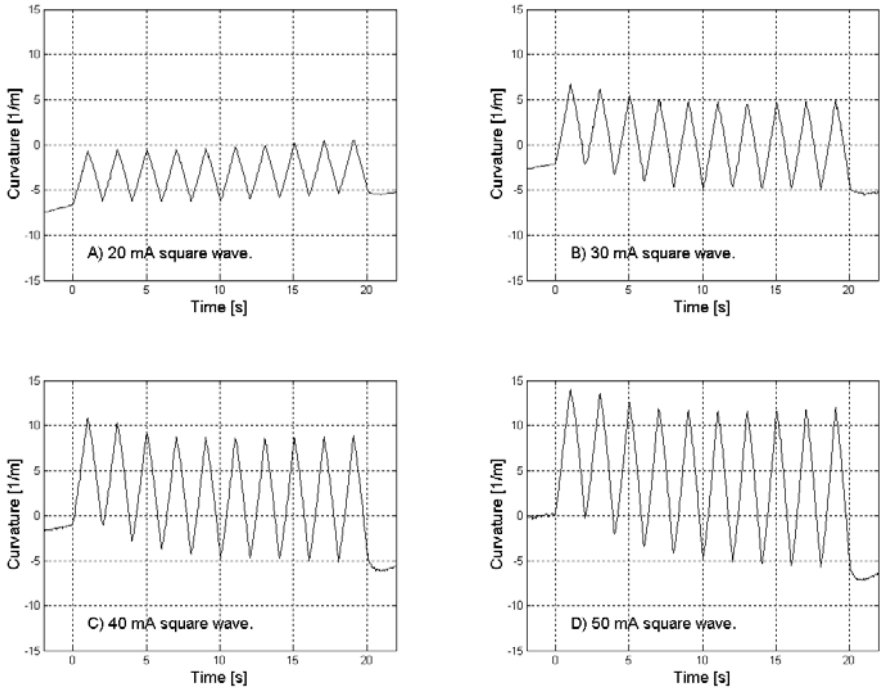

Figure 6.7: Curvature of a deflecting trimorph plotted versus Time for four different current square wave amplitudes. A) 20 mA current square wave. B) 30 mA current square wave. C) 40 mA current square wave. D) 50 mA current square wave.

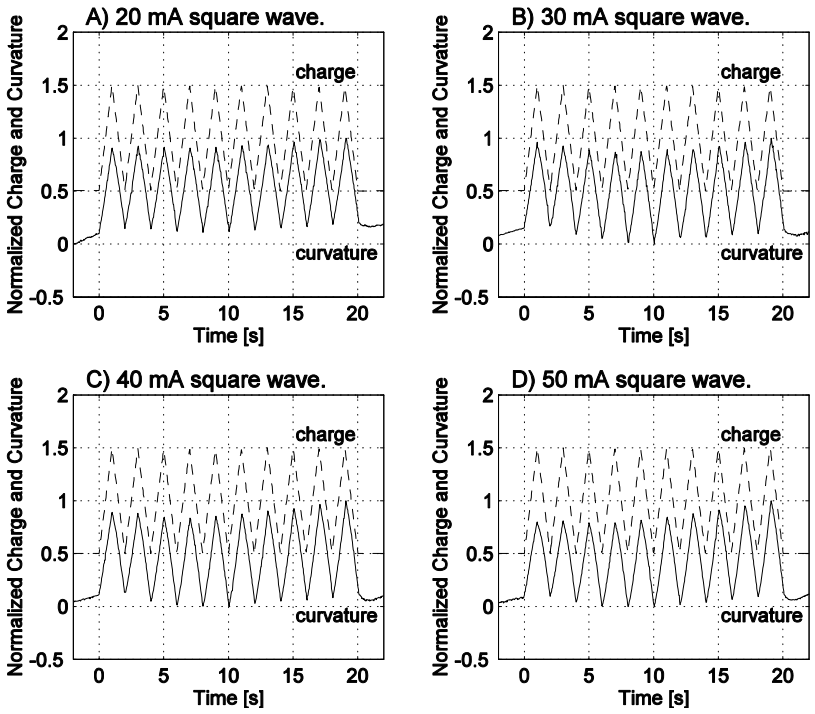

Figure 6.8: Normalized charge and normalized curvature vs. time. Both charge and curvature have been scaled to a peak to peak magnitude of 1 for easy comparison. The charge is offset by 0.5 (normalized units) for clarity. Linear trends over the entire data set (1st order) were removed prior to normalization to remove the effect of a small current offset and a small error in the current measurement on both charge and curvature.

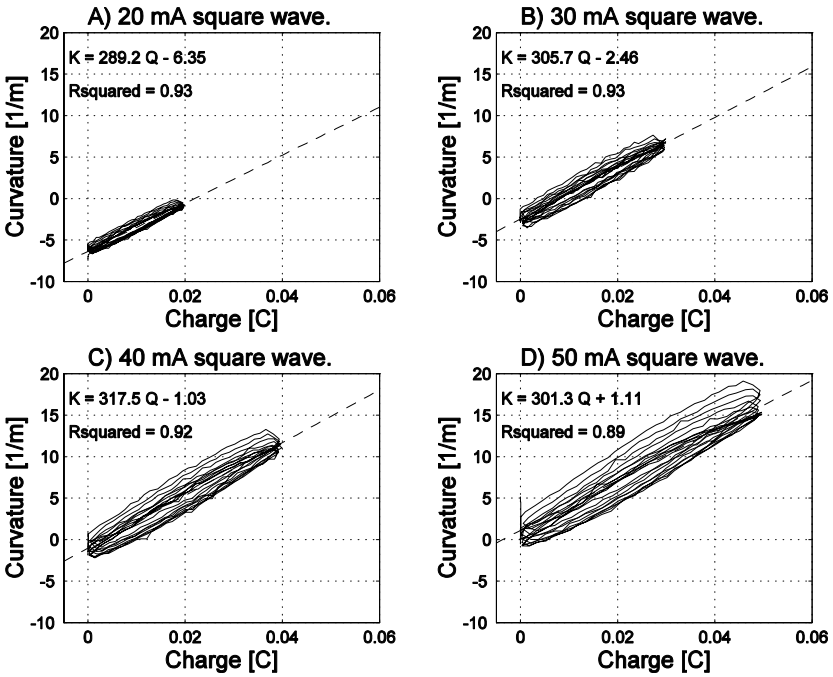

Figure 6.9: Curvature vs. Charge plots for different square wave current amplitudes. A) 20 mA. B) 30 mA. C) 40 mA. D) 50 mA.

The curvature can be related to the strain/charge ratio using the equations for the deflection of a trilayer. But first it is of interest to compare the charge vs. time plots with the curvature vs. time plots (Figure 6.8). The total charge and the curvature appear highly correlated.

To confirm that there truly is a relationship, we can plot the curvature as a function of charge as shown in Figure 6.9.

Shown below (Figure 6.10) is the variation in curvature / charge ratio (averaged over 10 cycles) as a function of the current square wave amplitude. The curvature / charge ratio increases up to 40 mA and then drops slightly.

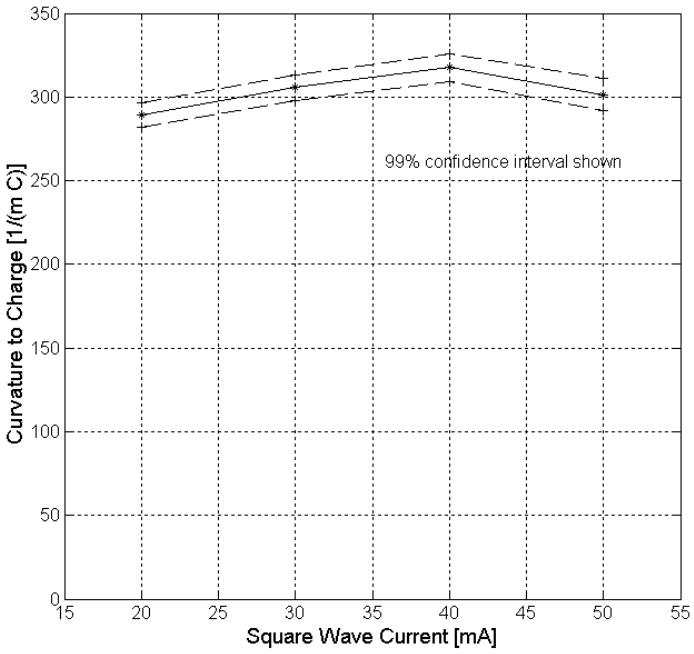

Figure 6.10: Curvature / charge ratio as a function of the current square wave amplitude. There is about a 10% variation in the measured curvature / charge ratios. Dashed lines show the 99% confidence interval for the linear fits shown in Figure 6.9.

Analyzing the Expected Curvature / Charge Density Ratio

The model derived in Chapter 4 predicts that the curvature / charge density ratio is given by:

$$\frac{K}{\rho} = \frac{3\alpha}{2h_g}\left[\frac{(1+\gamma)^2 - 1}{(1+\gamma)^3 + (1/e - 1)}\right], \qquad (1)$$

where K is the curvature, ρ is the charge density, $\alpha = 1 \times 10^{-10}\ m^3C^{-1}$ is the strain/charge ratio, γ is the ratio $\frac{h_p}{h_g}$ (h_p = 12 μm and h_{gel} = 104 μm are the thickness of the polymer and the gel layers), and e is the ratio of the polymer to gel Young's moduli $\frac{E_p}{E_g} = \frac{1GPa}{7.3MPa}$. The Young's moduli for the polymer and the gel and nylon mesh were measured in

independent experiments[4]. The strain/charge ratio was measured by J. Madden in his thesis (Madden, 2000).

Curvature / charge ratios found from the plots above (Figure 6.9) are converted to curvature / charge density by multiplying by the volume of one of the polymer strips (see Table 1). These curvature / charge ratios can be compared with the predictions of the model curvature calculated using the geometry and material properties of the strips.

Table 1: Measured and Modeled Curvature / charge and Curvature / charge Density Ratios. The volume of the strips is 12 μm × 38 mm × 6 mm.

Current Amplitude	K / Q [C^{-1} m^{-1}]	K / ρ [C^{-1} m^2]
20 mA	289	0.790×10^{-6}
30 mA	306	0.790×10^{-6}
40 mA	317	0.867×10^{-6}
50 mA	301	0.823×10^{-6}
Expt Mean	*303*	0.83×10^{-6}
Theory	*326* ±41	0.89×10^{-6} $\pm 0.08 \times 10^{-6}$

The model curvature / charge density ratio is 326±41 C^{-1} m^{-1} (with no free parameters fitted to the data). Error bounds are due to uncertainties in measurement of the geometry and material properties.

The mean experimental result is very close to the theoretically predicted result (7% difference in magnitude and within the errors of the theoretical calculation).

Conclusions

New actuators have been built that operate in air without the need for a liquid electrolyte solution. Video measurements of the motion of the trilayer actuators have been made and used to calculate curvature / charge density ratios.

The experimental curvature / charge density ratios closely match the theoretical calculations using only the geometric dimensions of the polymer actuator and independently measured material properties. As a consequence, the equations describing the deflection generated by polymer actuator muscles can be used as an engineering tool to create new actuators. If the force and displacement requirements of a design are known, the model can help determine the required geometry for the trimorph.

The trilayer operation in air also holds great promise for new engineering designs as it greatly simplifies the packaging of conducting polymer artificial muscle. By using a solid electrolyte, there is no need for a liquid electrolyte container. Force can be scaled up if need be by stacking trilayers one on top of each other without sacrificing large displacements (demonstrated in Chapter 5) or, as is done in the next chapter, by designing a trimorph that is considerably wider.

Future measurements will include a confirmation that the theoretical equations are also able to predict force output from trilayers accurately and that stacking of the trilayers will increase the force output without significantly compromising displacement. Work also remains to understand the actuator lifetime, the effect of ambient temperature on performance, and the energy efficiencies that can be achieved.

[4] Measurements of the gel properties are shown in the Appendix A "Measurement of Gel Electrolyte Properties".

Reference List

1. Madden, John D. Conducting Polymer Actuators, Ph.D. Thesis. Cambridge, MA: Massachusetts Institute of Technology; 2000.

2. Noda, A. and Watanabe, M. Highly conductive polymer electrolytes prepared by in situ polymerization of vinyl monomers in room temperature molten salts. Electrochimica Acta. 2000; 45:1265-1270.

3. Wallace, G.G. , Ding, J., Zhou, D., and Spinks, G.M. Ionic Liquids: An Elixir for Inherently Conducting Polymer Based Artificial Muscles. World Congress on Bioartificial Muscles 2002; Albuquerque, New Mexico.

7. Position Feedback Loop Using a Conducting Polymer Actuator and Strain Gage

Feedback control is often used in engineering to counteract the effect of unknown disturbances. In nature, mammals use feedback to regulate diverse functions including the cardiovascular system, hormone levels, body temperature, visual tracking, or position control. In a mechanical system, feedback control can change the basic response of the system; an active automobile shock absorber for example changes its stiffness and viscosity in response to driving conditions.

The work described in this chapter is an important step towards an all polymer position feedback loop. The mechanical feedback control of animals in nature is unique because all the elements of the feedback loop are made of similar high molecular weight materials. Mammalian muscle incorporates an actuator (the skeletomuscular fibers) and position and velocity sensing (the muscle spindle fibers). The muscle spindles send signals along the nerves to neurons in the spinal cord. The neurons are programmed to activate the muscles if there are sudden changes in the muscle position. When a physician taps the tendon of your knee, the sudden pull on the tendon causes the spindles to signal the neurons and the neurons invoke a muscle contraction to counteract the apparent extension. Just within the muscle bulk, nature includes energy storage (ATP, fatty tissue), information transmission (nerves), energy delivery (blood vessels), sensing (muscle spindles), and of course actuation.

Human engineering has yet to replicate a muscle with nature's full suite of capabilities. However the construction of a feedback loop with a conducting polymer actuator and conducting polymer strain gage is big step towards a muscle like system. With conducting polymer batteries, wires, and transistors, all of the elements needed to build an artificial muscle exist within a single class of man made materials. Conducting polymer muscles will one day be built with completely integrated feedback loops. Such muscles will not only be able to track a desired path but will also be able to regulate their own material properties such as stiffness and viscosity.

The actuator for the feedback loop described in this chapter is a conducting polymer trimorph. The trimorph is wider (100 mm) than it is long (30 mm) to give greater force, as is described in Section 7.2. The position sensor is a flexible fabric (Lycra[1]) coated with conducting polymer. When the fabric is stretched, the resistance of the coating changes. If the fabric is attached to the polymer muscle, the resistance of the fabric becomes a measure of the muscle position. A computer monitors the resistance and controls the voltage or current applied to the actuator to keep the resistance at a constant value.

This chapter describes the first demonstration of feedback using a conducting polymer strain gage and a conducting polymer actuator. When testing the feedback loop, limitations of both the actuator and the strain gage become apparent. As will be seen, the poor step response and the long settling time of the conducting polymer coated strain gages combined with the limited strain rate of the actuator mean that succesful operation is only possible at low frequencies. At low strain rates, a linear model can be used to predict the behaviour of the feedback system. Being the first feedback loop with

[1] Lycra is a trademark of Dupont Corp.

conducting polymer actuator and strain gage and the first modeling of such a feedback system, these trials mark an important milestone in the development of conducting polymer engineering.

The chapter first presents test results of work aimed at the fabrication of polypyrrole coated Lycra strain gages, largely following the construction methods of De Rossi and refined somewhat by Spinks (De Rossi, Della Santa and Mazzoldi, 1999; Spinks, Wallace, Liu and Zhou, 2003; Spinks, 2002; Spinks, G. G. Wallace and et al. 2002). After the section on strain gages, the fabrication of the higher force trimorph is described. In the final section, models of the feedback system are developed and the first results of feedback tests for step and ramp disturbances are presented.

7.1. Conducting Polymer Strain Gages

For most stretched materials, both longer length and smaller cross sectional area increase the resistance according to the formula $R = \rho L / A$, where ρ is the resistivity, L is the length, and A is the cross-sectional area. The change of resistance is used to advantage in the manufacture of strain gages.

The common metric used to compare strain gages, called the gage factor K, is defined as:

$$K = \frac{\Delta R / R}{\Delta L / L}$$

where R and L are the resistance and the length of the gage. Typical gage factors[2] for metal fall between 2-4 and for silicon can be as high as 50-150. For some applications, the maximum strain and the stiffness of the strain gage are also important parameters.

A high maximum strain is important to consider for gages to be used in a flexible actuator system. Spinks et al. have used coated Lycra gages at strains up to 100% (Spinks, Wallace, Liu, and Zhou, 2003). Conducting polymer actuator linear strains are at least a few percent and traditional gage materials (nickel, silicon) have maximum strains of a few tenths of a percent. In addition, a gage with low stiffness will impede the actuator motion less.

Strain gages based on conducting polymers were first reporeted by De Rossi, who used a fabric coating technique developed by Milliken Corporation to coat Lycra fabric with conducting polymer (De Rossi, Della Santa, and Mazzoldi, 1999; Kuhn and Kimbrell, 1989). When the coated Lycra is stretched the resistance changes. The high maximum strain, low stiffness, and conformability of the lycra strain gages make them good candidates for use as flexible strain gages and they have been incorporated into a number of research devices, including a position sensing glove and leotard suit (De Rossi, Della Santa, and Mazzoldi, 1999; De Rossi, D., Carpi, F., Lorussi, F., Mazzoldi, A., Scliningo, E. P. and Tognetti, A., 2002) and a knee sleeve worn to monitor excessive deceleration during sports (Wallace and Steele, 2001).

De Rossi measured gage factors of about 13 on chemically coated Lycra. He also found that the hysteresis of the strain gages varied considerably with the direction of the stretch. The Lycra used is a directional fabric with a much greater stiffness in one direction than in the other. A second group working on Lycra strain gages also found

[2] Gage factors are taken from product and technical data sheets at www.entran.com amd www.omega.com.

that gages stretched in the compliant direction have large hysteresis and are not useful for position measurement while gages stretching in the stiffer direction show far less hysteresis (Spinks, G. G. Wallace, and et al. 2002; Spinks, Wallace, Liu, and Zhou, 2003).

For this thesis, it was hoped that the materials and fabrication presented by De Rossi and Spinks were mature enough to be used immediately. However, in the experiments described below, several obstacles to the implementation of a reliable strain gage using conducting polymer coated Lycra are found. The poor step response and limited number of cycles before the response degrades form particularly big obstacles. At the end of the chapter, some new methods of manufacture are suggested that might improve the gages.

As is shown later in the chapter, in spite of the limitations, if the feedback is designed to keep the strain gage length constant in the face of low frequency external disturbances, the coated Lycra gages can be effective. The small length excursions may also extend the lifetime of the gages.

Fabrication of Strain Gages

To coat Lycra with chemically oxidized polypyrrole, two aqueous solutions are prepared (De Rossi, Della Santa, and Mazzoldi, 1999; Spinks, 2002; Kuhn and Kimbrell, 1989). The first solution is 0.02 M pyrrole and 0.006 M 1,5-Napthalenedisulfonic acid tetrahydrate. The second solution is 0.046 M of ferric (III) chloride. Equal volumes of each solution are mixed and poured into a container. The Lycra is immersed in the mixed solution and the container is immediately placed into a refrigerator at 4°C. The solution is stirred every 20-30 minutes and removed after 2 h. After deposition, the Lycra strips are rinsed with distilled water.

In an effort to improve the lifetime of the gages, some of the chemically coated strain gages were subsequently coated with electrochemically grown polypyrrole. The electrochemically grown polypyrrole has higher conductivity and better mechanical properties than the chemically oxidized polypyrrole. The electrochemical growth was done at –40°C in a solution of 0.05 M pyrrole, 0.05 M tetraethylammonium hexafluorophosphate, and 1 vol % water in propylene carbonate. Deposition was voltage controlled between 2 and 3 V versus the Cu counter electrode for 4 hours. Unfortunately, lifetime does not appear to be significantly different for chemically and electrochemically coated gages but the resistance of electrochemically coated gages is lower because of the thicker layer of polypyrrole.

Strain Gage Measurements

Measurements of the change in resistance as a function of position were made in both the flexible and the less flexible directions of the coated Lycra. Electrical attachments were made with alligator clips or by weaving fine gold wire directly into the lycra/polypyrrole composite fabric.

Measurements typical of the coated strain gages are shown in Figure 7.1. The left and the right plots in the figure are for different strain directions of the Lycra material. As can be seen, changes in the resistance of the coated fabric differ depending on the stretch direction. The more compliant direction has a much more useful response over

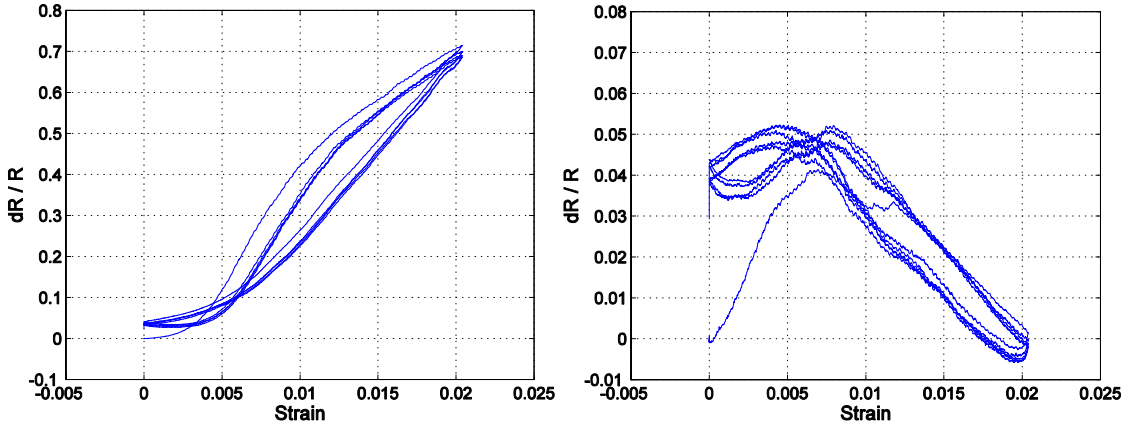

Figure 7.1: Strain gage of a double coated (chemically and then electrochemically coated) Lycra strain gage. Response at a strain rate of 10^{-3} /s (0.1 mm/s) in the more compliant (left) and in the less compliant (right) directions. The left plot is for lycra more compliant in the direction of the gage with a gage factor of around 42; in the flat section at low strain, the strain gage is slack. The right plot is for lycra which is stretchier in the direction perpendicular to the gage. The gages were not slack at any point in the measurement.

the range of a few percent strain and so all further results presented use the more compliant direction.

The gage factor varies considerably between individual samples. Age, location within the sample, and stretch history all affect the response. Freshly made gages or gages that were stored in well sealed containers have gage factors of between 6 and 10. Sample aging of double coated gages in some cases can give a marked increase in the gage factor: a gage factor of 60 was measured for one sample. The mechanism for the large increase in gage factor is not at all clear and as a consequence of the changes, each gage had to be calibrated before use. The changes in gage factor that I observed were not mentioned in the papers by De Rossi et al. or Spinks et al. but they paid little attention to lifetime issues.

Ramp Response

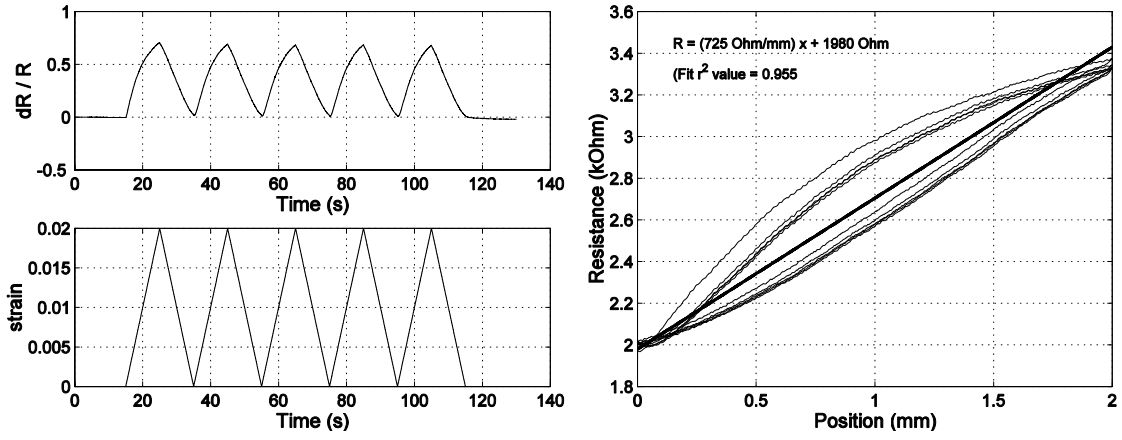

Figure 7.2: Ramp response (0 to 2 mm) of a 100 mm long polypyrrole coated lycra strain gage. Left: time response; Right Resistance versus Position. The straight line in the right hand plot is a linear fit to the data.

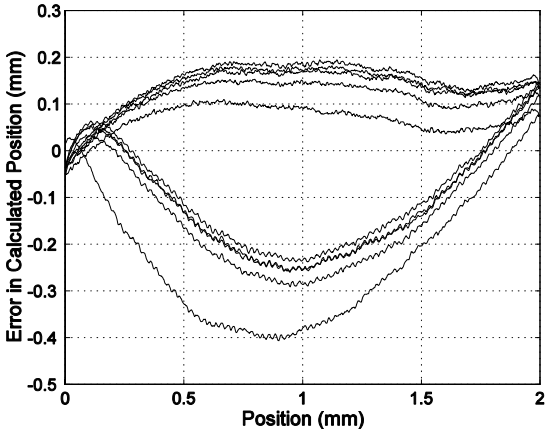

Figure 7.3: Error for the calibration of the strain gage shown in Figure 7.2. The maximum error over a 2mm ramp cycle is 0.4 mm.

Good responses to cycling position ramps are shown in Figure 7.2. The measurements shown are within the first 20 cycles for a chemically and subsequently electrochemically coated sample at a strain rate of 0.2 %/s. The ramp strain response is repeatable and gives a decent indication of position (gage factor = 36, $\Delta R = 725\Omega / mm \cdot \Delta x$, where x is the gage length). Using the linear fit to the resistance versus position curve to calculate the position, the maximum error is 0.4 mm or 20% of the total deflection over the five cycles shown (Figure 7.3).

Unfortunately, the repeatability does not last and the stretch history of the gage causes large changes in response. Lifetime tests of a sample undergoing a ~10% cycling ramp strain drifted by about 25% of the peak to peak response after 100 cycles and by over 100% after 1000 cycles. The shape of the response also varies with the number of cycles, sometimes becoming non-monotonic (giving two possible positions for any given resistance).

After several tens of cycles or cycles at strains of 5-10%, the response of the gage becomes erratic. Figure 7.4 shows the ramp response of a double coated strain gage to a ~1% cyclic extension after large strain cycles. The right hand plot of Figure 7.4 shows that the resistance (plotted vs. position) has become a useless predictor of the actual position.

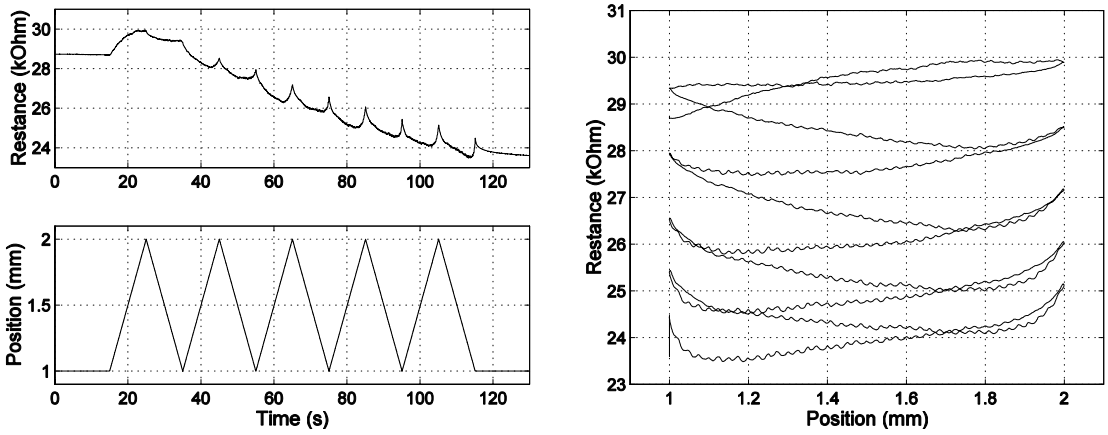

Figure 7.4: Bad strain gage response to a triangle wave position 1mm up and down at 0.1 mm/s

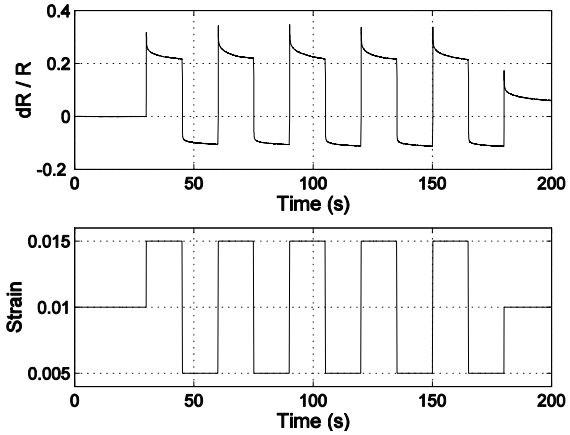

Figure 7.5: Step response of a polypyrrole coated lycra strain gage.

In conclusion, under slow ramped cycling (~0.1 %/s) the strain gages can measure the position. Hysteresis of the response limits the accuracy (in measurements shown here the maximum error was ~20% of the strain range) and the gage lifetime is limited to only a small number of cycles (around 30 or 40). Clearly there is a need for further development work and suggestions for directions are made later in the chapter.

Step Reponse

Like the ramp response, the step response can be repeatable over a small number of cycles. Figure 7.5 shows the step response to a 0.5% strain over 5 cycles. The considerable overshoot in the positive direction (extension) makes the measurement of position versus time difficult at short times. The overshoot for the step extension varies with step size and can be 60% of the steady state response. When stepping in the negative direction, there is no overshoot but instead a gradual decay to the steady state value. Moreover, for a large number of cycles, the repeatability of the response shown in Figure 7.5 does not last.

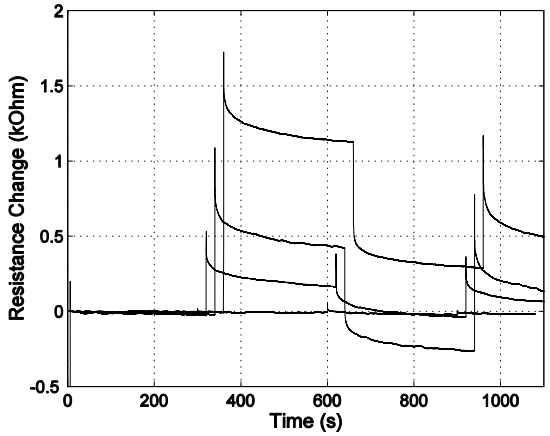

Figure 7.6: Response of a coated Lycra strain gage after more than 40 cycles to a positive and negative step of 0.01 mm, 0.1 mm, 0.3 mm and 0.5 mm (strain changes of ±0.01%, ±0.1%, ±0.3% and ±0.5%). The responses are each offset by 20 s for clarity. The response to the negative strain step is negative only for the 0.3 % step. Furthermore, the response to the second positive going step is considerably smaller than the response to the first positive going step.

Some of the erratic behaviour typical of gages after they have been cycled at 1% or 2% more than 40 or 50 times is shown is shown in Figure 7.6. The responses to strain changes of ±0.01%, ±0.1%, ±0.3%, and ±0.5% are superimposed to allow easy comparison. Steps in the positive direction show a large resistance spike followed by a slow decay. When the step direction is reversed, the 0.3% strain response is the only response to show a resistance lower than the starting resistance. Note also that the magnitude of the response to the second positive step (at $t \approx 900$ s) is much smaller than that of the first step.

Even at low cycle numbers, the overshoot in extension and the long settling time of the step response makes the conversion of gage resistance to position difficult. Improvements are needed before gage step responses are useful for strain measurement. As will be seen later in this chapter, during feedback tests for step changes, the control is able to restore the gage resistance but the gage length is not kept constant.

Stiffness

It is useful to know the stiffness of the gage as well as its resistive properties. A

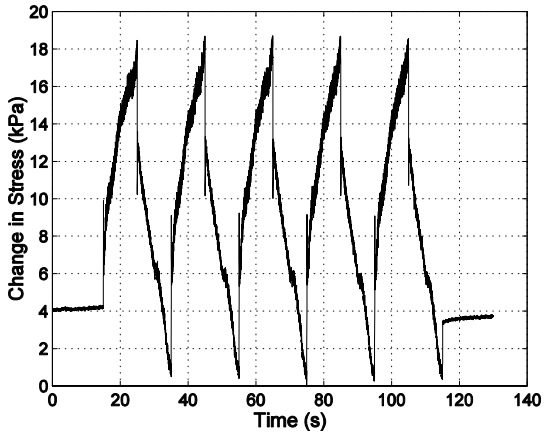

Figure 7.7: Stress Response of a polypyrrole coated Lycra strain gage at 0.2 mm/s. The Young's modulus of the strain gage is about 610 kPa.

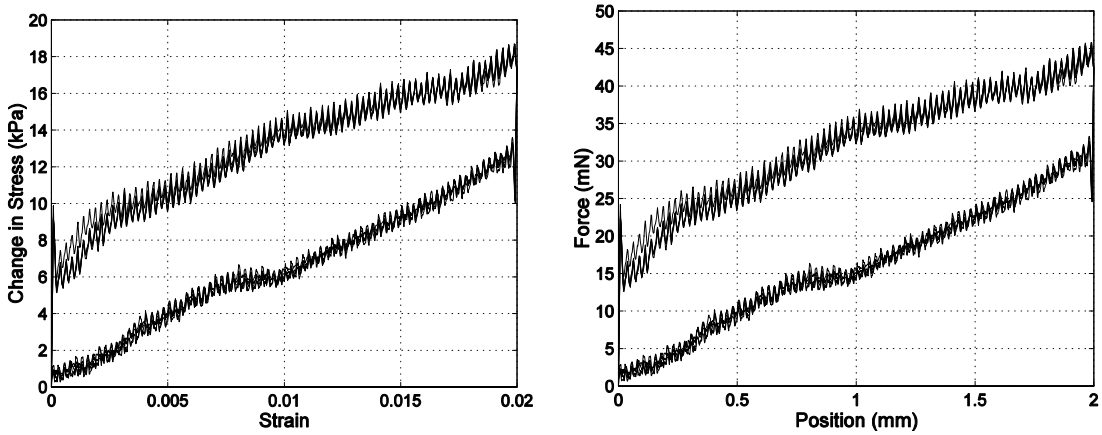

Figure 7.8: Stress vs. Position and Force versus Position for a coated lycra strain gage. The spring constant is approximately 14.5 mN/mm and the stiffness is 590 kPa. L = 100 mm, W = 4.9 mm, h = 0.5 mm. The high frequency ripple is noise from the force measurement.

gage with a high stiffness can obstruct the motion it is trying to measure. Figure 7.7 shows the stress response of a Lycra strain gage (100 mm long, 4.9 mm wide, and 0.5 mm thick) to a cyclic ramp position. Figure 7.8 shows the measured stress versus strain and the force versus position for the same data. The peak to peak force change is about 45 mN (including hysteresis) for a 2 mm position change. If the hysteresis is ignored, the stiffness is 590 kPa and the spring constant is 14.5 N/m. The polymer muscle used later in this chapter generates forces greater than 100 mN and is easily able to deflect the polymer by more than 2 mm.

Limitations for Application of Coated Lycra Strain Gages

In conclusion, polypyrrole coated strain gages can provide some measure of position (or strain). Step responses are not accurate. Overshoot in extension at short times and slow decay after motion make the measurements very time dependent. Furthermore, after about 40 cycles, the responses are no longer repeatable.

But, for low frequency ramps the strain gages can provide a satisfactory measure of position. As long as the total number of cycles is limited to only 20 or 30, the response is repeatable and good enough for use in a laboratory demonstration of feedback control.

In the feedback experiments presented in Section 7.3, the strain gage is attached to the polymer actuator at one end and to a stepper motor at the other end. During the tests, as the stepper motor moves, feedback drives the actuator to keep the gage length constant for low velocity ramps.

Directions for Improvement

The lifetime and repeatability of the lycra coated strain gages are huge obstacles to their wide use as a position sensor. Improvements can be expected with better manufacturing but first, the mechanisms that effect the changes must be understood.

The polypyrrole forms bridges between the fiber strands in the Lycra. During cycling, these bridges may break or may be permanently deformed. The polypyrrole might also detach from the underlying fibers over time. Thicker high quality electrochemical coatings should improve the mechanical properties of the coating.

The properties of the polypyrrole itself also change over time due to solvent loss and oxidation by the environment. A coating to encapsulate the polymer could chemically stabilize the strain gage while at the same time providing additional mechanical support. Strain gages potted in polyurethane and in silicone were developed as part of the work for this thesis but test results so far are inconclusive.

Results in a recent paper by Spinks et al. suggest that there may be less hysteresis at much greater strains of 10-60% (Spinks, Wallace, Liu, and Zhou, 2003). Potting the pre-stretched coated Lycra gages in a flexible material might give more reproducible results.

7.2. Higher Force Trimorph Actuators

The actuator used for the feedback is similar to the trilayer actuators presented in Chapter 6. To increase the force generated, the geometry is changed to a long wing like structure (Figure 7.9). Two rigid carbon fiber strips are attached across the two edges of the actuator that constrain the actuator to bend in only in the shorter direction. The first

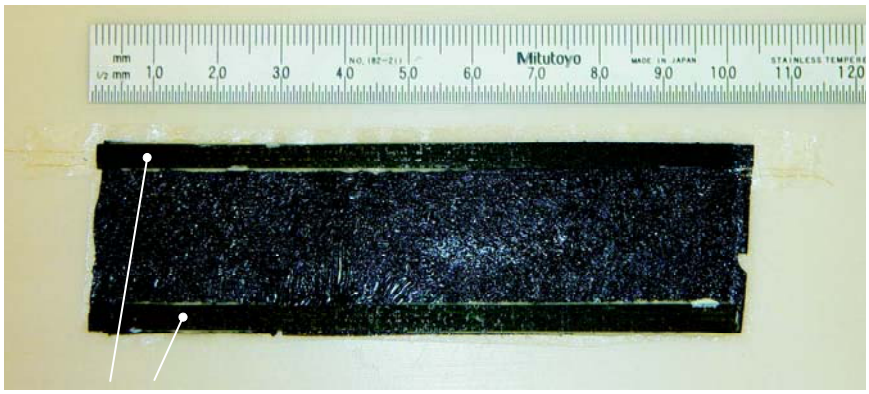

Figure 7.9: Completed trimorph. There are two carbon fiber strips on each long edge of the trimorph to constrain the bending to curling around the long axis only. Thin gold wires protruding from both ends make electrical contact to the upper and lower polymer films. The ruler dimensions are in mm. The trimorph is about 220 μm thick where there are no carbon fiber strips.

high force actuators using this design were built in the lab by Bryan Schmid, working as an undergraduate research student.

For the purposes of modeling the control system in Section 7.3, the displacement / charge ratio is needed. The expected curvature / charge ratio can be calculated using the model equation from Chapter 4:

$$\frac{K}{Q} = \frac{1}{LWh_p}\frac{K}{\rho} = \frac{1}{LWh_p}\frac{3\alpha}{2h_g}\left[\frac{\left(1+{h_p}/{h_g}\right)^2 - 1}{\left(1+{h_p}/{h_g}\right)^3 + \left({E_g}/{E_p} - 1\right)}\right], \qquad (1)$$

where K is the curvature, ρ is the charge density (Q/volume) in the polymer, α is the strain to charge ratio, E_p and E_g are the elastic moduli of the polymer and gel, h_p and h_g are the thicknesses of the polymer and the gel layers, and W and L are the width and length of the conducting polymer layer.

The measured h_p is 17 μm and h_g is 92 μm. The width of the wing is W = 100 mm and the length of the wing is L = 30 mm. The polymer strain to charge ratio and elastic moduli are the same as those used in Chapter 6 ($\alpha = 10^{-10}$ C/m^3, E_p = 1 GPa, E_g = 7.5 MPa). For a trimorph of length 22 mm, the curvature / charge ratio is:

$$\frac{K}{Q} = 19\frac{1}{\mathrm{m}\cdot\mathrm{C}}. \qquad (2)$$

If the trimorph is close to being straight, the movement of the end can be approximated as a linear motion Δy that is related to the curvature[3]:

$$\Delta y = L^2 K. \qquad (3)$$

The total length of the wing is L = 30 mm but the length that actually curves is reduced by the width of the two carbon fiber strips to L = 22 mm and so the linear motion / charge ratio is

[3] For small curvatures, $\frac{\Delta y}{L} \approx \frac{L}{R} = LK$.

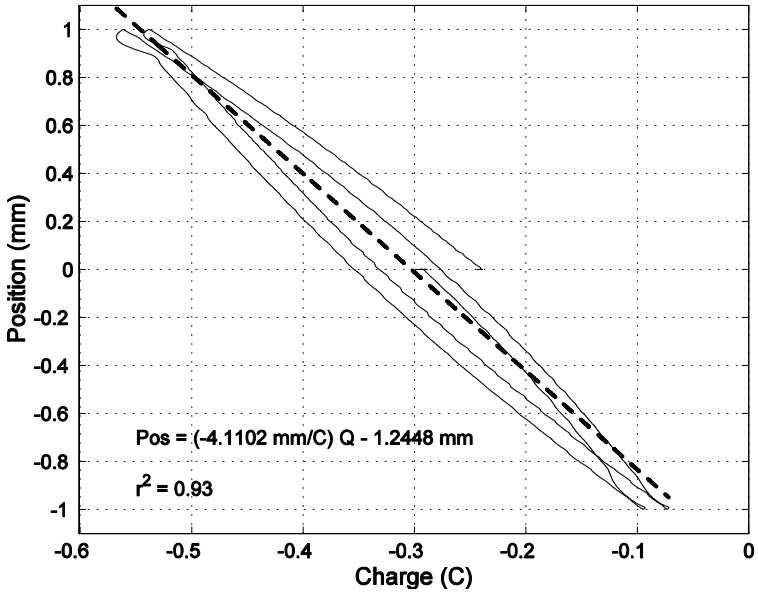

Figure 7.10: Displacement (Pos) versus Charge (Q) at Constant Force (isotonic). The position/charge ratio is -4.11 mm/C.

$$\frac{\Delta y}{Q} = L^2 \frac{K}{Q} = 9.2 \text{ mm C}^{-1}. \quad (4)$$

The linear motion / charge ratio was experimentally measured and was found to be 4.1 mm/C (shown in Figure 7.10). The difference between the measured value and the model value could arise for a number of reasons. If in spite of the carbon fiber stripes there is any bending in the width direction, the force required to bend in the other direction will increase and so the displacement / charge will decrease. There may also be some current leakage through the electrolyte. The experimentally measured value is used in the control model in Section 7.3.

7.3. Feedback Control to Maintain Constant Strain Gage Length

Position feedback control tests were conducted with two types of disturbances. Tests for both types of disturbances used a constant set point for the gage resistance rather than tracking a changing set point. Step position responses prove to be difficult to control because of the erratic strain gage response. Ramped position responses are easier to control. A disturbance is introduced by moving one end of the strain gage that is attached to a stepper motor as shown in Figure 7.11 and Figure 7.12. The actuator moves to keep the gage length constant. If the feedback is effective at maintaining a constant gage length, the peak strains and the number of cycles that the gage is subjected to are kept small which should extend the useful life of the gages.

The actuators used for the tests are the trimorph winglets presented in Section 7.2. The winglets produce forces up to hundreds of mN and displacements greater than 10 mm. Peak velocities are slow and are on the order of 0.5 mm/s.

Feedback control was implemented using a digital approximation to a PID loop. The control was programmed in Visual Basic and runs in a real time extension of the

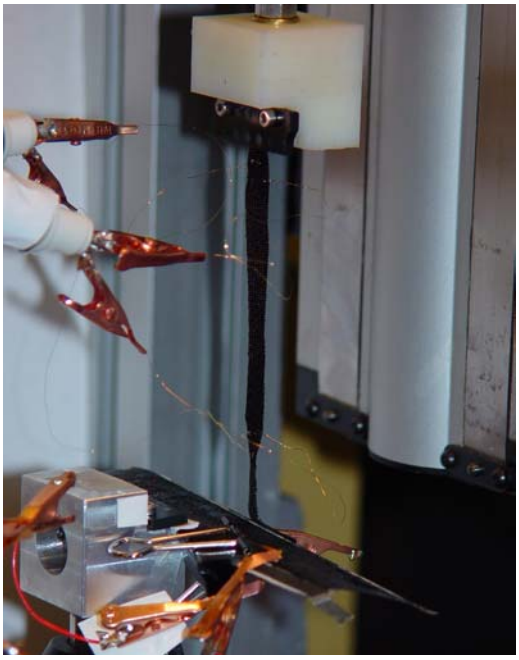

Figure 7.11: Photograph of the experimental setup for feedback testing. The wide black polymer actuator is shown in the lower part of the picture and is curled slightly downwards. The polypyrrole coated lycra strain gage is the thin black strip that stretches from the actuator up to the white clamping block. The clamping block is mounted on a motorized stage that moves in the vertical direction.

Windows 2000 operating system[4]. Update rates for the control loop can be as high as 10 kHz (which is far faster than needed since the actuator response is typically on the order of seconds).

The polymer muscle is controlled with either current or voltage input. Both types of control have been implemented. At low frequencies, the polymer behaves like a capacitor with a position that is proportional to the charge. Since the voltage determines the charge and hence the position, using only a proportional gain controller will give a

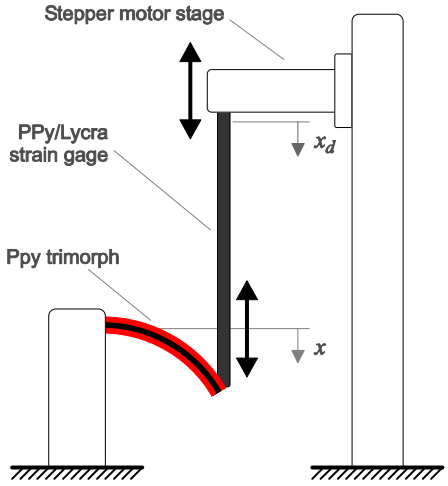

Figure 7.12: Diagram of apparatus for feedback control testing.

[4] WinRT from BSquared, Cambridge, MA.

steady state error. Proportional and integral control is therefore used for voltage control of the polymer actuator.

Using current input, when the set point position is reached and the error goes to zero, a proportional gain only controlled current will also drop to zero, no charge is exchanged, and the polymer should not move. The steady state error is zero with proportional control and no integral control. Only proportional gain is used for the controller for current input to the actuator.

Controller design for a conducting polymer muscle must take into account the limited potential range that can be applied at the double layer. Instead of limiting the double layer potential, the simple controllers presented here limit the potential or the current applied to the entire system. Limiting the voltage or the current adds a non-linearity to the controller because the voltage or current will saturate at high controller gains. In the experiments, saturation is observed and does limit the maximum actuator velocity. Peak velocities are around 0.25 to 0.5 mm/s.

Model of the System

For the purposes of analyzing the feedback control system, models of the polymer actuator and strain gage are presented in this section. Block diagrams of the control systems are shown in Figure 7.13.

Many of the relationships used to describe the system are actually approximations. For the actuator, curvature rather than position is proportional to charge but the approximation is very good at low curvatures. Furthermore, at extreme voltages that degrade the polymer, the relationship between charge and curvature breaks down. For the strain gage (as discussed in Section 7.1), the strain gage models the position as

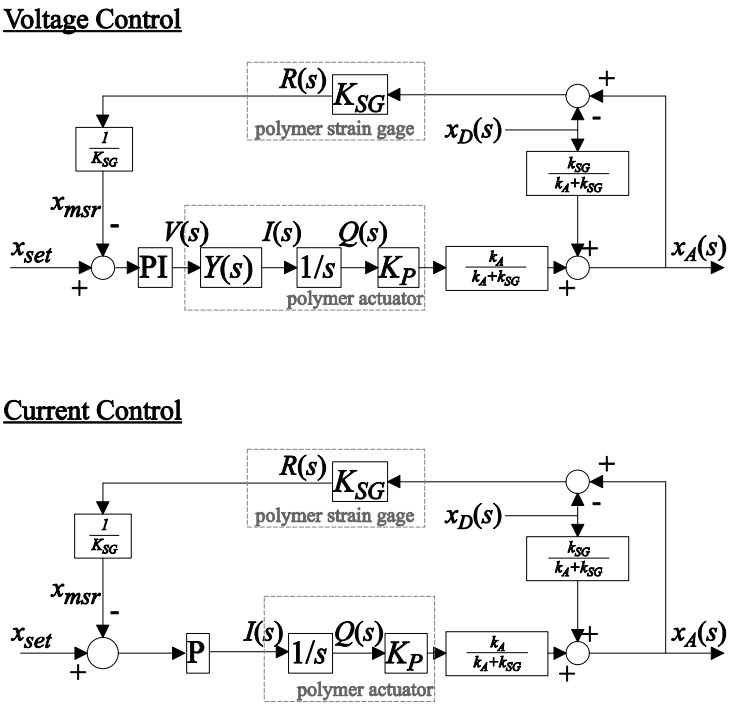

Figure 7.13: Block diagrams of the control for a voltage controlled and current controlled feedback loop. The meaning of the variables is described in the text.

perfectly proportional to resistance, ignoring the hysteresis, time dependence, and the erratic high frequency behavior that are difficult to model. Finally, the high frequency response of the system should also include inertial and damping effects but for low actuator response rates these terms are not important. In spite of the many approximations, the simple linear relationships are useful to better understand issues of actuator control and stability.

The trimorph actuator is treated as a charge to position transducer in series with a spring (as described in Chapter 4):

$$x_A = \mathrm{K}_P Q + \frac{1}{k_A} F, \tag{5}$$

and the strain gage is approximated as a position to resistance transducer:

$$R = \mathrm{K}_{SG}(x_A - x_D) + R_o, \tag{6}$$

where x_A is the actuator position, x_D is chosen as the position at which the strain gage force is zero, Q is the charge transferred to the actuator, R is the strain gage resistance, R_o is the resistance for $x_A = x_D$, K_P is the actuator position to charge ratio, k_A is the actuator spring constant, and K_{SG} is the strain gage resistance to position ratio.

Since the force on the actuator is equal to the extension force of the strain gage $F_{SG} = k_{SG}(x_A - x_D)$, x_A can be expressed a function of Q and x_D:

$$x_A = \left(\frac{k_A}{k_A + k_{SG}}\right)\mathrm{K}_P Q + \left(\frac{k_{SG}}{k_A + k_{SG}}\right)x_D. \tag{7}$$

If the actuator is much stiffer than the strain gage, disturbances on the system imposed by changes in the position x_D will have very little effect on the actuator position. On the other hand, if the strain gage is much stiffer than the actuator, the actuator can have great difficulty moving.

Voltage and Current Input Models of the Actuator

The input to the actuator is a current or a voltage depending on the type of control used. Since the actuator position x_A is expressed above as a function of charge, the input current or voltage need to be converted to a charge to write the complete actuator transfer function.

With a current input, the charge Q is simply the integral of the current. In the Laplace domain,

$$Q(s) = \frac{1}{s} I(s), \tag{8}$$

and so the transfer function relating the actuator position x_A to the control current I is:

$$G_{A,I}(s) = \frac{x_A(s)}{I(s)} = \frac{Q(s)}{I(s)}\frac{x_A(s)}{Q(s)} = \frac{1}{s}\left(\frac{k_A}{k_A + k_{SG}}\right)\mathrm{K}_P, \tag{9}$$

where K_P is the position / charge ratio of the actuator.

For a voltage input, the voltage to current transfer function is the admittance of the polymer trimorph, $Y(s)$. The transfer function relating x_A to the actuator voltage V is:

$$G_{A,V}(s) = \frac{x_A(s)}{V(s)} = \frac{I(s)}{V(s)}\frac{Q(s)}{I(s)}\frac{x_A(s)}{Q(s)} = Y(s)\frac{1}{s}\left(\frac{k_A}{k_A + k_{SG}}\right)\mathrm{K}_P. \tag{10}$$

In this section, to keep the model simple, the admittance $Y(s)$ is approximated as a series resistor R and capacitor C:

$$Y(S) = \frac{sC}{1 + sCR}, \qquad (11),$$

instead of using the much more complicated diffusive elastic model impedance model derived by J. Madden (Madden, 2000) and described in Chapter 2. The measured electrical impedance of the actuator used for feedback is shown in Figure 7.14. The RC model used to fit the experimental data is shown with a dashed line. The values in the model are R = 9 Ω and C = 4 F, to give a time constant of 36 s (or ω = 28 mHz). The simpler admittance makes it possible to find the inverse Laplace transform and solve the impulse response function.

Open Loop Transfer Function with the Strain Gage

The PID control algorithm on the computer compares the measured position to a set point position. For controller design, the open loop transfer function should relate the input to the actuator (either current or voltage) to the position measured by the strain gage. Referring to Figure 7.13, for a voltage input we can write the measured position $x_{msr}(s)$ as

$$x_{msr}(s) = -x_D + \left\{\frac{k_{SG}}{k_A + k_{SG}}\right\}x_D + \left\{\left(\frac{k_A}{k_A + k_{SG}}\right)\left(Y(s)\frac{1}{s}K_P\right)\right\}V(s), \qquad (12)$$

and for a current input we write

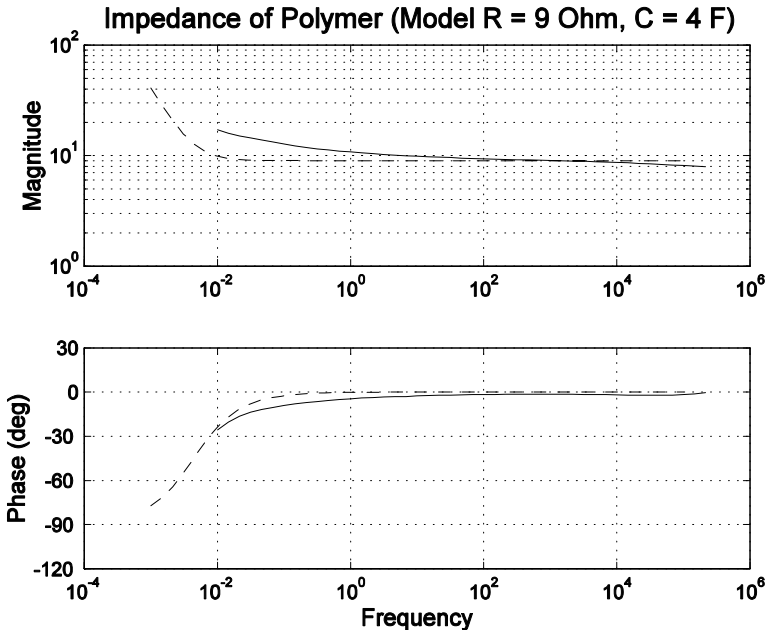

Figure 7.14: Measured Admittance versus Frequency (in Hz) of the conducting polymer actuator used in the feedback control experiments (solid line) and a series resistance and capacitance circuit model (dashed line) used to approximate the polymer actuator impedance. At low frequencies the polymer actuator electrical response is capacitive. At high frequencies, the response is resistive. (The actuator impedance response was only measured to 0.01 Hz. More complete low frequency impedances that clearly show the low frequency capacitive behaviour have been extensively measured by J.Madden (Madden, 2000)).

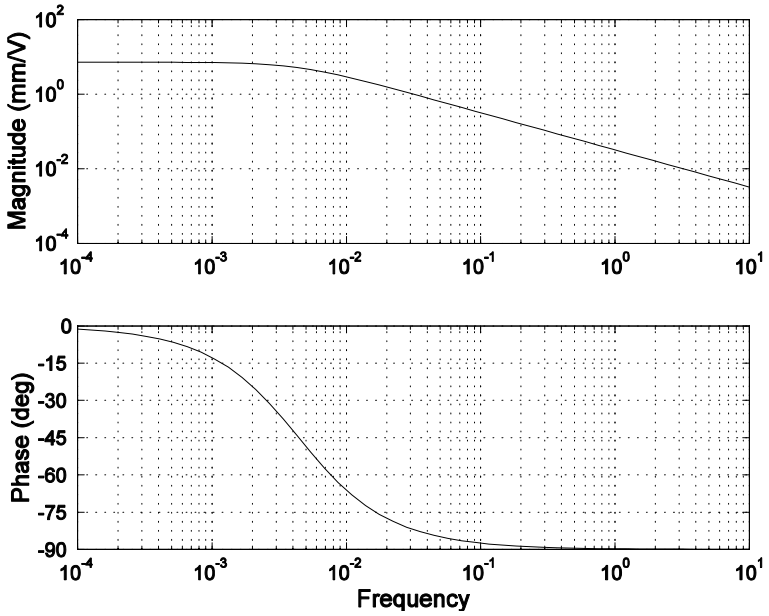

Figure 7.15: Open loop transfer function versus Frequency (in Hz) for strain gage measurement output and voltage input to the actuator.

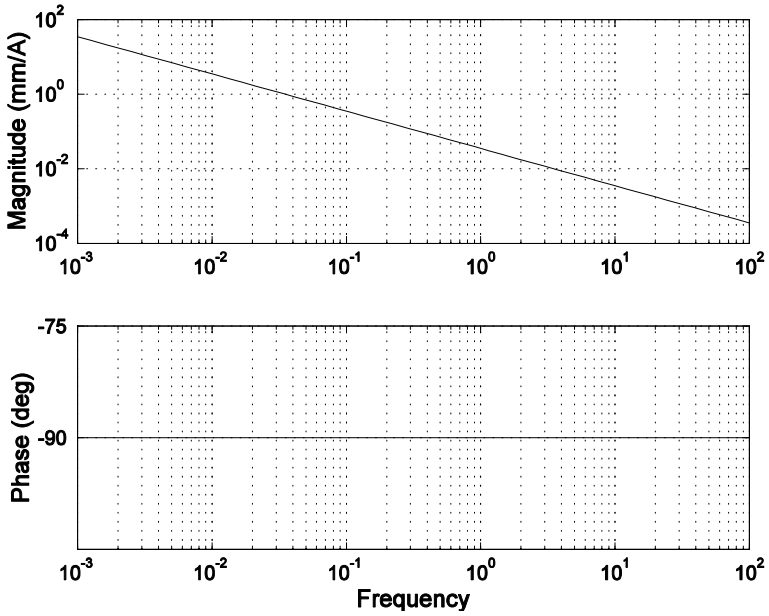

Figure 7.16: Open loop transfer function versus Frequency (in Hz) for strain gage measurement output and current input to the actuator.

$$x_{msr}(s) = -x_D + \left\{\frac{k_{SG}}{k_A + k_{SG}}\right\}x_D + \left\{\left(\frac{k_A}{k_A + k_{SG}}\right)\left(\frac{1}{s}K_P\right)\right\}I(s). \qquad (13)$$

The lower case *k*'s are the spring constant of the actuator (k_A) and of the strain gage (k_{SG}).

The (measured position)/current and the (measured position)/voltage transfer functions are the open loop transfer functions that can be used to check stability of the control design. The variables K_P, k_{SG}, and k_A were measured in independent experiments and were found to be K_P = 4.11 mm/C, k_{SG} = 14.5 mN/mm, and k_A = 11 mN/mm. The

values of R and C used for the admittance model are R = 9 Ω and C = 4 F, as given above. The open loop transfer functions for both current and voltage input are plotted in Figure 7.15 and Figure 7.16.

Both open loop transfer functions have phase margins of 90° which means they should always be stable under proportional control. As mentioned though, the control models ignore inertial and damping terms that will come into play at higher frequencies and can limit the maximum gain used for feedback. The double layer voltage at which material degradation occurs is another practical limit on the maximum system gain.

Closed Loop Transfer Functions

Referring back to the block diagram in Figure 7.13, the closed loop transfer functions are found to be:

$$x_A(s) = \left(\frac{F(s)}{1+F(s)}\right)x_{set} + \left(\frac{F(s)+r_{Spr}}{1+F(s)}\right)x_D, \tag{14}$$

where for current control

$$F(s) = P \cdot \frac{1}{s} \cdot \left(\frac{k_A}{k_A + k_{SG}}\right)\mathrm{K}_P, \tag{15}$$

and for voltage control

$$F(s) = \left(P + \frac{I}{s}\right) \cdot Y(s) \cdot \frac{1}{s} \cdot \left(\frac{k_A}{k_A + k_{SG}}\right)\mathrm{K}_P. \tag{16}$$

The variable r_{Spr} is a ratio of spring constants:

$$r_{Spr} = \frac{k_A}{k_A + k_{SG}}, \tag{17}$$

where as before, k_A and k_{SG} are the spring constants of the actuator and strain gage.

At high frequencies, where the control is not effective, the response should be dominated by the relative spring constants of the actuator and the strain gage while it should not depend at all on the resistance set point (see equation (7)). Indeed, as $s \to \infty$, $F(s) \to 0$ for both current and voltage input and so $x_A(s) \to r_{Spr} \cdot x_D(s)$.

At low frequencies, the control will be effective at tracking the resistance set point. The control will also be effective at maintaining a constant strain gage length or, in other words, at following the position disturbance x_D. Again, taking the limit as $s \to 0$

$$x_A(s \to 0) = x_{set} + x_D, \tag{18}$$

as expected.

The closed loop transfer functions for voltage control are plotted in Figure 7.17 and Figure 7.18. The cutoff frequency of the control as plotted is around 0.7 Hz. The gains P and I match those used in the next section for control with a ramp waveform x_D disturbance ("Response to a Ramp Disturbance"); gains were chosen during the experiments to keep the voltage within the voltage limits when the x_D is not changing (P = 26.6 V/Ω, I = 26.6 V/Ω/s). If the gains are set too high, the controller becomes a bang-bang controller, switching between the maximum and minimum applied voltages. Saturation of the applied voltage becomes a practical limit to the frequency of operation as the rate can no longer increase and the control cannot maintain the set point.

By taking the inverse Laplace transform of the function x_A/x_D, the impulse response function is found to be of the form:

$$h(t) = r_{Spr}\delta(t) + Ae^{-a_1 t} + Be^{-a_2 t}, \tag{19}$$

where A = 3.34 mm/mm, B = -0.35 mm/mm, a_1 = 4.05 s^{-1}, a_2 = 0.35 s^{-1}, and r_{Spr} = 0.44. The values depend on r_{Spr}, K_P, the controller gains P and I, and the R and C values of the admittance model. In the next section of this chapter, this impulse response function is convolved with the ramp input for comparison to the actual system response.

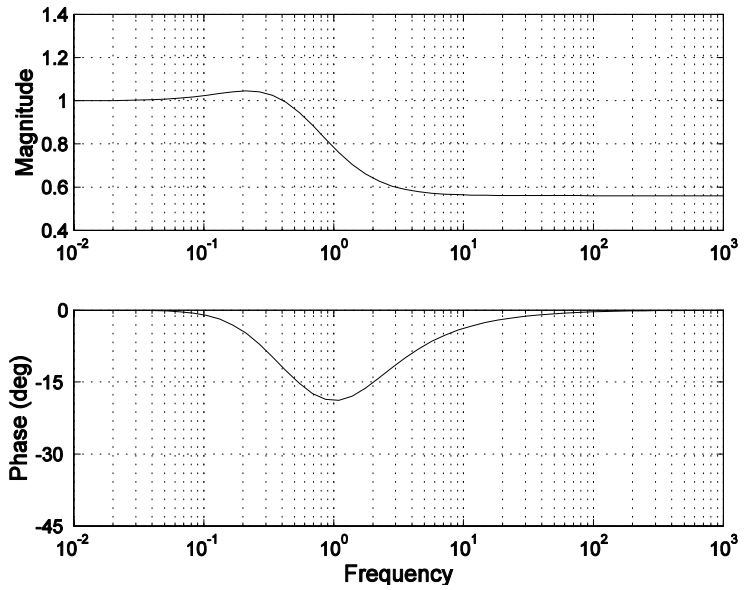

Figure 7.17: Voltage Control Closed Loop Transfer Function versus Frequency (in Hz) for (Actuator Position) / (Disturbance Position).

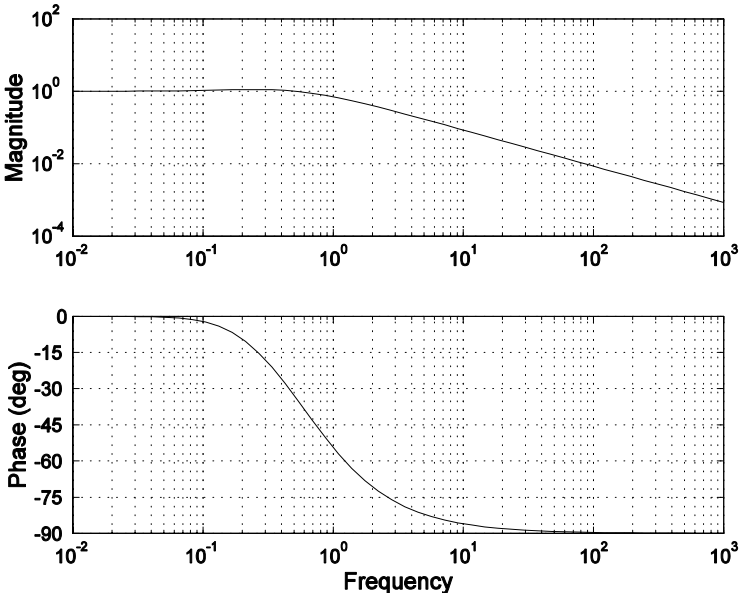

Figure 7.18: Voltage Control Closed Loop Transfer Function (actuator position) / (set point position) versus Frequency (in Hz). The cutoff frequency is about 0.7 Hz.

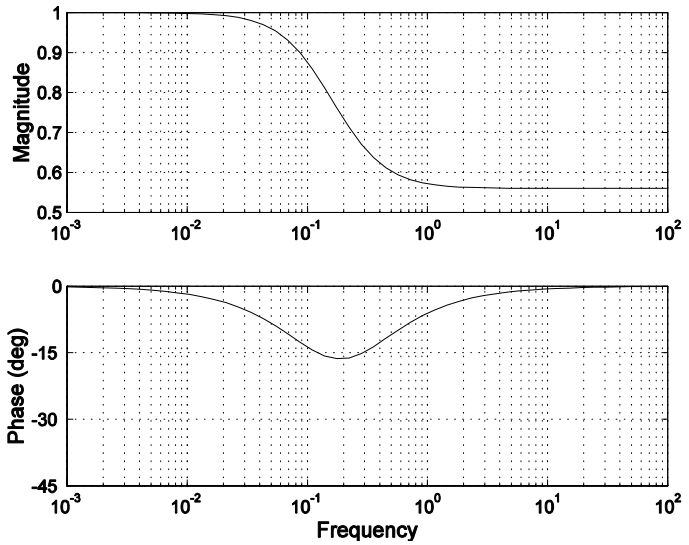

Figure 7.19: Current Control Closed Loop (Actuator Position) / (Disturbance Position). Frequency is in Hz.

The closed loop transfer functions for current control are plotted in Figure 7.19 and Figure 7.20. Again, the gain P was chosen so that the current was not limited during periods of unchanging x_D (P = 4.0 A/Ω). The value for K_P that was used was not the same as that used in the ramp experiments. While the same trimorph was used, through the course of the experiments that were run over two weeks between the first ramp experiments and the step response experiments, the value of K_P dropped from 4.11 mm/C to around 0.5 mm/C. The cutoff frequency of about 0.2 Hz is a bit lower than that of the voltage control model and is partly a consequence of the reduced position / charge ratio. As will be seen in the subsection on step response, in the feedback tests using current control the performance of the control loop is limited by the current limits and is greatly hampered by the erratic behavior of the strain gage.

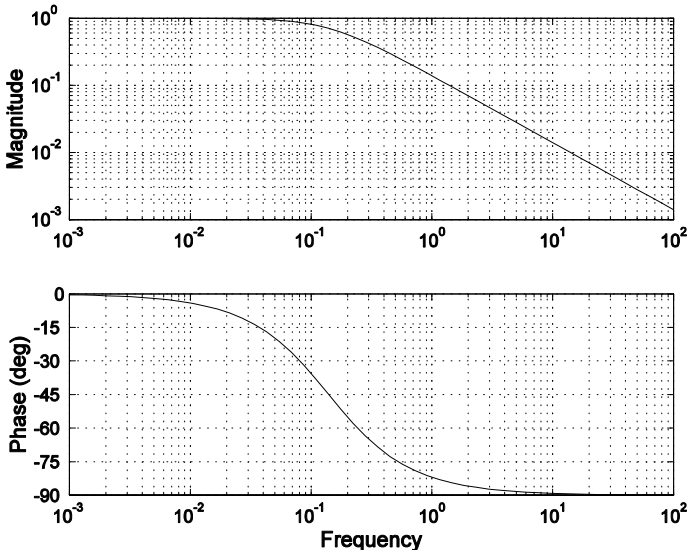

Figure 7.20: Current Control Closed Loop Transfer Function for (Actuator Position) / (Set Point Position). Frequency is in Hz.

Again, the impulse response function can be found by taking the inverse Laplace transform of the closed loop response and is found to be of the form:

$$h(t) = (1 - r_{Spr})\delta(t) + Ae^{-at}, \tag{20}$$

where A = 0.492 mm/mm, a = 0.88 s^{-1}, and r_{Spr} = 0.44. A simulated step response will be shown along with the feedback test results for step response.

Response to a Ramp Disturbance

Feedback was used successfully to keep constant gage length in response to low velocity disturbances. The feedback tests for the ramp response use voltage control with a PI controller.

Figure 7.21 shows the position disturbance and the gage resistance for a series of four experiments. In the first experiment (top row) feedback was off and the resistance

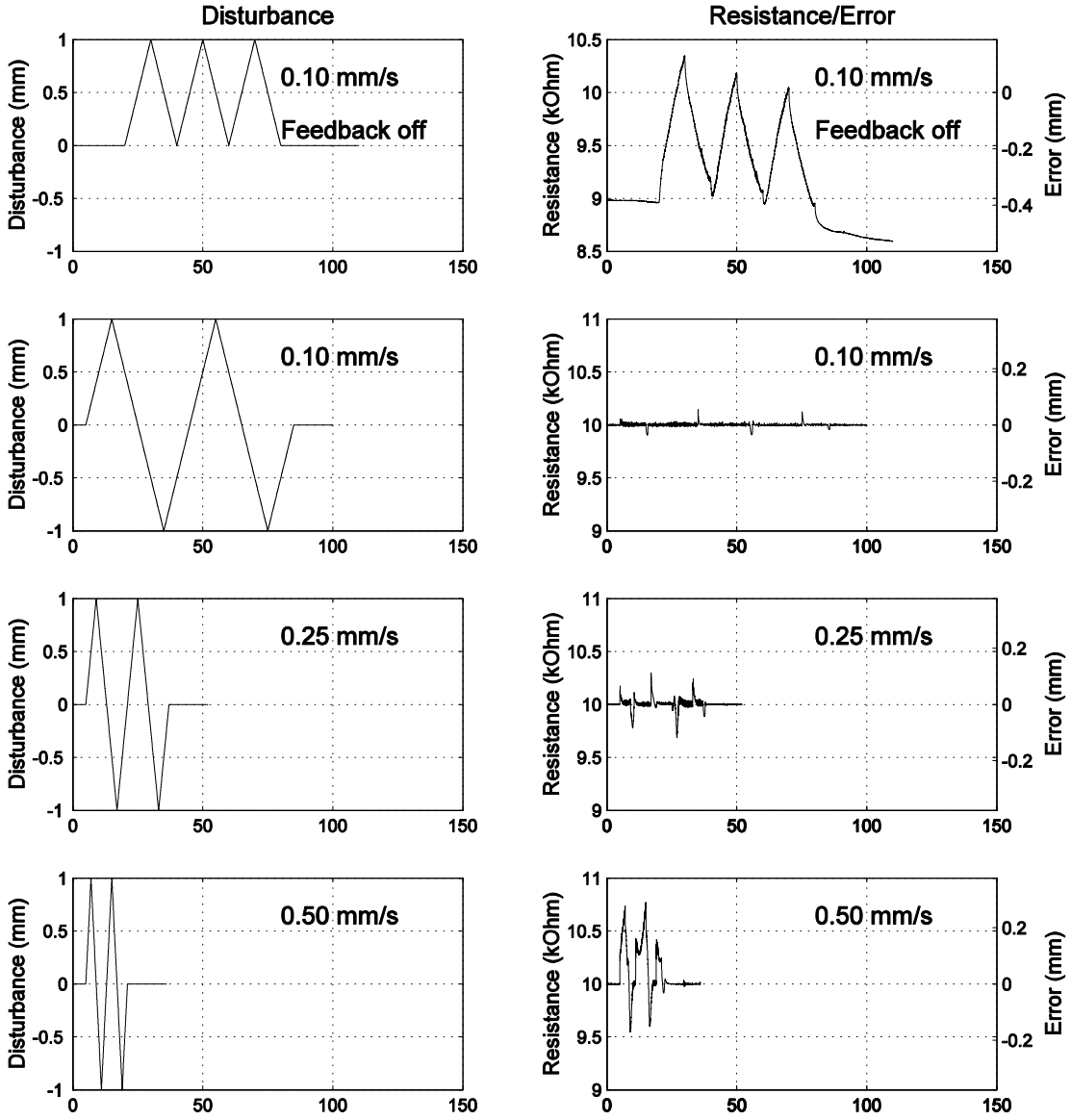

Figure 7.21: Feedback Response through time (in s) to ramp disturbances at different rates.

response to a 1 mm ramp at 0.1 mm/s was measured. In the other three experiments, feedback endeavors to keep the strain gage length constant during ±1 mm ramps at different rates. Figure 7.22 shows the resistance, voltage, current, and charge plotted versus time for the three feedback experiments. The peak voltage was limited to ±3 V to reduce damage to the polymer from electrochemical degradation. The nominal position as given by the strain gage calibration (2660 Ω/mm) is marked on the right side of the resistance versus time plots.

In the upper plot, with feedback off, the actuator displacement is ~0.4 mm. Even with feedback off, the 1 mm disturbance changes the strain gage length by only 0.4 to 0.5 mm. Because the actuator is compliant, the total displacement is split between the strain gage (length change 0.4 to 0.5 mm) and the actuator (displacement of 0.5 to 0.6 mm). This was shown in the model of the (actuator position) / (disturbance position) in the previous section.

However, in the feedback tests, the actuator must move the full 1 mm to keep the gage length constant. As the rate increases, the actuator isn't able to maintain the constant length of the strain gage. At 0.1 mm/s the standard deviation of the error is 3.4 μm (9 Ω) or around 0.4 % of the 1 mm ramp amplitude. The control is effective at tracking the disturbance position. The largest errors at this rate (the maximum error = 53 μm or 142 Ω) occur when the ramp disturbance changes directions at ±1 mm. When the ramp direction changes, the settling time to tracking the new direction is about 1 s.

At 0.25 mm/s the control does not keep up as well, particularly when the ramp changes directions at ±1 mm. The standard deviation from the set point is 6 μm (15 Ω) and the peak error, which again occurs when the ramp changes directions, is 118 μm (314 Ω). Here, the settling time after the change in direction is slightly more than 1 s when changing from a negative to a positive ramp and 1 to 2 s when changing from a positive to a negative ramp.

Finally, at 0.5 mm/s, the control becomes much less effective. At the rate of 0.5 mm/s there is a 90 μm (237 Ω) standard deviation from the set point. The peak error of 290 μm occurs at the disturbance position of +1 mm but is due to the control falling behind the ramp rather than difficulties in tracking the change of direction. In fact, as shown in Figure 7.23,the error drops to about 200 μm almost immediately after the direction changes. It is interesting though to look more closely at the errors. When the ramp is decreasing (with the voltage and current positive), the error settles to 0 mm in 2 to 3 s. However, the ramp position is increasing (with the voltage and current negative), the error does not settle and the polymer actuator falls behind the stepper motor. During the positive direction ramp, the voltage saturates at the –3 V limit, impeding the control and limiting the maximum velocity of the polymer.

Table 7-1: Standard deviation from set point and peak errors.

Rate	Std Error (μm)	% of Disturbance Amplitude	Peak Error	Peak % of Deviation
0.10 mm/s	6 μm	0.6 %	53 μm	5 %
0.25 mm/s	19 μm	2 %	118 μm	12 %
0.50 mm/s	90 μm	9 %	290 μm	29 %

A comparison of the errors at each different disturbance rate is given in Table 7-1.

Simulations of the system were run in Matlab (Mathsoft, Woburn, MA) using the impulse respones found earlier (Equation (19)). The simulated tracking errors are shown in Figure 7.24. The experimental time taken to settle the tracking to close to zero after a change in ramp direction is in fact quite close to the simulated time at 0.10 mm/s and 0.25 mm/s but the magnitudes of the errors are off by a factor of around 2. At 0.50 mm/s the experimental error and simulation error do not look similar on the upward ramp

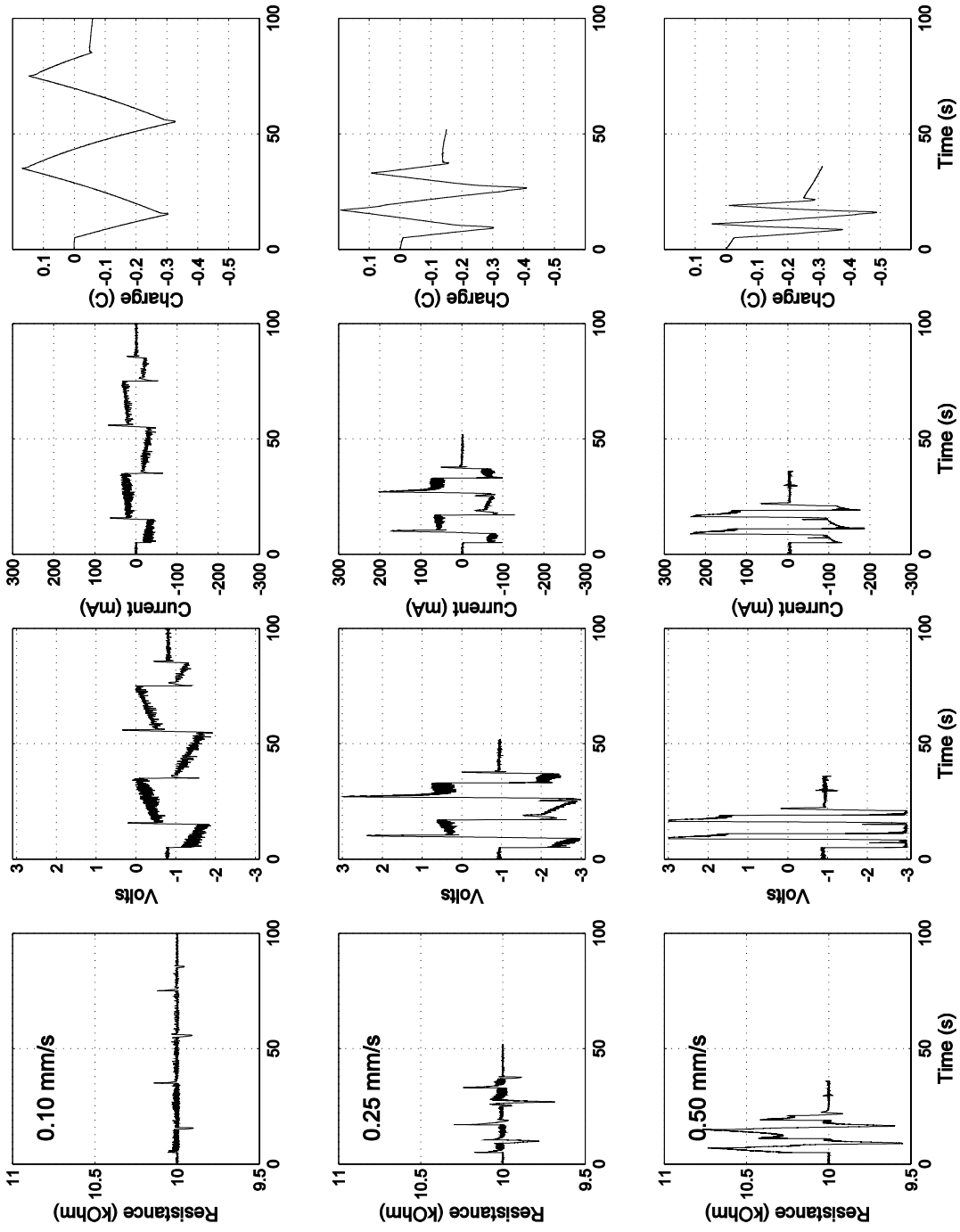

Figure 7.22: Resistance, Voltage Current, and Charge versus Time in Response to a Ramp Disturbance.

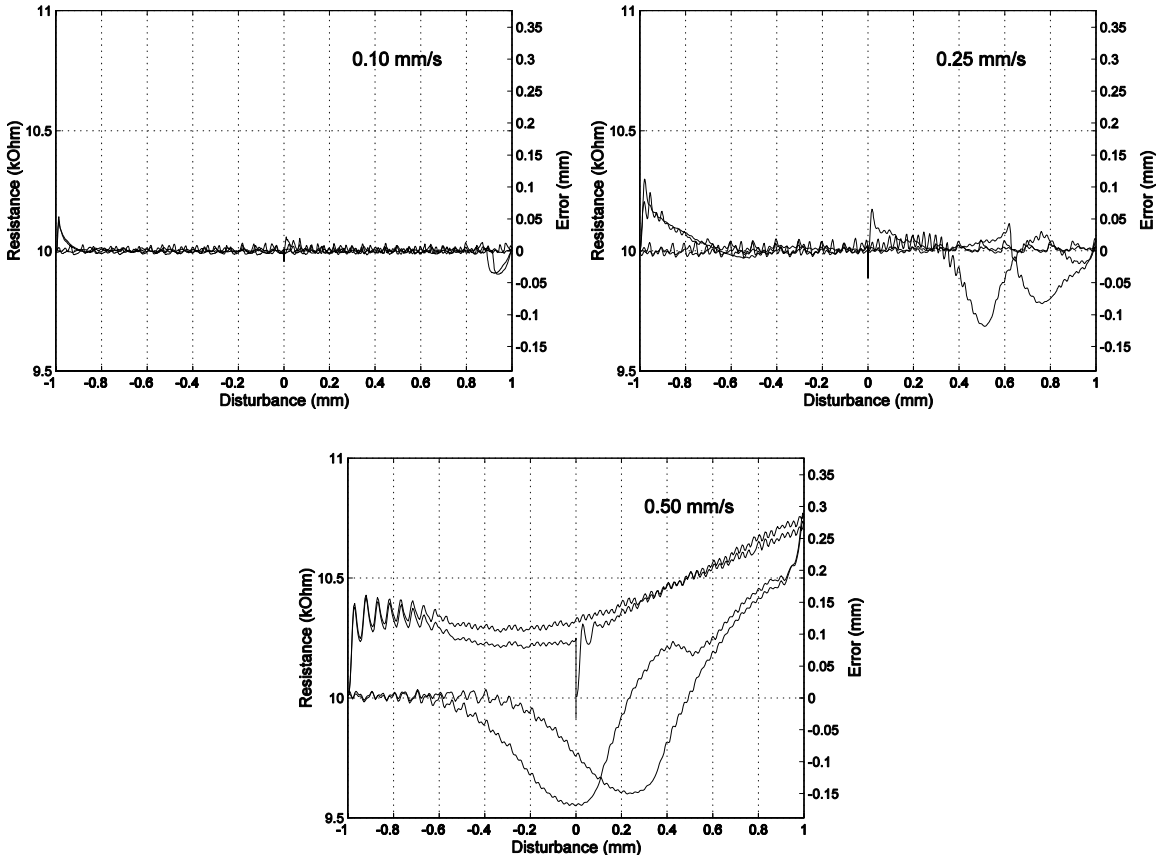

Figure 7.23: Resistance and Error versus the Disturbance Position (for a ramp disturbance).

because of the experimental voltage limits that are not modeled for the simulated results.

The simulation models the errors well. The largest errors occur after changes in direction of the ramp disturbance and the modeled settling times are close to the experimentally measured values.

Returning again to the experimental results, at the low tracking rate, the charge passed is close to proportional to the displacement of the trimorph (see Figure 7.25). However, as the rate increases, the displacement is no longer proportional to the amount of charge that has passed through the polymer. The charge that is passed in one direction is much higher than in the other. Quite likely, the polymer is being damaged in spite of the voltage limit. The voltage during the testing goes further towards the negative direction than it does towards the position direction and so this results in overoxidation of one electrode only.

The overoxidation of the polymer muscle brings up two issues. First, the potential limits that were used are too generous and should be narrowed to prevent polymer damage. Second, for long term operation, as the polymer is damaged, the strain to charge ratio is expected to decrease because there is less electroactive polymer. If the actuator has to perform consistently for long periods of time, overoxidation must be prevented by limiting the double layer voltage.

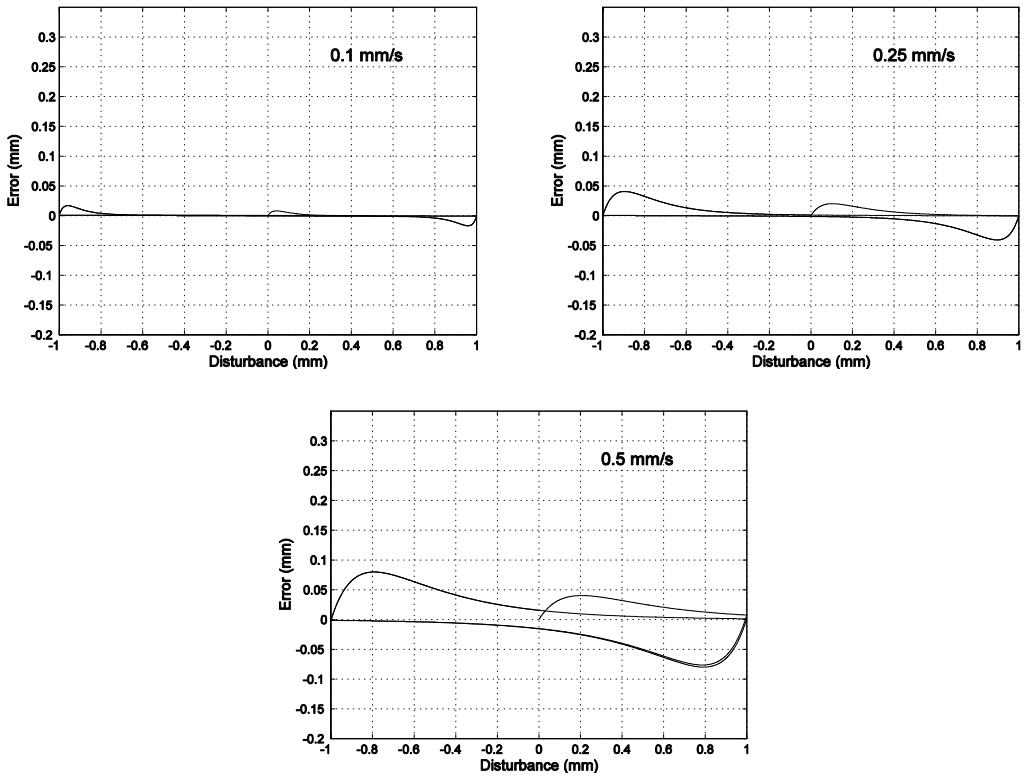

Figure 7.24: Simulated Error versus the Disturbance Position (for a ramp disturbance). The scale on the plots is chosen to match closely the scale of the plots in Figure 7.23 to allow easy comparison.

Response to a Step Disturbance

In Section 7.1, the coated Lycra strain gage response to a step change in length was shown to be an unreliable indicator of position. Nonetheless, the control responses to step length change are included here because they demonstrate the use of current control rather than voltage control.

Responses to a 1 mm step disturbances under proportional current control are shown in Figure 7.27 for three different limiting currents. Because the gage responses cannot easily be converted to a position, an equivalent position axis is not included in the plots. Integral and derivative terms are not used. The strain gage resistance response to 1 mm steps with feedback off is shown in the upper two plots of the Figure 7.27 for reference. When using feedback, the controller set point is 10.5 kΩ and the position disturbance is a 60 s, 1 mm step. Plots of the resistance, current, charge, and voltage versus time are shown in Figure 7.28.

Under current control, the maximum current is limited to try to avoid damage to the polymer. Responses are shown in Figure 7.27 and Figure 7.28 for each different current limit and it can be seen that the saturation current is reached at the 50 mA, 100 mA, and the 200 mA limits. Nonetheless, the strain gage resistance is restored to 10.5 kΩ for all three limiting current values (50 mA, 100 mA, 200 mA).

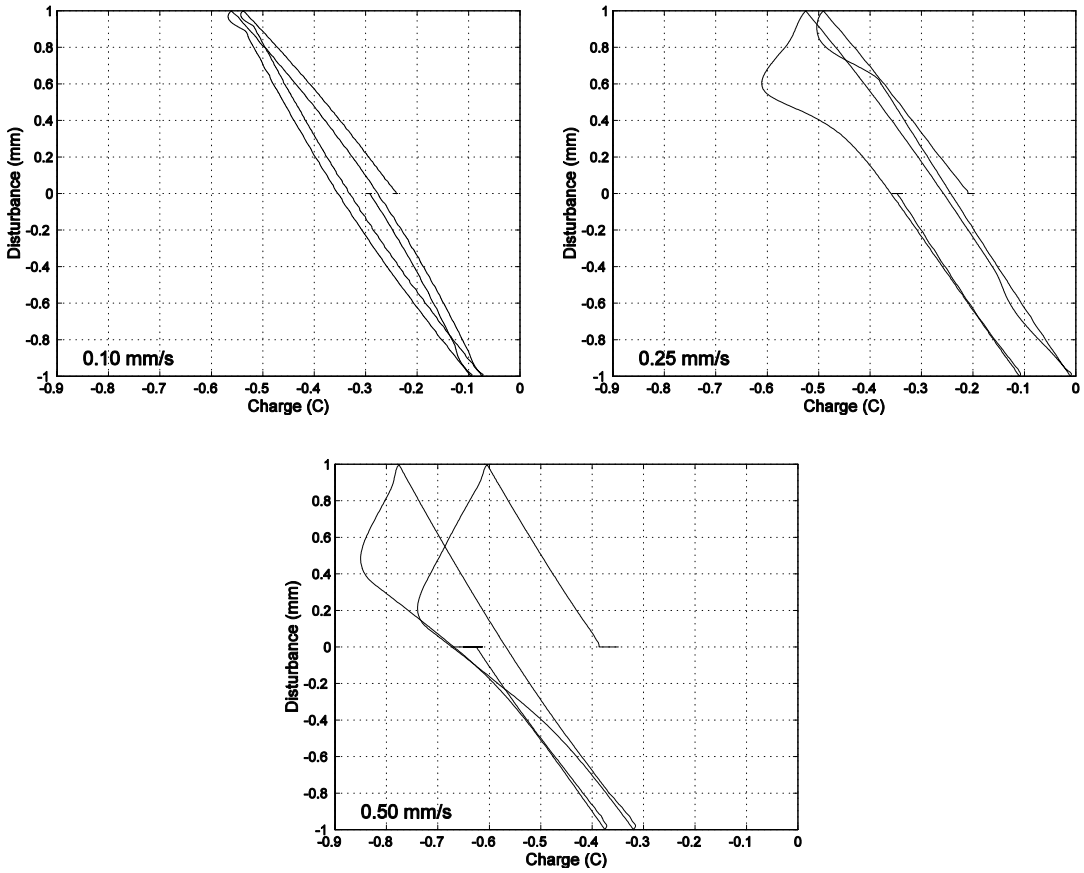

Figure 7.25: Disturbance plotted versus the charge passed to the actuator. At the lowest rate (upper left, 0.10 mm/s) the charge is close to proportional to the displacement. At the middle rate (upper right, 0.25 mms), there is a large negative shift in the amount of charge passed at a positive displacements of 0.4 to 1 mm. The shift corresponds to a period when the voltage applied to the polymer has reached the potential limits. At the fastest rate (lower plot, 0.5 mm/s), the negative shift in charge is even greater as the polymer spends more time at the potential limits.

Unfortunately, the resistance is not a good indicator of position for the step responses. Position of the actuator is extracted instead from video taken of the experiments and is shown in Figure 7.26.

For all three limiting currents, the position overshoots the 1 mm displacement after the step. The overshoot is a consequence of the strain gage behavior. If the strain gage is stretched and then returned to its starting point (as shown in the top of Figure 7.27), the resistance does not immediately return to the starting point but remains elevated. To return the resistance to the starting point, the actuator must shorten the gage below its starting length and so must go beyond the 1 mm displacement that would keep the gage length constant. After the overshoot, as the gage resistance gradually decays towards its starting point, the actuator position also decays towards the expected 1 mm displacement.

In the 50 mA test, after the step returning towards the starting point, the resistance has jumped to a higher value. The actuator moves to shorten the strain gage by almost1.5 mm before the resistance returns to the set point of 10.5 kΩ. The charge plotted in Figure 7.28 also shows an increase after the reverse step from 1 mm to 0 mm. Significant shifts

in the DC resistance of the strain gages was observed during step response tests of the strain gages only and so the shift is not entirely unexpected.

The simulated response of the system is shown in Figure 7.29. The error in the simulation converges to zero faster than the experimental error in part because the simulation does not include current limits.

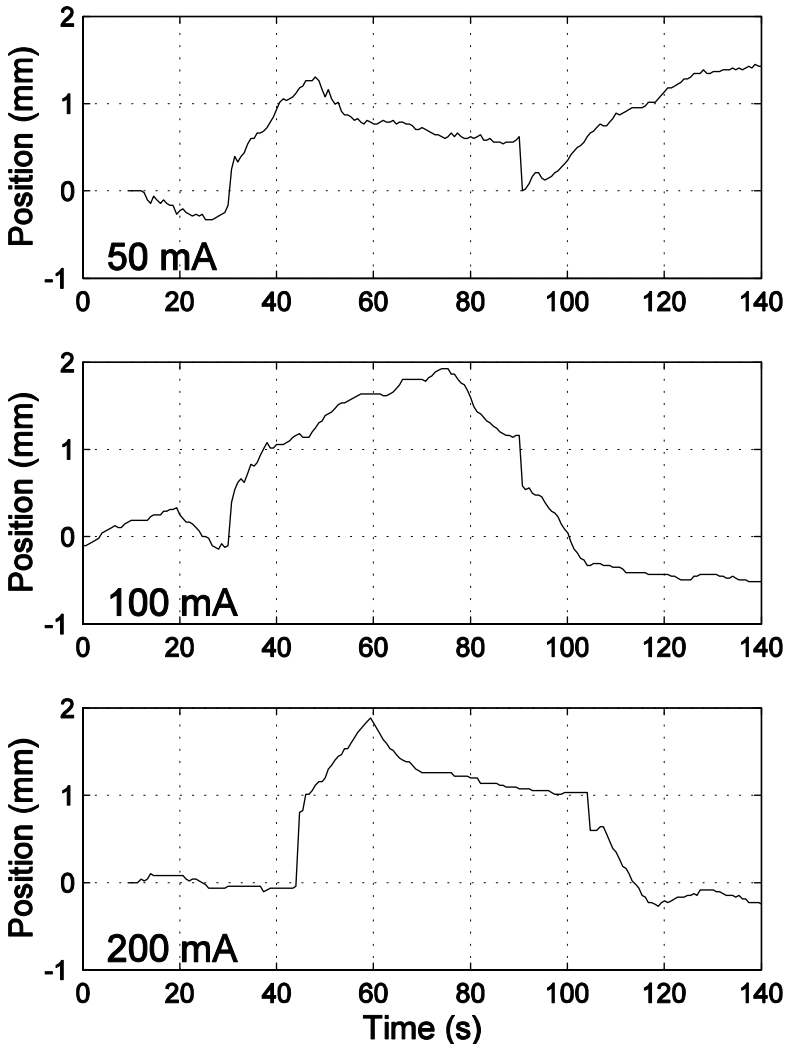

Figure 7.26: Position of the actuator as measured from the video. A 1 mm step is applied from t = 30 s to t = 90 s. Ideally the actuator would track the disturbance perfectly. The positions were extracted from video taken during the experiments (pixel resolution in the video is about 0.2 mm/pixel).

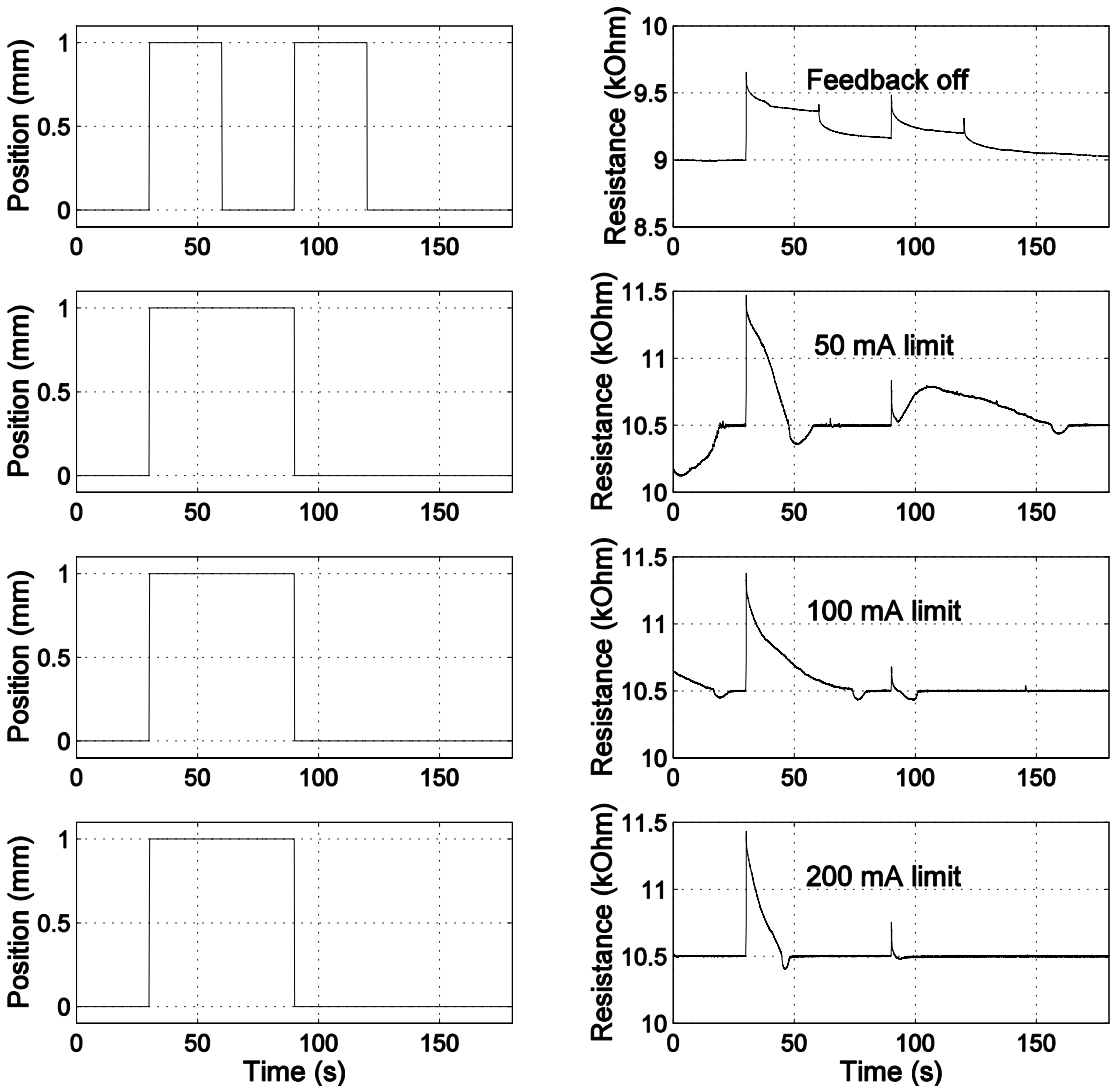

Figure 7.27: Step response with 50 mA, 100 mA, and 200 mA current limits on the proportional controller. Response to two 1 mm steps with the feedback off is shown for comparison.

The large drift and considerable overshoot of the strain gage response to a step disturbance make control of position uncertain even if the gage resistance can be well controlled and so the polymer strain gages should be used only where the maximum strain rates are limited. Improvements are needed in the strain gage before true step response control can be achieved.

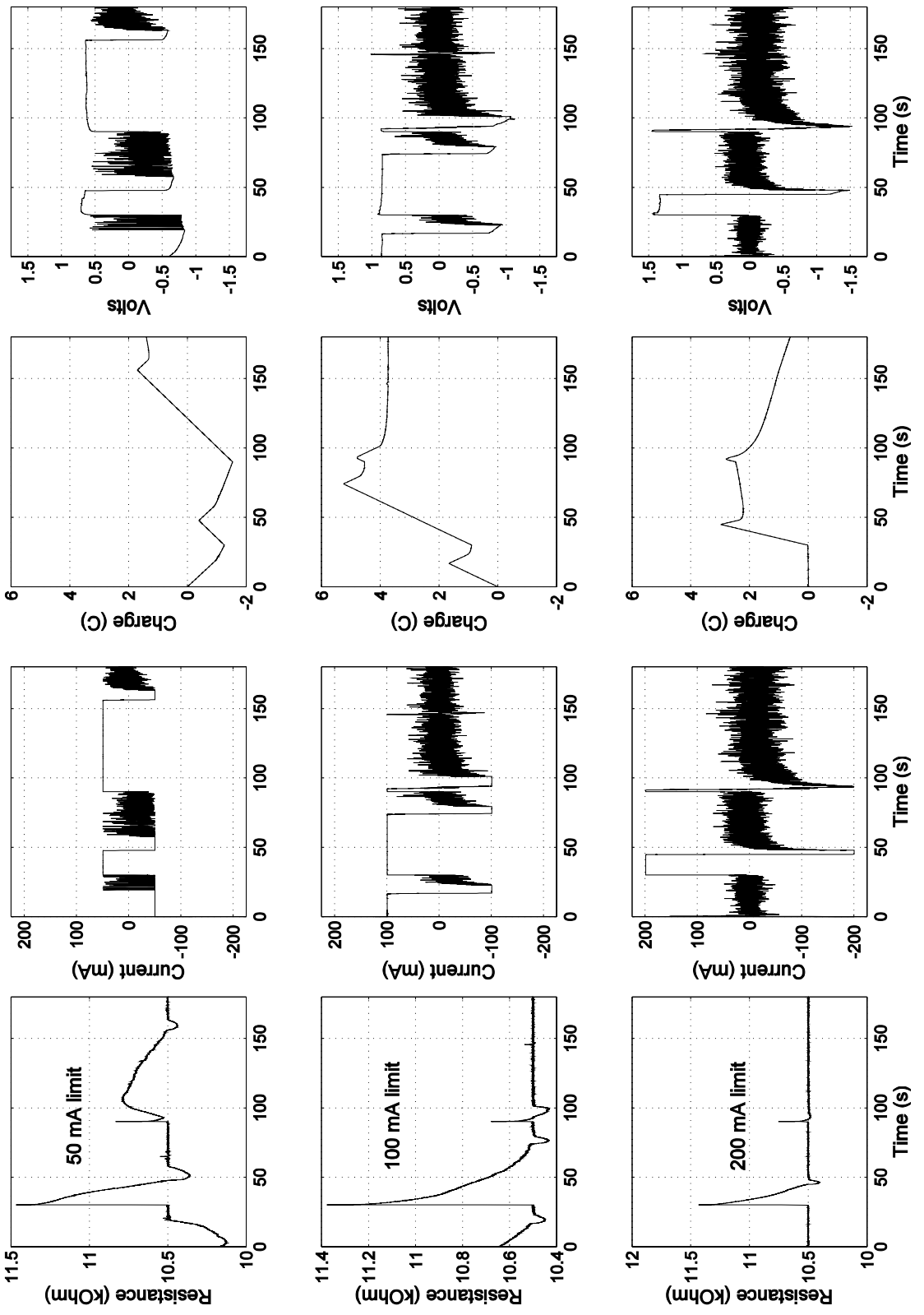

Figure 7.28: Resistance, Current, Charge, and Voltage versus Time in response to a 1 mm step change in position.

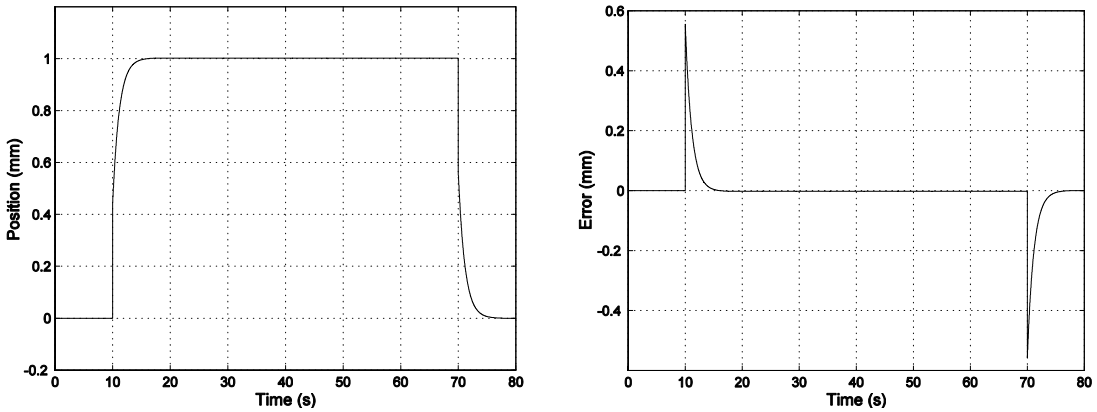

Figure 7.29: Simulated actuator position (left) and position error (right) for a step response. The error decays in 5 to 6 s, which is much faster than the errors decay in the experimental results (~20 s at 200 mA).

7.4. Conclusions

For the first time, feedback control of position has been implemented using a conducting polymer actuator and a conducting polymer strain gage. Succesful operation of the feedback loops presented here is an important step towards all polymer position feedback loops for position or force control or for dynamic changing of material stiffness and viscosity.

In one instance, control was implemented with current control and in the other instance, control was implemented with voltage control. Difficulties with the response of the conducting polymer coated Lycra strain gages were circumvented by using feedback to keep the gage length constant and limiting the disturbances to low rates. The feedback loop was able track position disturbances successfully at rates of 0.1 and 0.25 mm/s. At the higher rate of 0.5 mm/s, the voltage limits imposed by the control to reduce polymer degradation impeded the controller and prevent successful tracking. A model developed for the control predicts the form of the observed errors as long as the control does not saturate. The settling time of the response is predicted well although the magnitude of the error is slightly underestimated.

Feedback response tests to a step change in position were less accurate. The feedback was able to control the system to maintain constant resistance but the resistance is not a good measure of the position. Significant improvements in the response of the strain gages are needed before step changes in position can be successfully tracked.

In both step and ramp response tests, the current or voltage limits were sometimes reached. These limits, which were imposed in an attempt to protect the polymer from electrochemical degradation, are also limits to the performance of the system.

Future work on feedback with a polymer actuator and strain gage should concentrate efforts to improve performance in three directions. First, the current strain gage technology limits their use to low frequencies and small numbers of cycles. As a consequence of the low cycle lifetime, the existing strain gages are more suitable for constant length feedback than they are for changing length experiments. The erratic step response also limits their use to situations where the disturbances have no high frequency

components. New strain gages must be developed with good step responses and good lifetimes.

The second direction for improvement should focus on improved control to avoid degradation. The imposition of current or voltage limits is a simple solution to protection of the polymer actuator. A better solution is to use resistance compensation to limit the double layer potential itself rather than the total voltage or the total current of the system (resistance compensation was first used by J. Madden (Madden, Cush, Kanigan and Hunter, 2000) and is discussed briefly in Chapter 2).

Finally, the third direction of effort for improved performance should be directed at the enhancing the power and durability of the actuator. As discussed in Chapter 2, there are several strategies for improving displacement, rate, and force.

Ultimately, the feedback loop should be implemented in an all polymer system. Conducting polymer transistors could be used to amplify the strain gage sensor signal and to drive the conducting polymer actuators. Conducting polymer transistors that have been built to date have current levels up to 100s of μA that are not able to drive the actuator currents of 100s of mA (Okuzaki, Ishihara and Ashizawa, 2003; Lu, Pinto and Macdiarmid, 2002; Nilsson, Kugler, Svensson and Berggren, 2002). But as the transistor current levels increase and the actuator drive currents can be decreased, integrated conducting polymer mechanical feedback loops systems will become a reality.

Reference List

1. De Rossi, D., Carpi, F., Lorussi, F., Mazzoldi, A., Scliningo, E.P., and Tognetti, A. Electroactive Fabrics for Distributed, Conformable and Interactive Systems. IEEE Sensors: IEEE.

2. De Rossi, D., Della Santa, A. and Mazzoldi, A. Dressware: Wearable hardware. Materials Science and Engineering C . 1999; 7(1):31-35.

3. Kuhn, Hans H. and Kimbrell, Jr. William C., inventors. Electrically conductive textile materials and method for making same . Milliken, assignee. USA 4803096. 1989 Feb 7.

4. Lu, J., Pinto, N.J. and Macdiarmid, A.G. Apparent Dependence of Conductivity of a Conducting Polymer on an Electric Field in a Field Effect Transistor Configuration. Journal of Applied Physics. 2002 Nov 15; 92(10):6033-6038.

5. Madden, John D. Conducting Polymer Actuators, Ph.D. Thesis. Cambridge, MA: Massachusetts Institute of Technology; 2000.

6. Madden, J.D., Cush, R.A., Kanigan, T.S. and Hunter, I.W. Fast contracting polypyrrole actuators. Synthetic Metals. 2000 May; 113:185-193.

7. Nilsson, D., Kugler, T., Svensson, P.O. and Berggren, M. An all-organic sensor-transistor based on a novel electrochemical transducer concept printed electrochemical sensors on paper. Sensors and Actuators B-Chemical. 2002 Sep 20; 86(2-3):193-197.

8. Okuzaki, H., Ishihara, M. and Ashizawa, S. Characteristics of conducting polymer transistors prepared by line patterning. Synthetic Metals. 2003 Apr 4; 137(1-3):947-948.

9. Spinks, G.M., G. G. Wallace and et al. Conducting polymers and carbon nanotubes as electromechanical actuators and strain sensors. Materials Research Society Symposium Proceedings 698 (Electroactive Polymers and Rapid Prototyping). 2002 ; 5-16.

10. Spinks, G.M., Wallace, G.G., Liu, L. and Zhou, D. Conducting Polymers Electromechanical Actuators and Strain Sensors. Macromolecular Symposia. 2003 Mar; 192:161-169.

11. Spinks, Geoff (University of Wollongong). Letter To: Peter Madden. 2002 Jan. Recipe for manufacturing conducting polymer strain gages.

12. Wallace, G.G. and Steele, J. News & Links - Intelligent knee sleeve to save costly sporting injuries [Web Page]. 2001 Nov 15. Available at: http:///www.tft.csiro.au/news/inteliknee.html.

8. Conclusion

Within this thesis progress towards building an integrated conducting polymer feedback loop has been described. Since they are relatively new materials, there is much to be learned about the properties and behavior of conducting polymers and about how these materials can be used in engineering systems.

To construct such a feedback loop made of only conducting polymer materials, the individual elements of the feedback loop – an actuator to move, a strain gage to measure position or force, and transistors to compute the control signal - must first be understood. Each element must also be tailored to operate within the system as a whole. In this thesis, much of the work focuses on improving the understanding and engineering of actuators. Experiments are also done to characterize conducting polymer based strain gages. The devlopment of conducting polymer transistors to compute the feedback signal is left as future research to be done.

In the development of conducting polymer actuators and a feedback loop with conducting polymer actuator and strain gage, the major contributions to the field that are presented in this thesis are:

1) A careful enumeration is made of how the properties of the conducting polymers and of the electrolyte in which they are operated can affect the performance of conducting polymer (Chapter 2). Understanding the relationships between material properties and performance is important in the search for new improved materials.
2) The voltage along the length of a long conducting polymer strip in electrolyte is measured for the first time as the strip is charged (Chapter 3). The measurements show that the charging is not uniform along the length and that the resistance of the polymer strip considerably affects the charging rate.
3) A mathematical description of the charging of a long conducting polymer strip in electrolyte is derived (Chapter 3). The model relates the material properties and geometry of the conducting polymer and electrolyte to the voltage, current and charge density at any position within the strip and for a given excitation frequency. In the limit of very high frequencies (short times) and very low frequencies (long times) the model matches the experimental results very well. More work is needed to convert the model from the Laplace domain to the time domain to prove that it also matches the experimental results at all times.
4) The model for the charging of a long conducting polymer strip is adapted to predict the charging for an arbitrary number of contact points (Chapter 3). Using the equation for an arbitrary number of contact points, an engineer can calculate the geometry and number of contact points needed to meet a specified strain requirement at a particular frequency.
5) A mathematical model is derived relating the deflection and force of a conducting polymer trimorph actuator to the charge density (Chapter 4). Bimorphs and trimorphs are often used to amplify the somewhat small strains of traditional conducting polymer actuators but no equations have yet been published for trimorphs and no equation have been published at all relating force to the ionic charge density.

6) In Chapter 5, the operation of conducting polymer trimorphs in liquid electrolyte is described and shown to behave as predicted in the model from Chapter 4. Results are also shown for the first time demonstrating that trimorph actuators can be stacked to build higher force actuators.
7) The displacement of trimorphs operating in air is shown to match the predicted displacement of the model from Chapter 4 very well (Chapter 6). With no free parameters, the model gives a good prediction of the experimentally measured displacement as a function of the ionic charge.
8) A first position feedback loop is operated using a conducting polymer actuator and a conducting polymer strain gage (Chapter 7). The actuator is a wide trimorph design to get high forces (~100 mN) and the strain gage is a polypyrrole coated Lycra fabric. The feedback loop successfully rejects ramp disturbances and the models of the feedback loop are able to describe the response. Rejection of step disturbances is less successful because of erratic high frequency strain gage response.

Further Work

There are many directions for future work that will give improvements in the performance of conducting polymer actuators. Here, some ideas are listed in three different categories. The first category is research that is a direct continuation of the work presented in this thesis. The second category involves new work that could improve the current conducting polymer actuator materials (primarily polypyrrole but also polyaniline and polythiophene). Finally, in the third category, projects for new materials are discussed.

Continuation of Thesis Work

Several topics should be investigated that are a continuation of research topics in this thesis.

1) The model developed to describe the voltage and charge in a long polymer strip (Chapter 3) has not been conclusively shown to match the experimental data at all times. Difficulties in inverting the Laplace transform could be circumvented by running a swept sine experiment to measure the transfer function. Alternatively, the time domain output can be calculated by running a time domain simulation of the differential equations.
2) The model from Chapter 3 predicts that multiple electrical contact points will give greater contraction rates. Future linear actuators should make use of several contact points to improve performance.
3) In Chapter 5, parallel stacks of trimorph actuators are shown to exert greater force than single trimorph actuators. In Chapter 7, a single trimorph was presented that exerts over 100 mN. Stacking many of the > 100 mN trimorphs will lead to actuators that exert well over 1 N.
4) Most of the trimorph strips that were built are quite short. However, if longer strips are made, then the charging along the length of the strips will be nonuniform (as described in Chapter 3). The model in Chapter 3 needs to be

adapted to describe a system with two conducting polymer strips[1]. If needed, multiple electrical contact points can also be engineered into the trimorph actuators.

5) Improved strain gages which have low stiffness and high gage factors will make integrated feedback loops much more reliable. In the existing coated Lycra strain gages, the cause of failure is not yet certain and should be investigated. However, new materials that are designed specifically to be strain gages could ultimately give better strain gage properties.

Work with Traditional Materials

The best performance possible with traditional materials has not yet been realized. Furthermore, different manufacturing techniques could lead to new actuators with interesting designs.

1) Changes to geometry can lead to significant changes in performance. The number of electrical contact points, the thickness of the film (which should generally be as thin as possible), the geometry of the electrolyte (which should also be as thin as possible), and the mechanical attachment design all need to be carefully assessed.
2) The gel electrolyte used for the trimorph actuators can be improved in few ways. The current recipe gradually separates over time (several weeks) so more stable chemistry is needed for long lifetime actuators. Improvements that can be made to the conductivity of the gel will improve efficiency and rate.
3) The current generation of actuator materials require large currents to do work because of the low electromechanical coupling (a large amount of the energy that is input into the actuators is stored in the polymer bulk capacitance). If there are large resistances external to the actuator, it might be better to build actuators that run electrically in series instead of in parallel so that the voltage applied to the entire system increases while the current decreases.
4) Making use of lithography techniques to shape conducting polymer actuators would give the designer many more choices for geometry. Inganas and Smela have made use of lithography on the millimeter scale (Jager, Inganas and Lundstrom, 2000; Smela, 1999) but lithography on the 10 mm or 100 mm scale can also create interesting actuators. Gold electrodes can be patterned to improve conductivity, lithography photoresists can become structural elements in the actuator, or multilayer devices can be created by patterning electrolyte gels as well as conducting polymers.
5) Creating anisotropic materials or anisotropic conditions (e.g. by pre-stretching or constraining the polymer) could increase the strains observed in the polymer. Smela and Gadegaard, for example, observed very large strains

[1] The charging model from Chapter 3 can be applied to a conducting polymer trimorph by treating the trimorph as two independent long polymer strips with an imaginary perfectly conducting counter electrode that sits in the gel electrolyte equidistant between the two conducting polymer electrodes. For each 'half' trimorph, the resistance of the gel is then half the total gel resistance. By symmetry, the voltage on each 'half' of the trimorph is equal to half the voltage across the trimorph.

perpendicular to a film of polypyrrole still attached to a substrate (Smela and Gadegaard, 1999).

6) Very large strains have recently been demonstrated using polypyrrole in our lab (> 15%, unpublished work by D. Rinderkinecht). These tremendous strains are very exciting and must be investigated further.
7) To make a truly integrated conducting polymer feedback loop, high current transistors should be developed that can drive the polymer actuators. Transistors are also needed to implement a control algorithm.

New Materials

The most exciting developments in conducting polymer actuators will be with new materials designed specifically with actuation in mind.

1) Much of the research effort should be directed towards increasing the strain / charge ratio. Increasing the strain / charge ratio will reduce the currents required to generate a given strain and should also increase the electromechanical coupling (because less electrical charge will be stored in the bulk material capacitance). At the same time, it is important that the total strain also be increased
2) Micro-structuring of the new actuator materials can be used to blend material properties. If the new actuator materials are very brittle, layering the actuator material between a flexible elastomer may produce high strain flexible actuators. Conductivity, strain, Young's modulus, and creep can all be dramatically changed by combining two or more distinct materials. Finally, if the micro-structuring is anisotropic, properties can be tailored to produce maximum strain in only one direction.
3) Block copolymers might create conducting polymer based actuators that are truly nano-structured. Alternatively, design of monomers with side groups that can cross-link might produce elastomer-like mechanical properties with the high conductivity of conjugated polymers.

Reference List

1. Jager, E.W.H., Inganas, O. and Lundstrom, I. Mircrorobots for micrometer-size objects in aqueous media: Potential tools for single-cell manipulation. Science. 2000 Jun 30; 288:2335-2338.

2. Smela, E. and Gadegaard, N. Surprising volume change in PPy(DBS): An atomic force microscopy study. Advanced Materials. 1999; 11(11):953-957.

3. Smela, E. A microfabricated moveable electrochromic "pixel" based on polypyrrole. Advanced Materials. 1999; 11(16):1343-1345.

Appendix A Measurement of Gel Electrolyte Properties

This appendix includes the measurement of the gel electrolyte Young's modulus and the measurement of the gel electrolyte electrochemical impedance.

Measurement of Modulus

The modulus of the gel electrolyte with a nylon mesh was measured using a Perkin Elmer[1] DMA 7e dynamic mechanical analyzer. The dynamic modulus was measured at 1 Hz. The modulus measured over a period of about 12 minutes is shown in Figure A.2. The average modulus over the measurement is 7.3 MPa but there is a large variance in the measured value over time.

The modulus of the gel is used in the calculation of the trimorph curvature / charge ratio in Chapter 6. Because the modulus of the gel is much lower than the modulus of the conducting polymer, the variations in the measured modulus have very little effect on the calculated curvature / ratio (see Chapter 6, Equation 1).

Measurement of Gel Electrolyte Impedance

Using a PAR VMP2 Impedance analyzer[2], the impedance of a thin layer of gel electrolyte was measured between 10 Hz and 200 kHz. The measured impedance is shown in Figure A.2.

The conductivity of the gel can be calculated using the geometry of the test cell and the resistance of measurement setup at the point closest to zero phase. The measurements were made on a $BMIBF_4$ gel sandwiched between two gold coated 25 mm

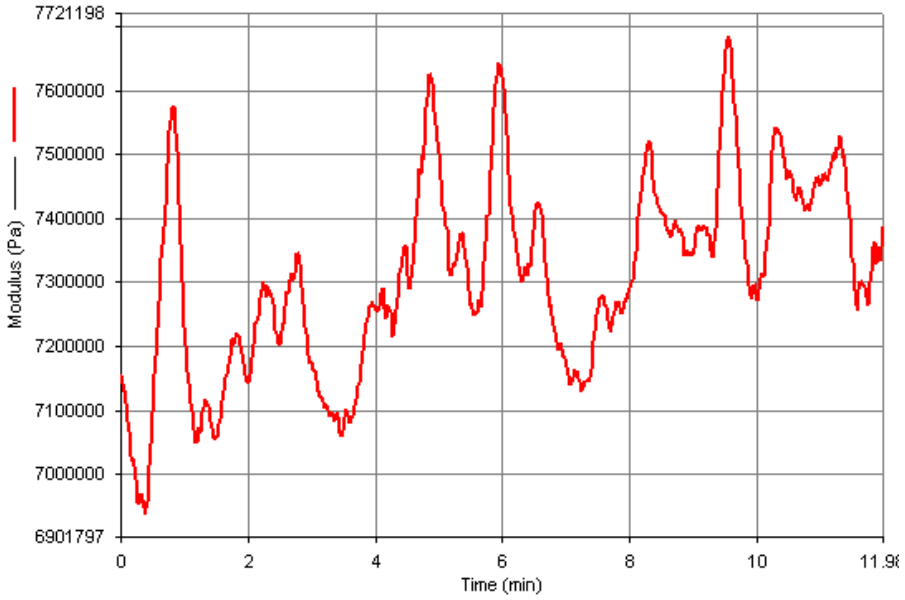

Figure A.1: Modulus of a $BMIBF_4$ gel. The average modulus over the measurement is 7.3 MPa.

[1] Perkin Elmer, www.pekrin-elmer.com.

by 75 mm glass slides. The gel thickness was measured to be 0.124 ± 0.2 mm. The conductivity is:

$$\sigma = \frac{h_{gel}}{R \cdot A} \tag{1}$$

where σ is the conductivity, h_{gel} is the thickness of the gel, A is the cross-sectional area of the gel, and R is the resistance. Substituting h_{gel} = 0124 mm, A = 1875 mm^2, and R = 42.8 Ω gives $\sigma = (1.6 \pm 0.25) \times 10^{-3}$ S/m.

A second sample of $BMIBF_4$ gel (not shown) had a thickness of 0.184 ± 0.2 mm and a resistance of 57.0 Ω. The conductivity of the second sample was calculated to be $(1.72 \pm 0.2) \times 10^{-3}$ S/m.

The average value of the two measurements is $(1.66 \pm 0.2) \times 10^{-3}$ S/m.

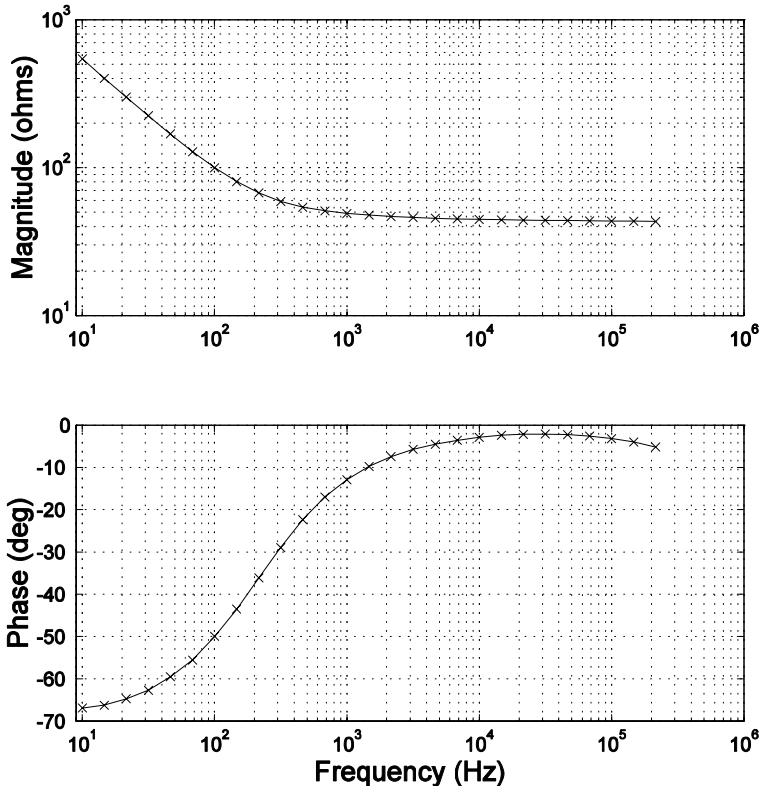

Figure A.2: Impedance of the $BMIBF_4$ Gel sandwiched between two gold coated slides. The series resistance of the gel (at the point closest to zero phase) is 42.8 Ω.

[2] Princeton Applied Research, Princeton, NJ.

Appendix B Matlab Frame by Frame Analysis

This appendix contains the code for the frame by frame analysis of the trimorph data.

File List

1) **domyruns.m**
   script file to do fits to the four trilayer video files.

2) **process.m**
   Matlab function to extract the position of the trimorph and to fit a circle.

3) **domyplots.m**

   Matlab file to make plots of the calculate curvatures.

domyruns.m

```
%
%   domyruns.m
%
% executes the automatic data analysis for TriNylon videos.
%
% Peter Madden, Nov. 11, 2002.
%

avifilenames = ['TriNylon20mA2sMatlab.avi'
          'TriNylon30mA2sMatlab.avi'
          'TriNylon40mA2sMatlab.avi'
          'TriNylon50mA2sMatlab.avi' ];

savefilenames = ['TriNylon20mAFrameAnalysis.mat'
          'TriNylon30mAFrameAnalysis.mat'
          'TriNylon40mAFrameAnalysis.mat'
          'TriNylon50mAFrameAnalysis.mat'];

ScaleX = [  0.15746545918960  % [mm/pix]
          0.15730109023428 %   [mm/pix]
          0.15746545918960 %   [mm/pix]
          0.15730109023428];

ScaleY = [  0.18490115882754
          0.18558429118774
          0.18604252400549
          0.18547008547009];


EchemONFrame = [    58
                76
                78
                74 ];       % found by looking at each frame until the red LED turns on

runstodo = [0 0 0 1];    % set to 1 if you want to calculate the run.



startstr = ['Start time: ',datestr(now)];
disp(startstr);
disp('');

for i = 1:4
   if runstodo(i)
      disp(['Processing file ', avifilenames(i,:)]);
      process(avifilenames(i,:), savefilenames(i,:), ScaleX(i), ScaleY(i));
   end
end

disp('');
disp(startstr);
disp(['End time: ', datestr(now)]);
```

process.m

```
function [Center, Rad, Sigma, Convergence, CovCenter, RadUncert] = ...
          process(avifilename, savefilename, ScaleX, ScaleY, startframe, stopframe, makeplots)
%
% function [Center, Rad, Sigma, Convergence, CovCenter, RadUncert] = ...
%           process(avifilename, savefilename, ScaleX, ScaleY, startframe, stopframe, makeplots)
%
% For processing of the TriNylon avi files.  20mA, 30mA, 40mA, and 50mA, 2s positive, 2s
negative.
%
% Peter Madden, Nov 11, 2002
%

movinfo = aviinfo(avifilename);

if ~exist('startframe')
   startframe = 1;
end
if ~exist('stopframe')
   stopframe = movinfo.NumFrames;
end
if ~exist('makeplots')
   makeplots = 0;   % don't display plots along the way
end

% Choose subregion of interest to get rid of the background rulers etc.
YHIGH = 333;
YLOW = 115;
XHIGH = 315;
XLOW = 137;

XSUBSIZE = XHIGH - XLOW + 1;
YSUBSIZE = YHIGH - YLOW + 1;
x = 1:XSUBSIZE;
y = 1:YSUBSIZE;
XM =  ones(1,YSUBSIZE)'*x;
YM =  y'*ones(1,XSUBSIZE);

tolp = 0.001;          % tolerance for least squares
tolg = 0.0001;         % gradient tolerance
r= 100;               % guess at radius

for i = startframe:stopframe
   mov = aviread(avifilename, i);

   disp(['Frame number ', num2str(i),' of ', num2str(movinfo.NumFrames), '.']);
   % extract just the part that of the image that
   % we are interested in:
   Im = RGB2GRAY(mov(1).cdata(115:333, 137:315,:));
   if makeplots
      figure, imshow(Im), title('Section of Image');
   end
```

```
DI = imadjust(Im, [], [0 1]);
if makeplots
   figure, imshow(DI), title('scaled image');
end
BWs = edge(DI, 'sobel', (graythresh(DI) * .1));
if makeplots
   figure, imshow(BWs), title('binary gradient mask');
end

se90 = strel('line', 3, 90);
se0 = strel('line', 3, 0);

BWsdil = imdilate(BWs, [se90 se0]);
if makeplots
   figure, imshow(BWsdil), title('dilated gradient mask');
end

BWdfill = imfill(BWsdil, 'holes');
if makeplots
   figure, imshow(BWdfill);
   title('binary image with filled holes');
end

PTSX = XM(BWdfill > 0.5);
PTSY = YM(BWdfill > 0.5);

if makeplots
   figure, plot(PTSX, PTSY, '.');
   axis([1 179 1 219]);
end

clear PTS;
PTS(:,1) = PTSX * ScaleX;
PTS(:,2) = PTSY * ScaleY;

%
% Fit to x = a + by + cy^2 and use the coefficient c to predict whether there
% is positive curvature or negative curvature.  The predicted sign of the curvature
% is used to seed the guess at an origin.
%
p = polyfit(PTS(:,2), PTS(:,1), 2);     % fit second order polynomial to data
if p(1) > 0
   Origin = [ (mean(PTS(:,1)) + 100)   mean(PTS(:,2))]';    % set origin to right of curve
   InvertFactor = 1;
else
   Origin = [ (mean(PTS(:,1)) - 100)   mean(PTS(:,2))]';    % set origin to left of curve
   InvertFactor = -1;
end

[x0n, rn, d, sigmah, conv, Vx0n, urn, GNlog, a, R] = ls2dcircle(PTS, Origin, r, tolp, tolg);

if makeplots
   theta = 0:0.1:2*pi;
   xp = rn*sin(theta) + x0n(1);
   yp = rn*cos(theta) + x0n(2);
   hold on; plot(xp/ScaleX, yp/ScaleY, 'r'); hold off;
```

```
    end
    Center(i,:) = x0n';
    Rad(i) = InvertFactor * rn;
    Sigma(i) = sigmah;
    Convergence(i) = conv;
    CovCenter(i,:,:) = Vx0n;
    RadUncert(i) = urn;
end

eval(['save ', savefilename, ' Center Rad Sigma Convergence CovCenter RadUncert ScaleX
ScaleY']);
```

domyplots.m

```
%
% domyplots.m
%
% For analysing .avi files for Trilayer Nylon experiments in air.
%
% Peter Madden, Nov. 11, 2002
%
avifilenames = ['TriNylon20mA2sMatlab.avi'
        'TriNylon30mA2sMatlab.avi'
        'TriNylon40mA2sMatlab.avi'
        'TriNylon50mA2sMatlab.avi' ];

savefilenames = ['TriNylon20mAFrameAnalysis.mat'
        'TriNylon30mAFrameAnalysis.mat'
        'TriNylon40mAFrameAnalysis.mat'
        'TriNylon50mAFrameAnalysis.mat'];


EchemONFrame = [    58
                76
                78
                74 ];       % found by looking at each frame until the red LED turns on

figuretext = ['A) 20 mA square wave.'
        'B) 30 mA square wave.'
        'C) 40 mA square wave.'
        'D) 50 mA square wave.' ];


for i = 1:4
   eval(['load ', savefilenames(i,:),';']);
   movinfo = aviinfo(avifilenames(i,:));
   eval(['Radius',num2str(i),' = Rad;']);
   Time = ((1:movinfo.NumFrames) - EchemONFrame(i))/movinfo.FramesPerSecond;  % shift
zero

   figure(1); subplot(2,2,i); plot(Time, 1./(Rad/1000), 'k'); grid on;
   % title(['Filename: ', avifilenames(i,:)]);
   text(1, -12, figuretext(i,:));
   xlabel('Time [s]');
   ylabel('Curvature [1/m]');
   axis([-2 22 -15 15]);
end
```

Appendix C Experiments on Coated Lycra Strain Gages

The experiments on Lycra strain gages that are described in Chapter 7 are a subset of all the experiments that were done. Several different ideas were tried to improve the properties of the strain gages but none were successful. Some of those experiments are briefly described here so that they are not repeated in the future by someone else.

Encapsulation of the Strain Gage

The changing response of the strain gages after a fairly low number of life cycles (described in Chapter 7) could be caused by a number of different mechanical failures. The polypyrrole coating of the strain gage could be separating from the underlying Lycra fabric, the fabric could be shifting, or the polypyrrole itself could be tearing. It was hoped that by encapsulating the strain gage into a flexible surrounding material, the electrical properties of the strain gage could be made more robust.

To keep the material as flexible as possible, the first attempt at encapsulation used silicone (manufactured by General Electric). A photograph of a strain gage embedded in

Figure C.1: Photograph of two polypyrrole coated lycra strips encapsulated in silicone. The silicone is nearly transparent and has been trimmed to be slightly larger than the coated Lycra strips. The ruler is marked in mm.

silicone is shown in Figure C.1. The response for the silicone gage turned out to be no better than those of uncoated gages (see Polymers, Pumps, Actuators Lab Book 7, April 2003).

Another attempt to coat the strain gages was made using a flexible polyurethane coating material as shown in (Kalex 04022, Elementis, NJ). Again the response was not markedly different from the response of the uncoated strain gages and the stiffness in this case was very high.

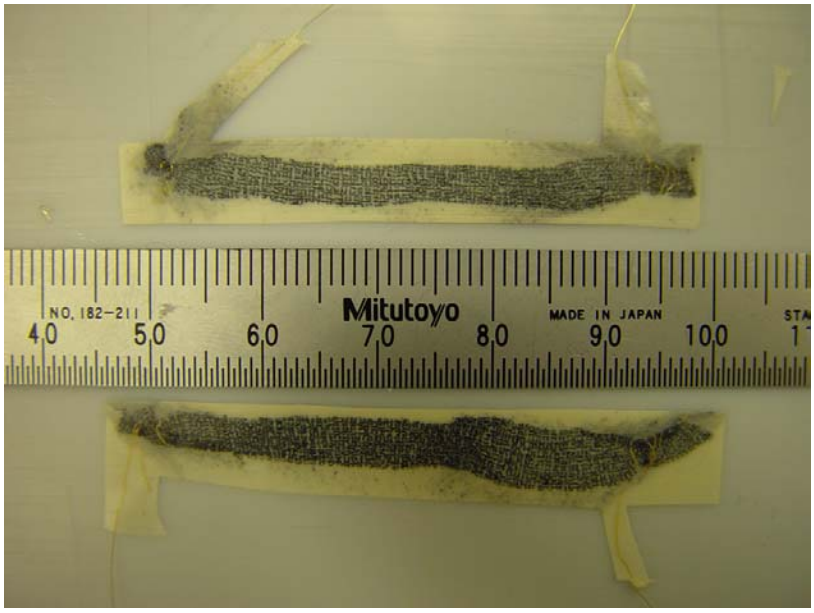

Figure C.2: Photograph of two polypyrrole cotaed Lycra strips encapsulated in a polyurethane. The tabs emerging to the sides are where the electrical contact is made to the strip with gold wires. The ruler is marked in mm.